INVESTIGATIONS INTO THE ACCUMULATION OF HEMATOPOIETIC CELLS IN THE SPINAL CORD IN A MURINE MODEL OF MOTOR NEURON DISEASE

by

Coral-Ann B. Lewis
B.Sc. (Kinesiology), Simon Fraser University, 2003

THESIS SUBMITTED IN PARTIAL FULFILLMENT OF
THE REQUIREMENTS FOR THE DEGREE OF

DOCTOR OF PHILOSOPHY

In the
Department of Biomedical Physiology and Kinesiology
Faculty of Science

© Coral-Ann B. Lewis 2011

SIMON FRASER UNIVERSITY

Summer 2011

APPROVAL

Name: **Coral-Ann B. Lewis**

Degree: **Doctor of Philosophy**

Title of Thesis: **Investigations into the Accumulation of Hematopoietic Cells in the Spinal Cord in a Murine Model of Motor Neuron Disease**

Examining Committee:

Chair: **Angela Brooks-Wilson**
Associate Professor - Department of Biomedical Physiology and Kinesiology, SFU

_____

Charles Krieger
Senior Supervisor
Professor – Department of Biomedical Physiology and Kinesiology, SFU

_____

Fabio Rossi
Supervisor
Associate Professor – Department of Medical Genetics, UBC

_____

Neil Watson
Supervisor
Professor – Department of Psychology, SFU

_____

Miriam Rosin
Internal Examiner
Professor – Deptment of Biomedical Physiology and Kinesiology, SFU

_____

Katerina Dorovini-Zis
External Examiner
Professor – Department of Pathology and Laboratory Medicine, UBC

Date Defended/Approved: August 12th, 2011

Declaration of Partial Copyright Licence

The author, whose copyright is declared on the title page of this work, has granted to Simon Fraser University the right to lend this thesis, project or extended essay to users of the Simon Fraser University Library, and to make partial or single copies only for such users or in response to a request from the library of any other university, or other educational institution, on its own behalf or for one of its users.

The author has further granted permission to Simon Fraser University to keep or make a digital copy for use in its circulating collection (currently available to the public at the "Institutional Repository" link of the SFU Library website <www.lib.sfu.ca> at: <http://ir.lib.sfu.ca/handle/1892/112>) and, without changing the content, to translate the thesis/project or extended essays, if technically possible, to any medium or format for the purpose of preservation of the digital work.

The author has further agreed that permission for multiple copying of this work for scholarly purposes may be granted by either the author or the Dean of Graduate Studies.

It is understood that copying or publication of this work for financial gain shall not be allowed without the author's written permission.

Permission for public performance, or limited permission for private scholarly use, of any multimedia materials forming part of this work, may have been granted by the author. This information may be found on the separately catalogued multimedia material and in the signed Partial Copyright Licence.

While licensing SFU to permit the above uses, the author retains copyright in the thesis, project or extended essays, including the right to change the work for subsequent purposes, including editing and publishing the work in whole or in part, and licensing other parties, as the author may desire.

The original Partial Copyright Licence attesting to these terms, and signed by this author, may be found in the original bound copy of this work, retained in the Simon Fraser University Archive.

Simon Fraser University Library
Burnaby, BC, Canada

STATEMENT OF
ETHICS APPROVAL

The author, whose name appears on the title page of this work, has obtained, for the research described in this work, either:

(a) Human research ethics approval from the Simon Fraser University Office of Research Ethics,

or

(b) Advance approval of the animal care protocol from the University Animal Care Committee of Simon Fraser University;

or has conducted the research

(c) as a co-investigator, collaborator or research assistant in a research project approved in advance,

or

(d) as a member of a course approved in advance for minimal risk human research, by the Office of Research Ethics.

A copy of the approval letter has been filed at the Theses Office of the University Library at the time of submission of this thesis or project.

The original application for approval and letter of approval are filed with the relevant offices. Inquiries may be directed to those authorities.

Simon Fraser University Library
Simon Fraser University
Burnaby, BC, Canada

Last update: Spring 2010

ABSTRACT

Transgenic mice over-expressing human mutant superoxide dismutase 1 (mSOD) develop motoneuron loss resembling amyotrophic lateral sclerosis (ALS), a fatal neurodegenerative disease. Bone marrow (BM) chimeric mice created by myeloablating and transplanting mice with green fluorescent protein (GFP)-labelled BM were used to study the recruitment of BM-derived cells (BMDCs) into the spinal cords of mSOD and control mice. Accumulation of GFP+ cells in mSOD spinal cord paralleled disease progression and significantly greater numbers of GFP+ cells were observed in mSOD spinal cord at symptomatic and disease end-stages compared to controls. GFP+ BMDCs expressed the macrophage markers CD11b and F4/80, which are also expressed by microglia. GFP+ BDMCs constituted 10-20% of total CD11b/F4/80 + cells within spinal cord, indicating the expansion of microglia within mSOD spinal cord is primarily through proliferation of resident microglia. Analysis of morphology and proximity of BMDCs to blood vessels revealed that only a fraction of BMDCs acquire the stellate morphology and Iba1+ immunophenotype characteristic of parenchymal microglia, and the majority of BMDCs remained in close proximity to blood vessels. Mice transplanted with BM from donors that express GFP in only CX_3CR1+ cells demonstrated that this population of cells accumulates within control and mSOD spinal cord. To determine whether myelosuppressive regimens alternative to irradiation potentiate BMDC accumulation in mSOD and control spinal cord, mice were treated with the chemotherapeutic Busulfex (BU) and transplanted with GFP+ BM. GFP+ cells were observed in the spinal cords of mSOD and control mice. Cytotoxic T-cells were also observed in control and mSOD spinal cord, suggesting the dose of BU used in this study has neurotoxic and neuroinflammatory effects. The differential accumulation of CX_3CR1+ BM cells and cells derived from definitive hematopoiesis was analyzed by transplanting irradiated mSOD and control mice with the $CX_3CR1^{+/GFP}$ fraction of BM cells along with red fluorescent protein (RFP) c-Kit+Lin-Sca1+ cells. Analysis of spinal cord at disease end-stage revealed $CX_3CR1^{+/GFP}$ and RFP+ cells in the spinal cords of mSOD and controls, indicating that circulating cells from the $CX_3CR1^{+/GFP}$ BM fraction and cells derived from definitive haematopoiesis are accumulate in spinal cord.

Keywords: bone marrow; hematopoietic stem cells; bone marrow transplant; mSOD mouse; amyotrophic lateral sclerosis; spinal cord; microglia

For my family.

ACKNOWLEDGEMENTS

TABLE OF CONTENTS

LIST OF FIGURES

LIST OF TABLES

GLOSSARY

AD	Alzheimer's disease
ALS	amyotrophic lateral sclerosis
APC	allophycocyanin
APP	amyloid precursor protein
BBB	blood-brain barrier
BDNF	brain-derived neurotrophic factor
BM	bone marrow
BMDC	bone marrow-derived cell
BrdU	bromodeoxyuridine
BSA	bovine serum albumic
BU	Busulfex
CFU-S	colony forming unit-spleen
CLP	common lymphoid progenitor
CMP	common myeloid progenitor
CNS	central nervous system
CSF	cerebrospinal fluid
Cy3	cyanine 3
DA	dopaminergic
DC	dendritic cell
EAE	experimental allergic encephalitis
EAE	experimental autoimmune encephalitis
EDTA	ethylenediaminetetraacetic acid
EdU	5-ethynyl-2'deoxyuridine
EPCR	endothelial protein C receptor
eYFP	enhanced yellow fluorescent protein
FACS	fluorescence-activated cell sorting
fALS	familial amyotrophic lateral sclerosis
FBS	fetal bovine serum
FITC	fluorescein isothiocyanate
G-CSF	granulocyte colony stimulating factor
GDNF	glial cell-derived neurotrophic factor
GFP	green fluorescent protein
GMP	granulocyte-macrophage progenitor
GVHD	graft-versus-host disease
HSC	hematopoietic stem cell

IP	intraperitoneal
IV	intravenous
JAM	junctional adhesion molecule
KLS	c-Kit+lin-Sca1+
KTLS	c-Kit+Thy1.1^{lo}lin-Sca1+
ManR	mannose receptor
MCAO	middle cerebral artery occlusion
M-CSF	macrophage colony stimulating factor
MDP	macrophage-dendritic cell precursor
MEP	megakaryocyte-erythrocyte progenitor
MHC	major histocompatibility complex
MO	monocyte
MPP	multipotent progenitor
MPS	mononuclear phagocyte system
MPTP	1-methyl-4-phenyl-1,2,3,6-tetrahydro-pyridine
mSOD	mutant superoxide dismutase-1
NGS	normal goat serum
PBC	peripheral blood cell
PBS	phosphate-buffered saline
PBST	0.3% Triton -X in PBS
PD	Parkinson's disease
PE	phycoerythrin
PECAM-1	platelet endothium cell adhesion molecule-1
PECy7	phycoerythrin-cyanine 7
PFA	paraformaldehyde
PSEN	presenilin
RFP	red fluorescent protein
SCF	stem cell factor
SLAM	signalling lymphocytic activation molecule
SOD1	superoxide dismutase 1
TBI	total body irradiation
TF	transcription factor
wt	wild type

AUTHOR CONTRIBUTIONS AND ORIGINAL PUBLICATIONS

Chapter 1

Lewis CA., Rossi FMV, Krieger C (2011) Bone marrow-derived cells as treatment vehicles in the central nervous system. *Regenerative Therapy Using Blood-Derived Stem Cells,* In Press.

Reproduced with changes by permission of Springer Publishing Company.

This book chapter was written by me and was reviewed by C. Krieger and F. Rossi; portions of this chapter were reproduced in Chapter 1 of this thesis.

Chapter 2

Solomon JN, Lewis CA, Ajami B, Corbel SY, Rossi FMV, Krieger C (2006) Origin and distribution of bone marrow-derived cells in a mouse model of amyotrophic lateral sclerosis. *Glia,* 53:744-53.

Reproduced by permission of Wiley-Liss, Inc.

My contribution to this study included: motor assessment of mice, tissue processing, cell quantification, immunohistology. The manuscript was written by J. Solomon with contributions from myself.

Chapter 3

Lewis CA, Solomon JN, Rossi FMV, Krieger C (2009) Bone marrow-derived cells in the central nervous system of a mouse model of amyotrophic lateral sclerosis are associated with blood vessels and express CX3CR1. *Glia,* 57(13):1410-19.

Reproduced with permission of Wiley-Liss, Inc.

My contributions to this study include overall design of study, bone marrow transplants, mouse husbandry/genotyping, tissue processing, histology, cell quantification, data analysis. The paper was put together and written by me.

Chapter 4

Lewis CA, Manning JW, Rossi FMV, Krieger C (2011) Bone marrow-derived cells accumulate in the spinal cord in a mouse model of Amyotrophic lateral sclerosis in the absence of irradiation. In preparation.

My contribution to this study included: mouse husbandry, genotyping, bone marrow transplants, tissue processing, and overall study design. J.W. Manning assisted in all experimental aspects and quantified cells. The paper was put together and written by me.

Chapter 5

Lewis CA., Ajami B, Rossi FMV, Krieger C (2011) Accumulation of CX3CR1+/GFP bone marrow cells and cells derived from definitive hematpoiesis in the spinal cord of a mouse model of amyotrophic lateral sclerosis. In preparation.

I was responsible for the overall design of this study and performed all experiments; the initial experimental paradigm was designed by B. Ajami and cell sorting was performed by J. Wong and A. Johnson. This paper was put together and written by me. S. Thakore and H. Mancell assisted with histology and cell quantification.

1: GENERAL INTRODUCTION AND LITERATURE REVIEW

1.1 Introduction

Neurodegenerative diseases are characterized by the death of specific populations of neurons, which due to a lack of regenerative potential, culminates in permanent and progressive disability. Pharmacological treatments for these disorders have been ineffective at slowing the disease process, due in part to the inability of drugs to reach sites of neurodegeneration. The CNS is surrounded by the blood-brain barrier (BBB), a specialized endothelial network that separates circulating blood from the extracellular space of the CNS. Tight junctions seal the apical surface between capillary endothelial cells and regulate the entry of blood-borne substances and cells into the CNS, largely preventing the influx of many drugs. However, it is well established that after receiving bone marrow (BM) transplants, donor cells are observed in the CNS of patients at autopsy in limited numbers (see: Unger et al., 1993; Appel et al., 2008) demonstrating that BM cells are capable of entering the CNS under some circumstances. Current research aims to exploit the ability of BM cells to enter the CNS and use these cells as vehicles to transport therapeutic substances into the CNS.

1.2   Discovery of the Hematopoietic Stem Cell

Stem cells are defined by two critical functional properties: the capacity for self-renewal, or division in which at least one daughter cell retains the properties of the stem cell and the production of differentiated progeny (McCulloch and Till, 2005). The diversity of the progeny produced by stem cells is variable, ranging from the totipotent zygote from which all extra-embryonic and embryonic tissues derive, to unipotent progenitors that give rise to a single lineage of daughter cells (Seita and Weissman, 2010). Between these two extremes, the multipotent hematopoietic stem cell (HSC) is the predecessor to all cells within the hematolymphoid system including erythrocytes, lymphocytes, granulocytes, and monocytes.

The existence of a single cell from which all cells of the hematopoietic system derive had been the subject of speculation since the late 19th century, however, it was not until the pioneering experiments of McCulloch and Till in the 1960s that its existence was confirmed. Employing experiments in which lethally irradiated mice received injections of limited numbers of syngeneic bone marrow cells, 10 days post-transplant investigators observed donor-derived, myeloerythroid cell colonies within the spleens of recipient mice (Seita and Weissman, 2010).

To determine whether the splenic colonies derived from a single multipotent cell or "colony forming unit-spleen" (CFU-S), in 1963 Becker and colleagues sublethally irradiated mice, injected them with BM and subjected them to a second dose of radiation. This second dose of radiation served two

purposes: to lethally myeloablate the host and to label individual donor BM cells through radiation-induced chromosomal damage, with the chances of multiple donor cells acquiring the same abnormal karyotype virtually impossible. Eleven days after BM transplantation, chromosomal analysis cells within the donor-derived splenic colonies confirmed that they derived from a single cell (Becker et al., 1963).

With the pluripotency of the CFU-S confirmed, Siminovitch and colleagues (1963) next investigated its capacity for self-renewal. Following irradiation and BM transplantation, single donor-derived splenic colonies were harvested, dissociated and transplanted into irradiated hosts. Serial transplantation of donor-derived cells similarly resulted in the formation of donor-derived, myeloerythroid colonies within the spleens of secondary recipients, demonstrating the ability of the CFU-S to self-renew (Siminovitch et al., 1963).

Although the CFU-S itself had yet to be identified, together the results of the above experiments conferred the functional properties of self-renewal and the capacity to produce fully differentiated progeny to the CFU-S and in doing so, demonstrated the existence of the hematopoietic stem cell (HSC).

1.2.1 Identification of HSCs and Myeloid Progenitors

Although colony-forming assays remain essential to functionally evaluating the ability of stem cells to proliferate and differentiate into clonogenic progeny, investigations into the expression patterns of a plethora of cell surface markers has enabled researchers to isolate HSCs and downstream progenitors from

whole BM (Table 1.1). Traditionally, the murine HSC population is identified as being c-Kit$^+$Thy1.1^{lo}Lin1$^{-/low}$Sca1$^+$ (KTLS) and is further subdivided based on the expression of CD34. HSCs capable of long-term reconstitution of the BM compartment (LT-HSCs) after myeloablation are CD34- while short-term reconstituting HSCs (ST-HSCs, also referred to as multipotent progenitors (MPPs)) are CD34+ (Zhu and Emerson, 2002).

More recently, the differential expression of members of the signalling lymphocytic activation molecule (SLAM) family of surface receptors, specifically CD48, CD150 and CD244 (Kiel et al., 2005), and endothelial protein C receptor (EPCR; Balazs et al., 2006) by hematopoietic stem and progenitor cells has also been employed to determine the primitiveness of hematopoietic progenitors (Kiel et al., 2005). The most primitive HSCs express EPCR and are identified as CD150$^+$CD48$^-$CD244$^-$ while MPPs are CD150$^-$CD48$^-$CD244$^+$ and EPCR negative; more restricted progenitor populations are characterized by CD150$^-$CD48$^+$CD244$^+$ expression (Kiel et al., 2005; Balazs et al., 2006).

The dominant hypothesis regarding cell fate determination from the MPP states that the first step is the restriction to either the lymphoid or myeloid lineage. The common lymphoid progenitor (CLP) is the earliest cell within BM that expresses IL-7Rα, and the IL-7/IL-7Rα signalling axis is essential for B and T cell development.   The CLP generates pro-T and pro-B cells that migrate to and mature within the thymus, natural killer cells, and a population of dendritic cells (DCs). Alternatively, myeloid progenitors reside with the IL-7R-c-Kit+Lin-Sca-1- population of BM cells and can be further fractionated based on the expression of

Fc$^\gamma$RII/III and CD34. The common myeloid progenitor (CMP) identified by

Fc$^\gamma$RII/IIIloCD34+ expression, gives rise to the downstream megakaryocyte-

erythrocyte progenitor (MEP, Fc$^\gamma$RII/IIIloCD34-) and the granulocyte-macrophage

progenitor (GMP, Fc$^\gamma$RII/IIIhiCD34+; Iwasaki and Akashi, 2007). The GMP

generates restricted progenitors for granulocytes (i.e. mast cells, basophils,

eosinophils and neutrophils), as well as the bipotent macrophage-dendritic cell

progenitor (MDP). The MDP is identified by Fc$^\gamma$RII/IIIhiCD34+ expression at

levels similar to the GMP along with the expression of the chemokine receptor

CX$_3$CR1 (Fogg et al., 2006).

1.2.2 Myelopoiesis

Within the BM compartment, the determination between HSC self-renewal

versus differentiation is dictated by the cytokine milieu within the stem cell niche

and by receptor/ligand interactions with surrounding stromal cells (Seita and

Weissman, 2010).   There are two niches within BM that are hypothesized to

regulate the cycling and differentiation of HSCs: the osteoblast niche and the

vascular niche. The osteoblast niche is home to the most primitive HSCs,

characterized as noncycling quiescent cells, which reside in close approximation

to endosteal osteoblasts (Lymperi et al., 2010). The vascular niche within BM

promotes HSC cycling and differentiation, in part by endothelial cell expression of

stem cell factor (SCF), the ligand for the receptor c-Kit expressed by HSCs,

which promotes cell proliferation (Hexner and Emerson, 2007).

The cellular events that direct HSC differentiation towards a single cell fate during hematopoiesis are not fully understood, however, in the steady state, the expression of transcription factors (TFs) by hematopoietic progenitors plays a central role in lineage commitment. There are two main theories regarding control of TF expression that differ in whether control is exerted intrinsically or extrinsically and are not mutually exclusive. The intrinsic theory claims that the expression patterns of TFs are initiated stochastically and that spontaneous alterations in levels of deterministic TFs tip the balance in favor of one lineage commitment over another. Alternatively, the extrinsic theory postulates that the induction of transcriptional programs is the result of signaling from external components to the progenitor cell (Zhu and Emerson, 2002).

In order to determine the role a given TF has during hematopoiesis, researchers often disrupt the expression of the TF at various stages of development and observe the effects this has on the generation of hematopoietic cells. Employing this experimental paradigm, three TFs, PU.1, GATA-1 and C/EBPα have been identified as being essential for myelopoiesis and in the case of PU.1 and C/EBPα, the regulation HSC self-renewal.

HSCs exhibit low-level expression of PU.1 and C/EBPα and experimental evidence suggests the reciprocal actions of these TFs regulate the rate of HSC self-renewal.   Although PU.1 knockout mice die during late embryonic or early post-natal stages of development, perturbation of PU.1 expression after birth

results in significantly reduced numbers of HSCs while disruption of C/EBPα

expression induces increased HSC proliferation (Zhang et al., 2004).

Within the MPP, an increase in the expression of PU.1 is hypothesized to

be the earliest step towards lineage commitment and the level of PU.1 up-

regulation has an instructive role in restriction of the MPP towards lymphoid

versus myeloid progeny. Low-level PU.1 expression drives differentiation to the

CLP while high-level PU.1 expression along with up-regulation of GATA-1,

generates the CMP (Zhu and Emerson, 2002). Ablation of PU.1 expression in

the BM of mature mice culminates in the loss of the CLP, CMP and GMP

progenitor populations identifying PU.1 as being essential to myelopoiesis

(Iwasaki and Akashi, 2007).

At the level of the CMP, GATA-1 and PU.1 physically inhibit the

transcriptional activity of each other and the interplay between these TFs is key in

cell fate determination from the CMP. An increase in the ratio of GATA-1 to PU.1

inhibits the expression of PU.1-driven genetic programs and results in

differentiation to the MEP while an decrease in this ratio along with the up-

regulation of C/EBPα results in differentiation to the GMP (Zhu and Emerson,

2002). Disruption of C/EBPα expression in BM results in the disappearance of

granulocytes, indicating C/EBPα is essential for the generation of the GMP from

the CMP (Iwasaki and Akashi, 2007).

From the bipotent GMP, PU.1 and its binding partner ICSBP activate the

monocyte lineage program while an increase in the level of C/EBPα restricts

7

differentiation of the GMP towards granulocytic fates. Ablation of PU.1 and/or

ICSBP in GMPs prevents the complete differentiation of these cells into

monocytes (MOs; Zhu and Emerson, 2002). Notably, perturbation of C/EBPα

within the GMP does not prevent the terminal differentiation into granulocytes as

it is suspected that C/EBPβ can functionally stand-in for C/EBPα (Iwasaki and

Akashi, 2007).

It should be noted that progenitors within BM exhibit lineage promiscuity

by the low-level expression of genes associated with their downstream progeny.

For example, CMPs are observed to express low levels hemoglobin and

myeloperoxidase, which are associated with erythrocytes and

granulocytes/macrophages, respectively (Laiosa et al., 2006). Lineage priming

or low level expression of genes associated with disparate lineage fates suggests

that rather than being immediately restricted, alternative differentiation programs

are gradually repressed, enabling progenitors to rapidly respond to homeostatic

disturbances by keeping multiple genetic programs available for transcription

(Iwasaki and Akashi, 2007).

1.2.3 Monocytes

In humans, MOs represent approximately 10% of peripheral leukocytes

and have a half-life of 3 days in the circulation (Yona and Jung, 2010). Based on

the differential expression of cell surface markers, human MOs can be divided

into three discrete populations. $CD14^{++}CD16^-$ "classical" monocytes comprise up

to 95% of circulating MOs, $CD14^+CD16^{++}$ "non-classical" or "patrolling" comprise

5% of circulating MOs, and a small population of CD14^{++}CD16^{+} "intermediate"

MOs has also been described (Tacke and Randolph, 2006). Murine MOs can be

divided into two roughly equal populations based on their expression of Ly6C and

the chemokine receptors CCR2 and CX$_3$CR1. Inflammatory or "classical" MOs

express high levels of Ly6C, CCR2, and low levels of CX$_3$CR1 while "resident"

MOs lack or express low levels of Ly6C and CCR2 but express high levels of

CX$_3$CR1 (Geissmann et al., 2008). These MO subpopulations correspond to the

classical and non-classical MOs of humans, respectively. In mice, peripheral

MOs constitute approximately 4% of circulating leukocytes and have a half-life in

the circulation of approximately 24 hours (Yona and Jung, 2010).

Along with distinct expression of antigenic markers, MO subpopulations

also exhibit differential physiological activities. Inflammatory MOs are recruited to

tissues after injury or infection and are associated with the promotion of

inflammation while resident MOs are associated with patrolling the vasculature

and the resolution of inflammation (Kamei and Carman, 2010). A recent study

also identified an extramedullary population of MOs located in the splenic red

pulp of mice, which may enable the rapid mobilization of MOs into the circulation

in response to injury or infection (Swirski et al., 2009).

1.2.4 The Mononuclear Phagocyte System

The mononuclear phagocyte system (MPS) is composed of hematopoietic

progenitors, blood MOs, dendritic cells, and tissue macrophages (Hume, 2006).

During inflammation, and to a lesser degree under steady state conditions,

circulating MOs are recruited to tissue compartments where they infiltrate and differentiate into macrophages. Macrophages are key players in the innate immune response and under inflammatory conditions their functions include phagocytosis, pro-inflammatory cytokine production and antigen presentation (Davoust et al., 2008). Similar to Kupffer cells in the liver or alveolar cells in the lungs, microglia represent a specialized population of tissue macrophages that reside within the CNS.

Microglia are highly ramified, stellate-shaped cells that extend long sinuous processes into their surrounding milieu. They reside within the parenchyma of the CNS and this location can be used to distinguish microglia from other populations of CNS-associated macrophages such as perivascular macrophages located between the glia limitans and basal lamina of blood vessels, and the meningeal macrophages located in the leptomeninges that surround the brain and spinal cord. In the steady state, these cells are highly dynamic, extending and retracting their processes as they survey their surrounding microenvironment; it is estimated that the entire extracellular space of the CNS is scanned every few hours (Nimmerjahn et al., 2005).

In their quiescent state, microglia exhibit a phenotype similar to that of immature myeloid cells, as they express only low levels of CD45, major histocompatibility complex (MHC) class molecules, and are poor antigen presenting cells; this can be contrasted with other populations of tissue macrophages that exhibit a more activated phenotype (Lull and Block, 2010). Activation by neuronal injury, proinflammatory mediators or foreign pathogens

induces stereotypic morphological changes in microglia including the retraction and thickening of their processes and cell body hypertrophy (Kreutzberg, 1996). As well, the expression of several cell surface molecules including MHC proteins is up-regulated. In the literature, microglial activation has often been referred to as a "double-edged sword", as the up-regulation of disparate factors can have deleterious or supportive effects on surrounding neurons. For example, microglial activation may be associated with increased production and release of reactive oxygen species, which are toxic to surrounding cells, and/or the production of trophic factors such as glial cell-derived neurotrophic factor, which support neuronal survival.

Unlike other populations of tissue macrophages, microglia express the stem cell marker CD34 and retain the ability to proliferate. In the osteopetrosis (op) mouse, a mutant deficient for the receptor to the mitogen macrophage colony stimulating factor (M-CSF), 40% reductions in the number of microglia are observed, supporting a role for M-CSF in microglia proliferation (Kreutzberg, 1996). Although it is well accepted that tissue macrophage populations in non-neuronal tissues are maintained to a variable degree by recruitment of MOs from the circulation whether or not this is also true for microglia has been greatly debated (Lawson et al., 1992).

1.3 BM Cell Entry into the CNS

1.3.1 The BBB and Monocyte Migration into the CNS

The BBB is a specialized endothelial network characterized by the presence of tight junctions between adjacent endothelial cells enabling the strict regulation of the transmission of blood-borne elements into the CNS. Tight junctions are composed of three different integral proteins: claudins, occludins, and junctional adhesion molecules (JAMs). Claudins homophilically bind to each other between the apical surfaces of endothelial cells forming the primary seal of tight junctions. In association with claudins, the extracellular loops of occludins form the paracellular barrier, while JAMs function as cell adhesion molecules between endothelial cells. The intracellular domains of occludins bind to the cytoplasmic zonus occludins, which link the occludins to the actin filaments of the cytoskeleton, forming continuous intramembranous fibrils between endothelial cells.

The transmigration or diapedesis of circulating leukocytes into tissue interstitium occurs in a stepwise manner beginning with marginilization, a process in which flowing red blood cells push free flowing leukocytes to the margins of blood vessels where they roll along the vessel wall, increasing their contact with endothelial cells. Selectins expressed by endothelial cells and leukocytes mediate the tethering of leukocytes to activated endothelium, which brings them into closer proximity. Activated endothelial cells secrete chemokines at their luminal surface that are presented to leukocytes by proteoglycans. Binding of chemokines to their corresponding receptors on leukocytes activates intracellular

signalling cascades that result in the clustering of integrin receptors in their plasma membranes. When integrin receptors (e.g. Mac-1) bind to their respective ligands (e.g. ICAM-1) expressed by endothelial cells, firm arrest of the leukocyte results. It should be noted that experimental evidence suggests that in brain and spinal cord white matter, leukocytes do not exhibit initial rolling and tethering along endothelium but rather undergo immediate arrest (Holman et al., 2011).

Upon arrest, MOs undergo morphological changes including actin-dependent spreading and polarization, developing a leading edge and urapod (Kamei and Carman, 2010). Endothelial cells extend microvilli containing clusters of adhesion molecules around adherent monocytes, forming a transmigratory cup that guides the migration of monocytes along the luminal surface of endothelium (Kamei and Carman, 2010). It is hypothesized that monocytes preferentially extravasate at points of relatively low levels of basal lamina and do so by dramatically altering their own morphology rather than by remodelling the basal lamina (Kamei and Carman, 2010). Transmigration across the endothelium can occur either paracellularly or transcellularly. Paracellular migration involves the deconstruction of tight junctions between endothelial cells providing a route for leukocytes into the interstitium, while transcellular migration occurs through the formation of a pore through the endothelial cell. When or if one route is preferred over the other is an area of active investigation.

1.3.2 BM Cell Entry into the Healthy CNS

Investigations of BM-derived cell (BMDC) migration into the CNS often employ BM chimeric rodent models in which the host's BM is replaced by BM that expresses a label such as green fluorescent protein (GFP), enabling the discrimination of BMDCs from host cells. These models are typically created by exposing host animals to myeloablative levels of radiation to deplete BM, followed by BM reconstitution via intravenous injection of donor BM cells. The successful reconstitution of the host's BM compartment is dependent on both the level of myeloablation achieved and the number of long-term reconstituting HSCs introduced into the host's circulation (Nevozhay and Opolski, 2006).

In the brains of BM chimeric rats, elongated BMDCs were observed on the abluminal surface of blood vessels in a perivascular position, as well as within the surrounding leptomeninges (Hickey and Kimura, 1988). These cells, commonly called perivascular cells or perivascular microglia, positively immunolabeled with OX-42, an antibody identifying macrophage/microglia in rats, indicating these BMDCs were perivascular and meningeal macrophages, respectively (Hickey and Kimura, 1988). Only very rare OX-42-positive, stellate-shaped donor BMDCs were observed in the brain parenchyma, suggesting that rarely BMDCs can acquire a microglial phenotype (Hickey and Kimura, 1988).

Similarly, in the brains of murine BM chimeras, BMDCs are observed in perivascular and meningeal locations one month after transplantation and these cells labelled with the monocyte/macrophage marker F4/80 (Kennedy and Abkowitz, 1997). At one year post-transplant, 30% of F4/80-positive cells in the

14

brain were of donor origin. However, investigators only rarely observed donor

BMDCs in the brain parenchyma, suggesting that the vast majority of BM-derived

macrophages were confined to perivascular and meningeal locations, with

BMDCs making only limited contributions to the parenchymal microglial

population (Kennedy and Abkowitz, 1997). More recent investigations have

shown that 2 weeks post-irradiation and transplantation BMDCs are observed

within the leptomeninges (Chinnery et al., 2010), and at 3 months post-

transplant, roughly 40% of the leptomeningeal macrophage population was

comprised of BMDCs; by 6 months this number increased to 70% (Vallieres and

Sawchenko, 2003), suggesting that leptomeningeal macrophages, like those in

most other tissues, are slowly replaced by BM-derived cells. All BMDCs in both

the leptomeninges and the cerebral cortex express the pan-hematopoietic

marker, CD45, and the vast majority of BMDCs also express the

macrophage/microglial marker Iba-1 (Vallieres and Sawchenko, 2003).

Consistent with previous results however, only ~0.1-0.25% of BMDCs within the

cerebral cortex were observed in parenchymal regions, the remainder being

found in association with blood vessels (Massengale et al., 2005; Chinnery et al.,

2010).

Although numerous reports have claimed that BMDCs make only modest

contributions to parenchymal microglial populations, there have been occasional

reports that BMDCs constitute up to 40% of the microglial pool in the healthy

CNS (Hess et al., 2004; Simard and Rivest, 2004). Despite isolated reports of

BMDCs making substantial contributions to the parenchymal microglia population

in healthy mice, this has not been the observation of many others (Hickey and Kimura, 1988; Kennedy and Abkowitz, 1997; Vallieres and Sawchenko, 2003; Chinnery et al., 2010).

In general, BMDC entry into the CNS appears to produce at least five specific types of cell populations within the CNS; these include the parenchymal microglia, perivascular microglia, leptomeningeal macrophages, other CD45-positive CNS populations that may express lineage markers at levels too low to be detected by immunohistochemistry, as well as T cells. Currently the general consensus among most investigators is that while BMDCs make significant contributions to the maintenance of CNS macrophage populations in areas lacking BBB (i.e. perivascular and leptomeningeal areas), BMDCs make only modest contributions to the parenchymal microglial pool in healthy irradiated BM chimeras.

1.3.3 BMDC Entry into the Diseased CNS

Injuries and neurodegeneration in the CNS are both associated with microgliosis, the activation and proliferation of microglia. Numerous studies employing BM chimeric mice have demonstrated that in various models of neurodegenerative disease the number of BMDCs that populate the CNS is significantly increased in affected areas.

1.3.3.1 Parkinson's disease

Parkinson's disease is associated with the selective degeneration of dopaminergic (DA) neurons that project from the substantia nigra to the striatum.

Clinically this culminates in bradykinesia, leading to akinesia with progressive

degeneration of DA neurons and consequently loss of independence. A

commonly used murine model for PD utilizes treatment of mice with 1-methyl-4-

phenyl-1,2,3,6-tetrahydro-pyridine (MPTP), a neurotoxin affecting DA neurons

(Jackson-Lewis and Przedborski, 2007). Mice with BM chimerism treated with

MPTP have been used to study the migration of BMDCs into the brain in this PD

model. Analysis of affected brains has consistently demonstrated significantly

increased BMDC density in areas of DA innervation compared to non-DA sites

and DA areas in untreated controls (Kokovay and Cunningham, 2005; Keshet et

al., 2007; Rodriguez et al., 2007). The numbers of BMDCs observed correlated

with the severity of neurodegeneration and suggests that neuronal degeneration

enhanced either the migration or proliferation of BMDCs within affected areas

(Rodriguez et al,. 2007). Identification of BMDC phenotypes using either CD68

or CD11b, yielded dissimilar results with approximately 50% of BMDCs in MPTP

treated mice immunolabeling with CD68 (Rodriguez et al., 2007) compared to up

to 90% of BMDCs labeling with CD11b (Kokovay and Cunningham, 2005),

suggesting a disparity between the sensitivities of these antigenic markers.

1.3.3.2 Alzheimers disease

The most common neurodegenerative disease of the elderly, Alzheimer's

disease (AD), is characterized by the formation of amyloid plaques, neurofibrillary

tangles, and neuron loss within grey areas of the cerebral cortex (El Khoury and

Luster, 2008). The vast majority of AD cases have a sporadic etiology however

genetic variations and mutations in amyloid precursor protein (APP) and presenilin (PSEN) genes are involved in the familial forms of the disease. The identification of these genes associated with the development of AD has enabled the creation of transgenic mice that express one or both mutated genes and these mice typically develop a phenotype similar to AD and provide a model with which to study the disease. Studies employing BM chimeric APP23 mice (Stalder et al., 2005) and APP/PSEN1 double transgenic mice (Malm et al., 2005) have shown that the total number of BMDCs observed in cortical regions was significantly increased in AD model chimeras compared to controls. Furthermore, in the brains of the APP23 chimeras, a significant portion of BMDCs were observed in brain parenchyma with increased BMDC density in cortical areas containing greater numbers of amyloid plaques, suggesting a positive correlation between BMDC migration and/or proliferation and levels of amyloid deposition (Stalder et al., 2005). This interpretation was supported by the observation that increased numbers of BMDCs were observed in APP23/PSEN1 mice transplanted at a time point when mice were symptomatic (21 months) compared to mice that received BM transplants presymptomatically (2.5 months) that were analyzed at symptom onset (9 months; Malm et al., 2005).

1.3.3.3 Amyotrophic lateral sclerosis

Characterized by the progressive degeneration of brain and spinal cord motoneurons, amytrophic lateral sclerosis (ALS) is a fatal neurodegenerative disease of humans typically diagnosed during the fifth decade of life. Although

primarily sporadic in etiology, there is a familial form of ALS seen in 10% of ALS cases, where 20% of these familial cases are attributed to mutations in the gene encoding superoxide dismutase 1 (SOD1). Transgenic mice that over-express mutant SOD1 (mSOD) develop motoneuron pathology similar to ALS and provide a model with which to study this disease.

Several groups have employed BM chimeras to study the migration of BMDCs into the spinal cord of the mSOD mouse model (Corti et al., 2004; Solomon et al., 2006; Chiu et al., 2009; Lewis et al., 2009). Increased numbers of BMDCs were observed in the lumbar spinal cords of mSOD mice compared to control mice at both the symptomatic and end-stages of disease (Solomon et al., 2006). Furthermore, the numbers of BMDCs in the mSOD spinal cord significantly increased between the symptomatic and disease end-stages, suggesting either continuous recruitment of circulating BM cells or the proliferation of BMDCs within the spinal cord (Solomon et al., 2006). BMDCs acquired a variety of morphologies and were observed in association with blood vessels in a perivascular position, and within the spinal cord parenchyma (Figure 3.1). The majority of BMDCs were observed to express the macrophage/microglial markers F4/80, CD11b and Iba-1 however BM-derived CD3+ T-lymphocytes were also observed (Solomon et al., 2006; Lewis et al., 2009). Although it has been reported that transplantation of wild-type BM into mSOD hosts resulted in significantly increased lifespan (Corti et al., 2004), this result has not been observed by other groups (Solomon et al., 2006; Chiu et al., 2009).

1.3.4 The Transdifferentiation of BM Cells

Previous studies have claimed that BM-derived cells in the CNS acquired the phenotypes of astrocytes (Eglitis et al., 1997), cardiac myocytes (Jackson et al., 2001), hepatocytes (Lagasse et al., 2000), and neurons (Brazelton et al., 2000; Mezey et al., 2000). Based on these observations, it was postulated that BMDCs had the potential to transdifferentiate or cross lineage boundaries and acquire non-hematopoietic lineage fates. Frequently the results of these studies could not be duplicated, nor could the functionality of transdifferentiated BM cells be verified, creating skepticism as to the validity of these observations. It was suggested that tissue damage played an integral role in inducing BMDC plasticity (Abedi et al., 2004) and studies employing CNS injury models such as aspiration injury to the cerebral cortex (Hess et al., 2004), middle cerebral artery occlusion (MCAO, a stroke injury model; Vallieres and Sawchenko, 2003), and others were carried out to determine if neuronal injury provided a microenvironment necessary to induce BMDC transdifferentiation. Examinations of BMDC phenotypes in these disease models were consistent with observations in the healthy CNS, namely that the vast majority of BMDCs acquired a macrophage phenotype (Vallieres and Sawchenko, 2003). Notably, although NeuN (a neuronal marker)-positive BMDCs were observed after MCAO, closer examination of these cells using confocal microscopy indicated that the immunostaining pattern was consistent with BMDC phagocytosis of NeuN-positive cells (Hess et al., 2004).

Further investigations into the transdifferentiation potential of BMDCs demonstrated that in BM chimeric mice, fusion events between BMDCs and Purkinje neurons, cardiac myocytes and hepatocytes occur (Alvarez-Dolado et al., 2003). Rather than transdifferentiating, BMDCs form heterokaryons with host cells, resulting in cells that demonstrate immunolabeling of both donor and host epitopes (Weimann et al., 2003; Corti et al., 2004). Furthermore, a recent study demonstrated that surface antigens of donor BM cells can be transferred to endogenous cell populations *in vivo* in a process termed trogocytosis, resulting in non-hematopoietic cells within the host that express the donor BM label (Yamanaka et al., 2009). The current consensus is that *in vivo,* BMDC differentiation is restricted to hematopoietic cell fates (Rodic et al., 2004).

Interestingly, an in depth investigation into the fusogenic nature of BMDCs with Purkinje neurons demonstrated that under conditions of systemic inflammation such as during dermatitis and after induction of experimental allergic encephalitis (EAE), significantly greater numbers of fusion events occur (Johansson et al., 2008). Investigators also employed parabiosis to connect the circulations of genetically distinct mice to determine if irradiation induced the fusion of BMDCs with Purkinje neurons and further demonstrated fusion events occur in the absence of both irradiation and BMDC contributions to microglia (Johansson et al., 2008). Analysis of the gene expression pattern by the donor nuclei of heterokaryons indicated that donor nuclei were reprogrammed to express Purkinje neuron-specific genes while hematopoietic gene expression was repressed. Further investigation into the phenomena of BMDC fusion events

may elucidate an additional therapeutic role for these cells (Johansson et al., 2008).

1.3.5 Identification of BMDCs that Enter the CNS

Although experiments that employ BM chimeric models provide valuable information on the migration of BM cells into the CNS and the functional fates they acquire, the clinical validity of this approach is questionable. Reconstituting patients' BM with genetically modified stem cells is certainly undesirable and could potentially have deleterious effects systemically. Therefore, identification of specific populations of BM cells capable of differentiating into microglia in the absence of whole BM transplantation might improve the clinical potential of BM cells as treatment vehicles.

To identify specific BM cell populations capable of migrating to the CNS, Hess and colleagues (2001) fractionated donor BM into isolated single HSCs which were expanded in culture and delivered into irradiated mice. When systemic injections of 100 HSCs were given, BMDCs were subsequently observed within the CNS where cells were histologically identified as perivascular cells and microglia (Hess et al., 2001). Given that the majority of BMDCs observed within the CNS of BM chimeras exhibit macrophage phenotypes, it appears likely that these cells derive from BM MOs or their precursors. To determine which populations of circulating MOs (i.e. inflammatory Ly-6C^{hi} or resident Ly-6C^{lo}) enter the CNS, Mildner and colleagues transplanted irradiated control mice with CCR2-negative GFP-positive BM. The ablation of CCR2

expression is hypothesized to hinder inflammatory MOs from leaving the BM compartment into the circulation (Serbina et al., 2006) and 4 weeks after BM transplant, significantly reduced numbers of circulating Ly-6C^{hi} MOs were observed (Mildner et al., 2007).

Analysis of the healthy brain of CCR2-GFP+ BM chimeras demonstrated substantially reduced BM-derived microglial engraftment. Similarly, in a cuprizone-induced model of demyelination within the corpus callosum, significantly greater numbers of BMDC engraftment was observed in mice that received CCR2+GFP+ BM transplants compared to mice that received CCR2-GFP+ BM after irradiation. The results of these studies support the hypothesis that CCR2 expression is requisite for the emigration of Ly-6C^{hi} MOs from the BM compartment and that the primary source of BM-derived microglia is the Ly-6C^{hi} (inflammatory) population of MOs (Mildner et al., 2007).

1.3.6 Contention Surrounding the Use of BM Chimeric Mice

A significant caveat associated with the irradiation/BM transplantation protocol used to create BM chimeras is the widespread effects that myeloablative levels of radiation have on the host.   Studies have indicated that in the two-week period after lethal irradiation of rats, there is apoptosis of endothelial cells within the rat blood-spinal cord barrier, permitting serum albumin to enter the CNS (Li et al., 2004). Furthermore, in mice, treatment of brain with 25Gy of radiation is associated with a neuroinflammatory response that persists for 2 to 3 months after treatment (Gourmelon et al., 2005). Although the level of exposure in this

experiment is significantly greater than that necessary to achieve high levels of BM chimerism, it has been demonstrated that 16 days after exposure to 10Gy of radiation, there is increased cytokine and chemokine expression within the CNS, including increased levels of the myeloattractant and CCR2 ligand CCL2 (Mildner et al., 2007).

Experiments aimed at teasing out the effects of irradiation on BMDC migration into the CNS have employed parabiosis to connect the circulations of genetically distinct mice, resulting in 50% chimerism of peripheral blood cells (PBCs). In the absence of irradiation/BM transplantation, essentially no BMDCs are observed in both the healthy and injured/diseased murine CNS (Massengale et al., 2005; Ajami et al., 2007; Mildner et al., 2007). Although these results suggest that the effects of irradiation are requisite for the migration of PBCs into the CNS, Ajami and colleagues created parabiotic pairs of GFP+ and GFP- mice and subjected the GFP- parabiont to myeloablative doses of radiation while protecting the GFP+ mouse from radiation exposure by using a lead shield. Five weeks after irradiation, an average of 78% of PBCs were GFP+ and the irradiated mouse was subjected to facial nerve axotomy (Ajami et al., 2007). However, similar to results from non-irradiated parabionts, very few GFP+ cells were observed near the inured facial nucleus and those that were observed appeared to be intravascular (Ajami et al., 2007). The results of this study suggest that not only is radiation necessary for BMDC engraftment into the CNS but so too is the presence of circulating BM progenitors that in that absence of

whole BM transplantation, would not normally enter the blood stream (Ajami et al., 2007).

Recently, an elegant series of experiments by Ginhoux and colleagues demonstrated that myeloid progenitors produced from primitive hematopoiesis during embryonic development make significant contributions to the adult microglial pool. Investigators employed transgenic mice with tamoxifen-inducible enhance yellow fluorescent protein (eYFP) expression under the control of the Runx 1 promoter; Runx1 is a transcription factor essential for successful hematopoiesis. Pregnant females were given injections of tamoxifen at various stages of gestation inducing the irreversible expression of eYFP by Runx1+ cells and their progeny. They found that when pregnant mice were treated with tamoxifen at E7.0-E7.25, 29.6 +/- 10% of microglia were eYFP+ while only 0.19 +/- 0.26% of circulating leukocytes were eYFP+. Treatment with tamoxifen at E8.5, a point in embryonic development characterized by definitive hematopoiesis resulted in few eYFP+ microglia, indicating that progenitors derived during definitive hematopoiesis make only minimal contributions to the adult microglial pool.

Accumulating evidence suggests that unlike other populations of tissue macrophages, microglial pools are maintained primarily through self-renewal rather than through the recruitment of myeloid progenitors from the circulation. As such, the necessity of preconditioning patients by exposing them to radiation in order to enhance the migration of BMDCs into the diseased CNS may limit the

clinical potential of these cells and alternative preparative treatment regimens should be investigated.

1.3.7 Alternative Myeloablative Treatment Regimens

Chemotherapeutic agents have been used in the clinic in concert with radiation or independently to myeloablate patients with blood cancers prior to receiving BM transplants and for experimental myelosuppression. Yeager and colleagues (1993) employed the alkylating agent Busulfan (BU) to myeloablate Twitcher mice, murine models of globoid cell leukodystrophy and transplanted them with wild type BM. When nine day-old mice were given single intrperitoneal injections of BU in doses ranging from 10mg/kg to 50mg/kg, donor BM reengraftment levels of over 80% were consistently observed at doses at and above 35mg/kg (Yeager et al., 1993).   Similarly, 10 to 12 week-old mice that received single doses BU at 40mg/kg followed by the transplantion of 20 million donor BM cells also demonstrated donor BM reengraftment at levels close to 80% by 4 weeks post-transplant which were maintained over a 12 to 13 week monitoring period (Hsieh et al., 2007).

BU has a long well documented history of clinical use and studies have observed BMDCs in the CNS following myelosuppression using Bu followed by BM transplant (Yeager et al., 1993; Espejel et al., 2009). Further investigations into BMDCs migration to the CNS following Bu treatment and BM transplantation might negate the notion that the preconditioning effects of radiation are required

for BMDC migration into the CNS, thereby improving prospects for BMDCs to be used as therapeutic vehicles clinically.

1.4 Amyotrophic lateral sclerosis

ALS is a fatal neurodegenerative disease typically diagnosed during the fifth decade of life and is associated with a lifetime risk of 1 in 1000 (Boillee et al., 2006). ALS is characterized by the progressive degeneration of both upper (cerebral) and lower (spinal cord, brainstem) motoneurons, culminating in loss of motor function. Clinically this initially presents as spasticity, muscle weakness and over the course of the disease advances to muscle atrophy, speech deficits and paralysis. Although the clinical course of ALS is highly variable, progressive motoneuron loss eventually results in the denervation of respiratory muscles and respiratory failure, most often leading to death 3 to 5 years after diagnosis (Barbeito et al., 2010).

The pathological hallmarks of ALS are similar to those observed in other neurodegenerative disorders and include the formation of protein aggregates and widespread astrogliosis and microgliosis. Current treatment options aimed at slowing motoneuron loss are limited, with the glutamate uptake inhibitor Riluzole the only pharmacological agent that has been demonstrated to successfully, albeit modestly extend survival in ALS patients (Cleveland and Rothstein, 2001).

ALS is a disease primarily of sporadic etiology with a plethora of aberrant physiological processes implicated in its pathogenesis including mitochondrial dysfunction, excitotoxicity, oxidative damage, and the formation of protein

aggregates resulting in cellular dysfunction (Strong et al., 2005). However, there

is a slight genetic aspect to ALS (termed familial ALS (fALS)) that is

indistinguishable from the sporadic form of the disease, which represents

approximately 10% of cases (Boillee, et al., 2006). Within the subset of fALS,

roughly 20% of cases are attributed to mutations in the gene encoding the

ubiquitously expressed, cytosolic protein Cu,Zn superoxide dismutase (SOD1;

Barbeito et al., 2010). Located on chromosome 21, to date over 125 different

mutations in the SOD 1 gene have been reported to cause ALS, with some

mutations affecting the structure of the protein and others the enzymatic active

site (Dion et al., 2009). SOD1 is a 32 kDa homodimeric protein that functions as

a free radical scavenger by catalyzing the reduction of superoxide, a byproduct of

cellular respiration to hydrogen peroxide. However, the pathogenicity of mSOD

does not appear to be related to its normal function and currently remains a

subject of intense investigation.

1.4.1 The mSOD Mouse Model of ALS

The development of transgenic mice and rats that over-express mSOD

has provided investigators with animal models that develop a motoneuron

pathology similar to that of ALS. In mSOD1 transgenic mice, progressive motor

neuron degeneration in the cervical and lumbar spinal cord manifests as muscle

atrophy and eventual hind-limb paralysis (Hall et al., 1998). The rate of disease

progression and time to end stage, defined as complete hind limb paralysis and

inability of the animal to right itself from a recumbent position, is dependent on

the specific type mutation in the SOD1 transgene and the level of over-expression (Bruijn et al., 2004).

Several transgenic mouse lines have been generated that over-express SOD1 mutations. The most common and well described transgenic mouse model used by investigators is the TgN(SOD1-G93A)G1H mouse (Hall et al., 1998). The G93A transgenic mouse over-expresses a human SOD1 mutation in which the amino acid glycine is substituted for alanine at residue 93 of the protein. At 120 days, mice have nearly complete hind-limb paralysis, the result of the degeneration of roughly 50% of cervical and lumbar motoneurons; thoracic motoneurons are largely spared (Hall et al., 1998).

Although created over 15 years ago by Gurney and colleagues (1994), how mSOD expression in mice (and humans) culminates in neurodegeneration has still not been elucidated. What is known is that pathogenic nature of mSOD is not due to a loss of function as the majority of mSOD variants retain at least partial normal enzyme activity. Furthermore, when the murine SOD1 orthologous gene is knocked-out, motoneuron dysfunction and degeneration are not observed and survival is not affected (Reaume et al., 2006). As such, it is now accepted that mSOD causes motoneuron degeneration through a toxic gain-of-function mechanism, although the nature of this mechanism has yet to be elucidated. After years of investigation, various pathological roles for mSOD have been suggested, including an increased propensity for misfolded mSOD to form intracellular aggregates, aberrant enzyme activity, disruption of axonal transport,

ER stress, mitochondrial dysfunction and glial dysfunction contributing to motoneuron death (Ilieva et al., 2009).

Evidence in support of non-cell-autonomous neuronal death in the mSOD model, which exhibits widespread astrocytosis and microgliosis that increases with disease progression, is very compelling. Although it has been demonstrated that mSOD expression in neurons alone is sufficient to cause motoneuron degeneration (Jaarsma et al., 2008), there is considerable evidence supporting a role for mSOD-expressing in exacerbating neuronal dysfunction and driving disease progression. When mSOD mice were crossed with PU.1-/- mice (a strain that does not develop macrophages or microglia) and transplanted with wild-type BM, resulting in a wild-type microglial pool, survival times in the mSOD mice were significantly extended (Beers et al., 2006). Similarly, the establishment of wild-type astrocyte populations within the spinal cords of mSOD mice via the transplantation of wild-type astrocyte-restricted precursors into the cervical spinal cord similarly resulted in prolonged survival (Lepore et al., 2008). Together the results of these and other studies paint a complex, multifaceted portrait of the pathological nature of mSOD that after over 15 years of investigation is still poorly understood.

1.5 Research Goals

The limited efficacy of pharmacologics as treatments for numerous neurodegenerative disorders has necessitated the research into alternative, novel treatment modalities. It is well established that under certain conditions,

BMDCs are capable of transmigrating into the CNS and typically acquire the

phenotypes of CNS-associated macrophages and microglia.   The ability of these

cells to circumvent the BBB, something the majority of pharmacologics cannot

do, underscores the potential of these cells to function as treatment vehicles to

deliver neurosupportive substances into the diseased CNS.   The goals of the

ensuing body of work are as follows: (1) to demonstrate that BMDCs enter the

spinal cord of the mSOD mouse model of ALS, (2) to investigate the phenotype

that BMDCs acquire once they have transmigrated into the CNS, (3) to begin to

determine which populations of cells within whole BM are capable of this

transmigration, (4) to investigate whether or not BMDCs are capable of migrating

into the CNS in the absence of irradiation by investigating alternative

myeloablative regimens.

1.6 Figures

Figure 1. 1 Hematopoietic hierarchy within BM.

Within the bone marrow compartment, HSCs are pluripotent progenitors giving rise to all myeloid and lymphoid cell types. The first step in lineage commitment is either the myeloid precursor (MP) or the lymphoid precursor (LP).   Cell differentiation within BM moves through downstream precursor populations of increasing lineage restriction eventually arriving at unipotent precursor cells (reproduced from Geissmann et al. 2010 with permission from AAAS).
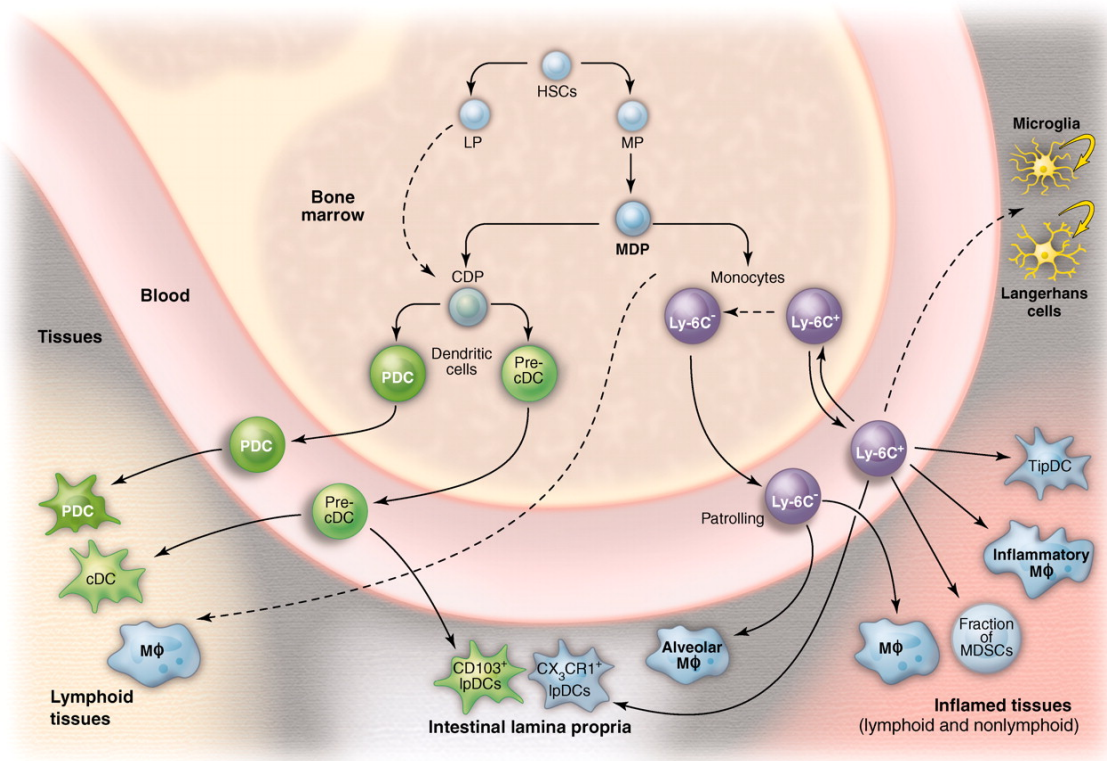
1.7 Tables

Table 1.1: Antigenic identification of HSC and progenitor cells

Flow cytometry enables the identification of progenitor populations within BM based on the combined expression/lack of expression of multiple antigenic markers (Iwasaki and Akashi 2007).

Progenitor	Antigenic Expression
long-term HSC	c-Kit$^+$Thy1.1^{lo}Lin$^{-/lo}$Sca-1$^+$CD34$^{-/lo}$
short-term HSC / MPP	c-Kit$^+$Thy1.1$^-$Lin$^{-/lo}$Sca-1$^+$CD34$^+$
common myeloid progenitor	IL-7R$^-$c-Kit$^+$Lin$^{-/lo}$Sca-1$^-$FcγRII/III^{lo}CD34$^+$
common lymphoid progenitor	IL-7R$^+$c-Kit^{lo}Lin$^{-/lo}$Sca-1^{lo}
megakaryocyte/erythrocyte progenitor	Lin$^{-/lo}$FcγRII/III^{lo}CD34$^-$
granulocyte-macrophage progenitor	Lin$^{-/lo}$FcγRII/III^{hi}CD34$^+$
monocyte-dendritic cell precursor	Lin$^{-/lo}$FcγRII/III^{hi}CD34$^+$CX3CR1$^+$

1.8 References

Abedi M, Greer DA, Colvin GA, Demers DA, Dooner MS, Harpel JA, Pimentel J, Menon MK, Quesenberry PJ (2004) Tissue injury in marrow transdifferentiation. *Blood Cells, Molecules and Diseases,* 32(1): 42-46.

Ajami B, Bennett JL, Krieger C, Tetzlaff W, Rossi FM (2007) Local self-renewal can sustain CNS microglia maintenance and function throughout adult life. *Nature Neuroscience,* 10(12): 1538-1543.

Alvarez-Dolado M, Pardal R, Garcia-Verdugo JM, Fike JR, Lee HO, Pfeffer K, et al. (2003) Fusion of bone-marrow-derived cells with purkinje neurons, cardiomyocytes and hepatocytes. *Nature, 425*(6961): 968-973. doi:10.1038/nature02069

Appel SH, Engelhardt JI, Henkel JS, Siklos L, Beers DR, Yen AA, et al. (2008) Hematopoietic stem cell transplantation in patients with sporadic amyotrophic lateral sclerosis. *Neurology, 71*(17): 1326-1334. doi:10.1212/01.wnl.0000327668.43541.22

Balazs AB, Fabian AJ, Esmon CT, Mulligan RC. (2006) Endothelial protein C receptor (CD201) explicitly identifies hematopoietic stem cells in murine bone marrow. Blood, 107(6): 2317-21.

Barbeito AG, Mesci P Boillee S (2010) Motor neuron-immune interactions: The vicious circle of ALS. Journal of Neural Transmission (Vienna, Austria : 1996), 117(8), 981-1000.

Becker AJ, McCulloch EA, Till JE (1963) Cytological demonstration of the clonal nature of spleen colonies derived from transplanted mouse marrow cells. Nature, 197, 452-454.

Beers DR, Henkel JS, Xiao Q, Zhao W, Wang J, Yen AA, Siklos L, McKercher SR, Appel SH. 2006. Wild type microglia extend survival in PU.1 knockout mice with familial amyotrophic lateral sclerosis. Proc Natl Acad Sci U S A. 103: 16021-16026.

Boillee S, Vande Velde C, & Cleveland DW (2006) ALS: A disease of motor neurons and their nonneuronal neighbors. Neuron, 52(1), 39-59.

Brazelton TR, Rossi FM, Keshet GI, & Blau HM (2000) From marrow to brain: Expression of neuronal phenotypes in adult mice. Science (New York, N.Y.), 290(5497): 1775-1779.

Bruijn LI, Miller TM, Cleveland DW (2004) Unraveling the mechanisms involved in motor neuron degeneration in ALS. Annual Review of Neuroscience, 27, 723-749.

Chinnery HR, Ruitenberg MJ, & McMenamin PG (2010) Novel characterization of monocyte-derived cell populations in the meninges and choroid plexus and their rates of replenishment in bone marrow chimeric mice. Journal of Neuropathology and Experimental Neurology, 69(9): 896-909.

Chiu IM, Phatnani H, Kuligowski M, Tapia JC, Carrasco MA, Zhang M, et al. (2009) Activation of innate and humoral immunity in the peripheral nervous system of ALS transgenic mice. Proceedings of the National Academy of Sciences of the United States of America, 106(49): 20960-20965.

Cleveland, D.W., Rothstein J.D. (2001) From Charcot to Lou Gehrig: deciphering selective motor neuron death in ALS. *Nature Reviews Neuroscience,* 2(11):806-19.

Corti S, Locatelli F, Donadoni C, Guglieri M, Papadimitriou D, Strazzer S, et al. (2004) Wild-type bone marrow cells ameliorate the phenotype of SOD1-G93A ALS mice and contribute to CNS, heart and skeletal muscle tissues. Brain : A Journal of Neurology, 127(Pt 11): 2518-2532.

Davoust N, Vuaillat C, Androdias G, & Nataf S (2008) From bone marrow to microglia: Barriers and avenues. Trends in Immunology, 29(5): 227-234.

Dion PA, Daoud H, Rouleau, GA (2009) Genetics of motor neuron disorders: New insights into pathogenic mechanisms. Nature Reviews.Genetics, 10(11), 769-782.

Eglitis MA, Mezey E (1997) Hematopoietic cells differentiate into both microglia and macroglia in the brains of adult mice. Proceedings of the National Academy of Sciences of the United States of America, 94(8): 4080-4085.

El Khoury J, Luster AD (2008) Mechanisms of microglia accumulation in alzheimer's disease: Therapeutic implications. Trends in Pharmacological Sciences, 29(12): 626-632. doi:10.1016/j.tips.2008.08.004

Espejel, S., Romero, R., & Alvarez-Buylla, A. (2009). Radiation damage increases purkinje neuron heterokaryons in neonatal cerebellum. *Annals of Neurology, 66*(1), 100-109.

Fogg DK, Sibon C, Miled C, Jung S, Aucouturier P, Littman, DR, et al. (2006) A clonogenic bone marrow progenitor specific for macrophages and dendritic cells. Science (New York, N.Y.), 311(5757), 83-87.

Geissmann F, Auffray C, Palframan R, Wirrig C, Ciocca A, Campisi L, et al. (2008) Blood monocytes: Distinct subsets, how they relate to dendritic cells, and their possible roles in the regulation of T-cell responses. Immunology and Cell Biology, 86(5): 398-408.

Geissmann F, Manz MG, Jung S, Sieweke MH, Merad M, Ley K (2010) Development of monocytes, macrophages, and dendritic cells. Science 327: 656-61.

Gourmelon P, Marquette C, Agay D, Mathieu J, Clarencon D (2005) Involvement of the central nervous system in radiation-induced multi-organ dysfunction and/or failure. British Journal of Radiography Supplements, 27: 62-68.

Gurney ME, Pu H, Chiu AY, Dal Canto MC, Polchow, CY, Alexander DD, et al. (1994) Motor neuron degeneration in mice that express a human cu,zn superoxide dismutase mutation. Science (New York, N.Y.), 264(5166), 1772-1775.

Hall ED, Oostveen JA, Gurney ME (1998) Relationship of microglial and astrocytic activation to disease onset and progression in a transgenic model of familial ALS. Glia, 23(3), 249-256.

Hess DC, Abe T, Hill WD, Studdard AM, Carothers J, Masuya M, et al. (2004) Hematopoietic origin of microglial and perivascular cells in brain. Experimental Neurology, 186(2): 134-144.

Hexner EO, Emerson SG (2008) Stem Cell Biology. In JE Karp (Ed) Hematopoietic Stem Cell Transplantation (pp. 3-18). New Jersey: Humana Press.

Hickey WF, Kimura H (1988) Perivascular microglial cells of the CNS are bone marrow-derived and present antigen in vivo. Science (New York, N.Y.), 239(4837): 290-292.

Holman DW, Klein RS, Ransohoff RM (2011) The blood-brain barrier, chemokines and multiple sclerosis. Biochim Biophys Acta, 1812(2):220-30.

Hsieh MM, Langemeijer S, Wynter A, Phang OA, Kang EM, Tisdale JF (2007) Low-dose parenteral busulfan provides an extended window for the infusion of hematopoietic stem cells in murine hosts. *Experimental Hematology, 35*(9), 1415-1420.

Hume DA (2006) The mononuclear phagocyte system. Current Opinion in Immunology, 18(1): 49-53.

Ilieva H, Polymenidou M, Cleveland DW (2009) Non-cell autonomous toxicity in neurodegenerative disorders: ALS and beyond. The Journal of Cell Biology, 187(6), 761-772.

Iwasaki H, Akashi K (2007) Myeloid lineage commitment from the hematopoietic stem cell. Immunity 26(6): 726-40.

Jaarsma D, Teuling E, Haasdijk ED, De Zeeuw CI, Hoogenraad CC (2008) Neuron-specific expression of mutant superoxide dismutase is sufficient to induce amyotrophic lateral sclerosis in transgenic mice. The Journal of Neuroscience : The Official Journal of the Society for Neuroscience, 28(9), 2075-2088.

Jackson KA, Majka SM, Wang H, Pocius J, Hartley CJ, Majesky MW, et al. (2001) Regeneration of ischemic cardiac muscle and vascular endothelium by adult stem cells. The Journal of Clinical Investigation, 107(11): 1395-1402.

Jackson-Lewis V & Przedborski S (2007) Protocol for the MPTP mouse model of parkinson's disease. Nature Protocols, 2(1): 141-151.

Johansson CB, Youssef S, Koleckar K, Holbrook C, Doyonnas R, Corbel SY, Steinman L, Rossi FM, Blau HM (2008) Extensive fusion of haematopoietic cells with Purkinje neurons in response to chronic inflammation. Nature Cell Biology 10(5): 575-83.

Kamei M & Carman CV (2010) New observations on the trafficking and diapedesis of monocytes. Current Opinion in Hematology, 17(1): 43-52.

Kennedy DW & Abkowitz JL (1997) Kinetics of central nervous system microglial and macrophage engraftment: Analysis using a transgenic bone marrow transplantation model. Blood, 90(3): 986-993.

Keshet GI, Tolwani RJ, Trejo A, Kraft P, Doyonnas R, Clayberger C, et al. (2007) Increased host neuronal survival and motor function in BMT parkinsonian mice: Involvement of immunosuppression. The Journal of Comparative Neurology, 504(6): 690-701.

Kiel MJ, Yilmaz OH, Iwashita T, Yilmaz OH, Terhorst C, Morrison SJ (2005) SLAM family receptors distinguish hematopoietic stem and progenitor cells and reveal endothelial niches for stem cells. Cell, 121: 1109-1121.

Kokovay E & Cunningham LA (2005) Bone marrow-derived microglia contribute to the neuroinflammatory response and express iNOS in the MPTP mouse model of parkinson's disease. Neurobiology of Disease, 19(3): 471-478.

Kreutzberg G. 1996. Microglia: a sensor for pathological events in the CNS. Trends Neurosci 19: 312-318.

Lagasse E, Connors H, Al-Dhalimy M, Reitsma M, Dohse M, Osborne L, et al. (2000) Purified hematopoietic stem cells can differentiate into hepatocytes in vivo. Nature Medicine, 6(11): 1229-1234.

Laiosa CV, Stadtfeld M, Graf T (2006) Determinants of lymphoid-myeloid lineage diversification. Immunity, 24:705-38.

Lawson LJ, Perry VH & Gordon S (1992) Turnover of resident microglia in the normal adult mouse brain. Neuroscience, 48(2): 405-415.

Lepore AC, Dejea C, Carmen J, Rauck B, Kerr DA, Sofroniew MV, et al. (2008) Selective ablation of proliferating astrocytes does not affect disease outcome in either acute or chronic models of motor neuron degeneration. Experimental Neurology, 211(2), 423-432.

Lewis CA, Solomon JN, Rossi FM, Krieger C (2009) Bone marrow-derived cells in the central nervous system of a mouse model of amyotrophic lateral sclerosis are associated with blood vessels and express CX(3)CR1. Glia, 57(13): 1410-1419.

Li YQ, Chen P, Jain V, Reilly RM, Wong CS (2004) Early radiation-induced endothelial cell loss and blood-spinal cord barrier breakdown in the rat spinal cord. Radiation Research, 161(2): 143-52.

Lull ME, Block ML (2010) Microglial activation and chronic neurodegeneration. Neurotherapeutics, 7(4):354-65.

Lymperi S, Ferraro F, Scadden DT (2010) The HSC niche concept has turned 31. Has our knowledge matured? Ann N Y Acad Sci., 1192:12-8.

Malm T, Koistinaho M, Muona A, Magga J, Koistinaho J (2010) The role and therapeutic potential of monocytic cells in alzheimer's disease. Glia, 58(8): 889-900.

Massengale M, Wagers AJ, Vogel H, Weissman IL (2005) Hematopoietic cells maintain hematopoietic fates upon entering the brain. The Journal of Experimental Medicine, 201(10): 1579-1589.

McCulloch EA, Till JE (2005) Perspectives on the properties of stem cells. Nature Medicine, 11(10), 1026-1028.

Mezey E, Chandross KJ, Harta G, Maki RA, McKercher SR (2000) Turning blood into brain: Cells bearing neuronal antigens generated in vivo from bone marrow. Science (New York, N.Y.), 290(5497): 1779-1782.

Mildner A, Schmidt H, Nitsche M, Merkler D, Hanisch UK, Mack M, et al. (2007) Microglia in the adult brain arise from ly-6ChiCCR2+ monocytes only under defined host conditions. *Nature Neuroscience, 10*(12): 1544-1553.

Nevozhay D, Opolski A (2006) Key factors in experimental mouse hematopoietic stem cell transplantation. *Archivum Immunologiae Et Therapiae Experimentalis, 54*(4): 253-269.

Nimmerjahn A, Kirchhoff F, Helmchen F (2005) Resting microglial cells are highly dynamic surveillants of brain parenchyma in vivo. *Science,* 308(5726):1314-8.

Reaume AG, Elliot JL, Hoffman EK, Kowall NW, Ferrante RJ, Siwek DF, et al. (1996) Motor neurons in Cu/Zn superoxide dismutase-deficient mice develop normally but exhibit enhanced cell death after axonal injury. Nature Genetics, 13(1), 43-47.

Rodić N, Rutenberg MS, Terada N (2004) Cell fusion and reprogramming: resolving our transdifferences. *Trends in Molecular Medicine,* 10(3): 93-96.

Rodriguez M, Alvarez-Erviti L, Blesa FJ, Rodríguez-Oroz MC, Arina A, Melero I, Ramos LI, Obeso JA (2007) Bone-marrow-derived cell differentiation into microglia: a study in a progressive mouse model of Parkinson's disease. *Neurobiology of Disease,* 28(3): 316-325.

Seita J, Weissman IL (2010) Hematopoietic stem cell: Self-renewal versus differentiation. *Wiley Interdisciplinary Reviews.Systems Biology and Medicine, 2*(6): 640-653.

Serbina NV, Pamer EG (2006) Monocyte emigration from bone marrow during bacterial infection requires signals mediated by chemokine receptor CCR2. *Nature Immunology, 7*(3): 311-317. doi:10.1038/ni1309

Siminovitch L, McCulloch EA, Till JE (1963) The distribution of colony-forming cells among spleen colonies. Journal of Cellular Physiology, 62, 327-336.

Solomon JN, Lewis CA, Ajami B, Corbel SY, Rossi FM, Krieger C (2006) Origin and distribution of bone marrow-derived cells in the central nervous system in a mouse model of amyotrophic lateral sclerosis. *Glia, 53*(7): 744-753.

Simard AR, Rivest S (2004) Bone marrow stem cells have the ability to populate the entire central nervous system into fully differentiated parenchymal microglia. *FASEB Journal.* 18(9): 998-1000.

Stalder AK, Ermini F, Bondolfi L, Krenger W, Burbach GJ, Deller T, et al. (2005) Invasion of hematopoietic cells into the brain of amyloid precursor protein transgenic mice. *The Journal of Neuroscience : The Official Journal of the Society for Neuroscience, 25*(48): 11125-11132.

Strong MJ, Kesavapany S, Pant HC (2005).The pathobiology of amyotrophic lateral sclerosis: A proteinopathy? Journal of Neuropathology and Experimental Neurology, 64(8), 649-664.

Swirski FK, Nahrendorf M, Etzrodt M, Wildgruber M, Cortez-Retamozo V, Panizzi P, et al. (2009) Identification of splenic reservoir monocytes and their deployment to inflammatory sites. *Science (New York, N.Y.), 325*(5940): 612-616.

Tacke F, Randolph GJ (2006) Migratory fate and differentiation of blood monocyte subsets. *Immunobiology, 211*(6-8): 609-618.

Unger ER, Sung JH, Manivel JC, Chenggis ML, Blazar BR, Krivit W (1993) Male donor-derived cells in the brains of female sex-mismatched bone marrow transplant recipients: A Y-chromosome specific in situ hybridization study. *Journal of Neuropathology and Experimental Neurology, 52*(5): 460-470.

Vallieres L, Sawchenko PE (2003) Bone marrow-derived cells that populate the adult mouse brain preserve their hematopoietic identity. *The Journal of Neuroscience: The Official Journal of the Society for Neuroscience, 23*(12): 5197-5207.

Weimann JM, Johansson CB, Trejo A, Blau HM (2003) Stable reprogrammed heterokaryons form spontaneously in Purkinje neurons after bone marrow transplant. *Nature Cell Biology, 5*(11): 959-966.

Yamanaka N, Wong CJ, Gertsenstein M, Casper RF, Nagy A, Rogers IM (2009) Bone marrow transplantation results in human donor blood cells acquiring and displaying mouse recipient class I MHC and CD45 antigens on their surface. *PloS One, 4*(12): e8489.

Yeager AM, Shinn C, Shinohara M, Pardoll DM (1993) Hematopoietic stem cell transplantation in the twticher mouse. The effects of pretransplant conditioning with graded doses of busulfan. *Transplantation,* 56(1):185-90.

Yona S & Jung S (2010) Monocytes: Subsets, origins, fates and functions. *Current Opinion in Hematology, 17*(1): 53-59.

Zhang P, Iwasaki-Arai J, Iwasaki H, Fenyus ML, Dayaram T, Owens BM, Shigenmatsu H, Levantini E, Huettner CS, Lekstrom-Himes JA, Akashi K, Tenen DG (2004) Enhancement of hematopoietic stem cell repopulating capacity and self-renewal in the absence of the transcription factor C/EBP alpha. *Immunity,* 21(6):853-63).

Zhu J & Emerson SG (2002) Hematopoietic cytokines, transcription factors and lineage commitment. *Oncogene, 21*(21): 3295-3313.

2: ORIGIN AND DISTRIBUTION OF BONE MARROW-DERIVED CELLS IN THE CENTRAL NERVOUS SYSTEM OF A MOUSE MODEL OF AMYOTROPHIC LATERAL SCLEROSIS

2.1 Abstract

Amyotrophic lateral sclerosis (ALS) is associated with increased numbers of microglia within the central nervous system (CNS). However, it is unknown whether the microgliosis results from proliferation of CNS resident microglia, or recruitment of bone marrow (BM)-derived microglial precursors. Here we assess the distribution and number of BM-derived cells in spinal cord using transplantation of green fluorescent protein (GFP)-labeled BM cells into myelo-ablated mice over-expressing human mutant superoxide dismutase 1 (mSOD), a murine model of ALS. Transplantation of GFP+ BM did not affect the rate of disease progression in mSOD mice. Mean numbers of microglia and GFP+ cells in spinal cords of control mice were not significantly different from those in asymptomatic mSOD mice and showed no change with animal age. The number of GFP+ cells and microglia (F4/80+ and CD11b+ cells) within the spinal cord of mSOD mice increased compared to age-matched controls at a time when mSOD mice exhibited disease symptoms, continuing up to disease end-stage. Although we observed an increase in the number of GFP+ cells in spinal cords of mSOD mice with disease symptoms, mean numbers of GFP+ F4/80+ cells comprised less than 20% of all F4/80+ cells and did not increase with disease progression.

Furthermore, the relative rates of proliferation in CD45+GFP- and CD45+GFP+ cells were comparable. Thus, we demonstrate that the microgliosis present in spinal cord tissue of mSOD mice is primarily due to an expansion of resident microglia and not to the recruitment of microglial precursors from the circulation.

2.2 Introduction

Amyotrophic lateral sclerosis (ALS) is a neurodegenerative disease characterized by the loss of neurons and motor neurons in the spinal cord, brain, and descending motor tracts. Approximately 10% of all ALS cases are dominantly inherited, and about 20% of these cases are associated with mutations in the Cu/Zn superoxide dismutase (SOD1) gene (Rosen et al., 1993). Mice over-expressing human mutant SOD1 (mSOD) transgenes develop a disorder closely resembling human ALS (Gurney et al.,1994; Hamson et al., 2002). The murine transgenic line G93A over-expresses human mSOD transgenes and develops rapidly progressive paralysis in one or more limbs at approximately 13 weeks of age due to loss of motor neurons with death occurring shortly thereafter (Gurney et al., 1994; Hall et al., 1998).

Although mSOD over-expression contributes to ALS, previous studies have shown that restricted over-expression of mSOD in neurons (Lino et al., 2002; Pramatarova et al., 2001) alone is not sufficient for the development of disease in mice. Clement and colleagues (2003) demonstrated that wild-type (wt) neurons in mSOD chimeric mice develop aspects of ALS pathology, whereas non-neuronal cells that do not express mSOD delay degeneration and extend

survival of mSOD-expressing motor neurons. These studies suggest that non-neuronal cells are involved in the pathogenesis of ALS. Other studies have demonstrated that there are elevated numbers of microglia within the spinal cord and brain of mouse models of neurodegenerative disease (Boillee et al., 2001; Hall et al., 1998; Hess et al., 2002). Microglia are part of the parenchymal, non-neuronal cell population within the central nervous system (CNS) and are involved in phagocytosis and the inflammatory response (Kreutzberg, 1996; Streit et al., 1999). Turnover of microglia in normal adult CNS is slow and is thought to occur by proliferation of CNS-resident microglia and the migration of microglial progenitors (monocytes) into the CNS through the blood-brain barrier (BBB) from the bloodstream (Lawson et al., 1992; Eglitis and Mezey, 1997). It has been proposed that engraftment of BM-derived microglia into the CNS is enhanced by a wide range of pathologies (Hess et al., 2004; Kreutzberg, 1996; Priller et al., 2001). These notions have led to the assumption that the microgliosis observed in a number of diseases leading to neuronal loss is at least in part due to increased recruitment of circulating progenitors across the BBB. However, the relative contributions from expansion of pre-existing tissue-resident cells and generation of new microglia from circulating progenitors have not been evaluated.

Here, we generated chimeric G93A mice by transplanting lethally irradiated recipients with bone marrow (BM) cells derived from transgenic mice that ubiquitously express green fluorescent protein (GFP), and we characterised the temporal and spatial kinetics of BM-derived cellular infiltration in the CNS of

this mouse model of ALS. Our results strongly suggest that the microgliosis observed in ALS is not a consequence of increased migration of BM-derived precursors into the CNS, but rather a result of the proliferation of pre-existing, resident microglia.

2.3 Materials and Methods

2.3.1 Animals

Two lines of mice over-expressing the G93A mutant human transgene for CuZn superoxide dismutase (SOD1) were used in this study, B6SJL- TgN(SOD1-G93A)1Gur (B6SJL) and B6.Cg-Tg (SOD1-G93A)1Gur/J (B6). Both G93A strains over-express mutant SOD1 (mSOD) by approx. 25-fold compared to non-transgenic wild-type (wt) littermates (Gurney et al., 1994). In both strains, mice that over-express mSOD manifest symptoms of motor neuron degeneration primarily in their hind limbs, resulting in weakness and eventual paralysis. The mice were obtained from Jackson Laboratories (Bar Harbor, ME), or locally bred from progenitor stock. The mice were maintained as hemizygotes by backcrossing mSOD transgenic males with wt females.

Genotype identification of mSOD mice was confirmed using a PCR assay of genomic DNA extracted from ear tissue based on a previously published protocol (Gurney et al., 1994; Hu et al., 2003). Control mice consisted of age-matched wt littermates that were phenotypically normal as well as PCR negative for human SOD1 and were sacrificed at the same age as mSOD littermates.

Mice that express enhanced green fluorescent protein (GFP; C57BL/6 GFP/CD45.1) were obtained from Dr. I. Weissman and were bred and maintained in a pathogen-free environment within the Biomedical Research Centre, University of British Columbia. The C57BL/6 GFP/CD45.1 mice express GFP ubiquitously under the control of the cytomegalovirus enhancer-chicken b-actin hybrid promoter (Wright et al., 2001).

All animals were supplied with food and water ad libitum. Protocols governing the use of animals were approved by review committees of Simon Fraser University and the University of British Columbia and were in compliance with guidelines published by the Canadian Council on Animal Care and are in accordance with the international guidelines including the NIH Guide for the Care and Use of Laboratory Animals, as well as the EEC Council Directive. Institutional approvals are available upon request.

2.3.2 Generation of bone marrow-chimeric mice

GFP+ transgenic mice were used as BM donors, as previously described (Corbel et al., 2003). Both mSOD transgenic mouse lines were used as BM recipients. Prior to transplantation, 6 week old mSOD (n = 23) and age-matched wt littermate mice (n = 23) were lethally irradiated (950-1100 rads), and 5 x 106 cells were injected into the tail vein of each animal. Controls consisted of age-matched non-transplanted mSOD (n = 8) and wt (n = 8) mice. An equal number of males and females, and equal numbers of mice from each transgenic line were used in this study.

The presence of GFP+ donor-derived leukocytes in the peripheral circulation of transplant recipients was analysed three weeks post transplant by fluorescence-activated cell sorting (FACS) on a a FACScan (Becton Dickinson; Franklin Lakes, NJ). Those mice with greater than 80% (a commonly accepted value) of GFP+ peripheral blood leukocytes were used for the experiments.

2.3.3 Motor Assessment

Mice were visually inspected daily for signs of disease. The rotarod test was used to evaluate motor function in both transplanted and non-transplanted mSOD and wt mice twice-weekly beginning at 8 weeks of age as previously described (Wilson et al., 2002). Mice were placed in the center of the rod and the latency to fall off the rotating rod was recorded. A value of 120 seconds was recorded for mice that remained on for the assigned maximum duration of rotation.

2.3.4 Tissue Processing

Animals were euthanized using blended CO_2 and O_2 at three time points: 11 weeks, 15 weeks, and at disease end-stage (approximately 18-21 weeks), being defined as the time when mice were unable to right themselves within 10 seconds, having been placed on their sides. mSOD mice were asymptomatic, or exhibited moderate or severe symptoms at the three respective time points. All mice were perfused transcardially with PBS (pH 7.4) followed by 4% paraformaldehyde (PFA; pH 7.4, w/v). Spinal cords were dissected out and stored in 4% PFA at 4oC for 48 hours, and then transferred to 20% sucrose (w/v

in PBS) at 4oC for 24 hours for cryoprotection. Tissue was suspended in M1

Embedding Matrix (Thermo Electron Corporation, Waltham, MA), sliced at a

thickness of 30 µm in a transverse plane using a microtome, mounted on gelled

slides and cover slipped with Vectashield mounting medium (Vector Laboratories,

Inc., Burlingame, CA), or suspended in an ethylene glycol-based cryoprotectant

solution (Watson et al., 1986) and stored at -20°C.

2.3.5 Immunohistochemistry

Free-floating spinal cord sections were permeabilized with 0.3% Triton X-

100 (v/v) in PBS at room temperature (RT), and blocked in 0.3% Triton, 3%

bovine serum albumin (BSA; w/v), and 25% normal goat serum (NGS; v/v) at RT

for 1 hour. For sections incubated with murine antibody, the blocking buffer also

contained anti-mouse IgG Fab fragments (1:500; Jackson ImmunoResearch

Labs, Inc., West Grove, PA). Sections were incubated in staining buffer

composed of 0.3% Triton, 3% BSA, and 10% NGS with primary antibody at 4°C

for 24 hours. Primary antibodies included: anti-F4/80 (1:1000; Serotec, Raleigh,

NC), anti-CD11b (Mac-1; 1:500; Serotec), anti-NeuN (1:500; Chemicon,

Temecula, CA), anti-GFAP (1:200; Calbiochem, San Diego, CA), anti-CD3e

(1:10; BD Pharmingen, San Diego, CA), anti-Ly-6G (Gr-1; 1:10; BD Pharmingen),

anti-CD45 PE (1:200; eBiosciences, San Diego, CA), anti-CD117 (c-Kit; 1:200;

eBiosciences), and anti-CD31 (PECAM-1; 1:1000; BD Pharmingen). Sections

were washed and incubated at RT for 2 hours in staining buffer with either Cy3-

congugated anti-IgG (1:500; Jackson ImmunoResearch Labs, Inc.), or

Alexafluor568-conjugated anti-IgG (1:1000; Molecular Probes, Carlsbad, CA). In each set of experiments, negative controls lacking primary or secondary antibodies were included.

2.3.6 Analysis

Spinal cord sections were visualized using a Zeiss Axioplan 2 microscope equipped for epifluorescence (Carl Zeiss, Inc., Thornwood, NY). Images were captured using a charge-coupled device (CCD; Qimaging, Burnaby, BC, Canada), and analysed using OpenLab 2000 software (Improvision Inc., Lexington, MA). Labeled sections were examined with a Zeiss LSM 5 Pascal Laser Scanning Confocal Microscope.

At a final magnification of 10 X, we examined every fifth spinal cord section in defined rostral and caudal regions. Rostral sections comprised upper to mid-thoracic levels (T2-T10), and caudal sections comprised mid- to lower lumbar levels (L2-L6). GFP+ cells were manually counted and the mean number of cells in each region was calculated. All evaluations were blinded. For each animal, 62 ± 2 sections were analysed for GFP+ cells visible in the focal plane and within the spinal cord parenchyma. For each animal an additional five lumbar sections were evaluated at 40 X magnification in order to positively identify GFP+ cells as microglia within either the left or right ventral quadrant of the spinal cord. At the level of L5, two cross-sectional areas per animal were evaluated, and the mean area was calculated.

SPSS and JMP software were used for statistical analysis. Rotarod tasks, spinal cord cross-sectional areas, and quantitative assessments of GFP+ cells or F4/80+ cells within the spinal cord were statistically evaluated using the Students-t test or ANOVA followed by Tukey's post hoc analysis where applicable. Statistical significance was determined at a = 0.05.

2.3.7 Bromodeoxyuridine Labelling

Beginning at 115 days of age, B6SJL mSOD mice (n = 3) received intraperitoneal injections with bromodeoxyuridine (BrdU) solution (10mg/ml; BD Pharmingen), once daily for five consecutive days. On the fifth day, mice were terminally anesthetized, perfused with PBS containing 5mM EDTA, and spinal cords were harvested. The spinal cords were homogenized and incubated in dispase II solution (2.4 units/ml) for 1 hour at 37°C. The digestion was stopped by adding PBS containing 5% FBS and the cell suspension was filtered through a 0.45μm nylon mesh. Samples were stained with directly conjugated anti-CD45-PE antibody (BD Pharmingen) and fixed in 2% PFA on ice for 5 mins, prior to staining of BrdU. BrdU staining was performed using the APC BrdU Flow Kit (BD Pharmingen) as per the manufacturer's instructions and analysed by flow cytometry on a FACScan. 7-amino-actinomycin D (7-AAD; a DNA dye) positivity was used to identify nucleated cells within the digested spinal cord samples.

2.4 Results

2.4.1 BM transplantation does not influence disease progression in SOD1-G93A mice

To investigate the spatiotemporal kinetics of the recruitment of blood-derived cells into spinal cords of mSOD mice, GFP+ BM cells were transplanted into 6 week old lethally irradiated mSOD mice (n = 23) and littermate controls (n = 23) to generate BM chimeric animals. Both mixed background B6SJL and inbred B6 mice were used as transplant recipients to minimize the effects of strain-specific differences on our analysis. The transplantation procedure was well tolerated by both G93A strains. To determine the frequency and degree of reconstitution of BM cells in transplanted mice the presence of GFP+ donor-derived leukocytes in the peripheral circulation of transplant recipients was analysed by FACS. Those mice that were effectively repopulated (>80% or more GFP+ peripheral blood cells), were included in this study (Fig. 2.1A). Mice that underwent the same irradiation protocol but did not receive BM transplants (n = 2) showed signs of radiation sickness and were euthanized within 10 days.

Gait and locomotion were examined using rotarod tests in order to evaluate motor coordination as a function of motor neuron degeneration. There was a significant decline in motor function of both B6SJL and B6 mSOD mice compared to wt controls beginning at 95 days of age ($P < 0.05$ for both groups). There was a significant difference in motor performance between B6SJL and B6 mSOD mice beginning at 106 days of age ($P = 0.001$; Fig. 1B and C). B6SJL mSOD mice declined significantly faster (Fig. 2.1B) than mSOD mice of the B6

strain (Fig. 2.1C). We did not find a significant difference in motor performance

between transplanted and non-transplanted mice of the same strain, indicating

that radiation treatment and BM transplantation do not play a role in disease

progression in mSOD mice under these conditions.

2.4.2 Distribution of BM-derived cells in the spinal cord of SOD1-G93A mice

The distribution of GFP+ cells in mSOD mice and age matched wt

littermates was analyzed at three time points: 11 weeks, 15 weeks, and disease

end-stage. The B6SJL mSOD mice reached 'end-stage' conditions (see above)

at 127 ± 4 (mean $\pm$ SEM) days of age (n = 4), while the B6 mSOD mice reached

the same criteria significantly later (P < 0.01, 152 ± 5 days of age, n = 3). We

examined the cross-sectional area of transverse spinal cord sections at the L5

level from mSOD and wt mice at all time points in order to assess the degree of

spinal cord atrophy. No differences in spinal cord cross-sectional size were

detected between mSOD and wt mice at 11 weeks and 15 weeks of age.

However, the cross sectional areas of mSOD spinal cords at end-stage were

significantly less (21% less) than wt littermates (P < 0.01). This indicates that

there is substantial loss of spinal cord neurons as a result of disease progression.

To assess the extent of BM-derived cellular entry, we examined every fifth

section of spinal cord from upper to mid-thoracic (rostral) and mid- to lower

lumbar segments (caudal) for each animal (n = 46). GFP+ cells were present in

the spinal cords of both mSOD and wt mice at all three time points (Fig. 2.2 and

2.3). There was some infiltration of GFP+ cells into wt mice by 11 weeks that did

not significantly increase with age, and similar numbers of GFP+ cells were

present in spinal cords of wt mice at all three time points. There were no

significant differences between the numbers of GFP+ cells in the spinal cords of

mSOD mice and wt mice at 11 weeks of age indicating that in transplanted

animals, a limited recruitment of cells from the circulation takes place

independently of the disease. In contrast, spinal cords of mSOD mice at 15

weeks of age had significantly greater mean numbers of GFP+ cells than wt mice

at any age and mSOD mice at 11 weeks of age (P < 0.001; Fig. 2.2 and 2.3).

This difference was detected in both thoracic and lumbar regions of the spinal

cord. Consistent with the notion that microgliosis gradually increases with

disease progression, spinal cords of mSOD mice at end-stage contained

significantly more GFP+ cells than mSOD and wt mice at both 11 weeks and 15

weeks, as well as wt age-matched controls (P < 0.001). On average, mSOD

mice at end-stage had a 4- to 5-fold increase in the number of GFP+ cells

compared to either pre-symptomatic mSOD mice or wt mice at end-stage. The

extent of GFP+ cell infiltration was similar between B6SJL and B6 mice. A

gender effect on GFP+ cell number was not detected. These data demonstrate

that in mSOD mice, the increase in GFP+ cell number in spinal cord with age is

associated with disease progression.

Examination of spinal cord sections revealed that GFP+ cells were

regionally distributed within the caudal spinal cord, and to a lesser extent in the

rostral spinal cord. Comparisons were made between GFP+ cell number in the

grey and white matter, and the dorsal and ventral hemicords. At both thoracic

and lumbar levels in the spinal cords of mSOD mice, there were significantly

more GFP+ cells in the ventral region than in the dorsal region (P < 0.05). These

regional differences were detected in both 15 week old and end-stage mSOD

animals (Fig. 2.2 and 2.3). In contrast, GFP+ cells in spinal cords of mSOD mice

at 11 weeks of age and wt mice at all three time points were uniformly distributed

between the dorsal and ventral hemicords. Significantly greater numbers of

GFP+ cells were found in the grey matter of spinal cords compared to the white

matter at the lumbar level in all mSOD mice (P < 0.05) whereas, GFP+ cells in wt

mice were evenly distributed between the grey and white matter at both levels.

Many GFP+ cells were found in the lumbosacral enlargement of mSOD mice, as

this area contains the motor neuron cell bodies that innervate muscles of the hind

limbs, which are prominently affected in G93A mutant mice. These data suggest

that the accumulation of BM-derived GFP+ cells in the spinal cord is increased by

local signals in this ALS model.

2.4.3 Microgliosis in the spinal cord

Using antibodies directed against the cell surface markers F4/80 and

CD11b of murine microglia, we evaluated the extent to which BM-derived

monocytes differentiate into microglia in the spinal cords of G93A mice (Fig. 2.4

and 2.5). Approximately 44% to 83% of BM-derived GFP+ cells expressed the

microglial marker F4/80 (Fig. 2.5; Table 2.1). Mice at 11 weeks of age exhibited

the lowest percentage of F4/80+ donor (GFP+) cells per section, and end-stage

animals had the highest percentage. The mean number of F4/80+ donor cells per spinal cord section increased significantly in mSOD mice from 11 weeks of age through end-stage (P < 0.01), but remained constant in wt mice, consistent with increased expression of this marker upon activation/maturation. No significant changes in the number of donor-derived CD11b+ cells in the spinal cord of mSOD or wt mice were measurable (Table 2.1). We also examined whether there was an increase in the percentage of CD11b+ cells that were donor-derived; however, a significant change in percentage was not detected in either mSOD or wt mice indicating that clonal expansion of donor-derived microglia was similar in both groups. The percentage of GFP+ cells that were CD11b+ was approximately 21 to 40% of the total number of GFP+ cells. We found that CD11b+ cells were much more frequent than F4/80+ cells both in mSOD and wt mice (Table 2.1).

The morphology of GFP+ cells within the spinal cord varied; some cells had spherical cell bodies, while others were spindle-shaped or ramified with thin processes. Almost all of the GFP+ cells that failed to stain for microglial markers were spherical in shape and did not exhibit processes suggesting that non-labelled cells were at an earlier stage of morphological differentiation. Using platelet endothelium cell adhesion molecule-1 (PECAM-1; CD31) markers to label the vascular endothelium, we found that GFP+ cells of varying phenotypes were present both within the vascular lumen and the parenchyma of the spinal cord (not shown).

The increased numbers of BM-derived microglia in affected areas of spinal cords of mSOD mice compared to controls suggested that mSOD mice have increased recruitment of microglial precursors from the circulation. We compared numbers of BM-derived (GFP+) and resident (GFP-) microglia at different time points in G93A mice. The percentage of F4/80+ microglia that were donor-derived comprised only 7% to 24% of the total number of F4/80+ microglia in BM-transplanted mice, and still lower percentages of CD11b+ cells that were GFP+ were observed at all time points in both mSOD and wt mice (approx. 1-3%; Fig. 2.5, Table 2.1). The percentage of GFP+ CD11b+ microglia appeared to be relatively equal in mSOD and wt animals at all time points, although there were slight differences in the percent of donor-derived F4/80+ cells between mSOD and wt mice ($P < 0.05$). These data suggest that although BM-derived cells enter the spinal cord and differentiate into microglia, their contribution to the total number of microglia in the spinal cord is limited, even in mSOD mice.

Virtually all GFP+ cells present within the spinal cord were positive for the pan-hematopoietic cell marker CD45 (data not shown). Since some of the GFP+ cells failed to label with microglial markers, we used antibodies against NeuN, GFAP, CD3, Ly-6G, and CD117. We did not find any convincing examples of GFP+ cells labelled with these markers and demonstrating a cell type appropriate morphology.

In order to determine the frequency and nature of the proliferation of hematopoietic cells in the spinal cords of mSOD mice, we used immunofluorescence staining of incorporated BrdU and flow cytometric analysis.

mSOD mice received intraperioneal injections for five consecutive days beginning at a time when they exhibited advanced disease symptoms (115 days of age). We examined the percentage of GFP+ and GFP- cells that exhibited BrdU staining coupled with immunofluorescence staining of CD45. Proliferation of both endogenous (CD45+GFP-) and BM-derived (CD45+GFP+) hematopoietic cells were identified. We found that the relative rates of cell proliferation in these spinal cord cell populations were similar, that is approximately 13% of all hematopoietic cells underwent replication.

2.5   Discussion

2.5.1   BM-derived cells infiltrate the parenchyma of mSOD spinal cord

This study demonstrates that transgenic mice that over-express mSOD have a progressive increase in BM-derived cell infiltration in spinal cord that is significantly larger compared to wt littermates. Although we did see some BM-derived cell infiltration in wt spinal cord, the extent of infiltration was significantly greater in mSOD mice than wt littermates at 15 weeks of age and at end-stage. No significant differences in GFP+ cell number were detected in mSOD mice at 11 weeks of age compared to age-matched wt animals, indicating that the extent to which GFP+ cell number increases is associated with the development of neurological debility. The chronology of increase in GFP+ cell number in spinal cord parallels the time course of microgliosis and microglial activation, as demonstrated by previous studies (Alexianu et al., 2001; Hall et al., 1998). These previous studies are consistent with our observations that there is a

greater number of microglia in the spinal cords of mSOD mice compared to age-matched controls beginning at 15 weeks of age.

We observed that the numbers of GFP+ cells were greater in caudal regions of spinal cord compared to rostral regions. This observation is of interest as neurological debility in mSOD mice is especially evident in the hindlimbs suggesting extensive motor neuron loss in the lumbar regions. Previous studies using the G93A mouse have demonstrated that there is prominent motor neuron cell loss and gliosis most notably in the ventral horns (Alexianu et al., 2001; Dal Canto and Gurney, 1995; Hall et al., 1998). In the present study, we showed that within the spinal cord of symptomatic mSOD mice, BM-derived cells are predominately localized to the ventral horns, particularly the grey matter, and less in the ventral white matter and dorsal regions, suggesting that the BM-derived cells are recruited to sites of neuronal degeneration.

The present experiments employed mSOD and wt mice of two different background strains. Transgenic mice of the B6SJL strain have been used extensively as a model of ALS (Gurney et al., 1994; Hall et al., 1998; Hamson et al., 2002; Hu et al., 2003). However, we were unsure whether the presence of BM-derived cells from GFP+ B6 mice in the CNS might result in an inflammatory response due to graft-versus-host disease (GVHD) or other reactions. Consequently, we performed similar protocols on mice isogenic to the donor strain (B6) and to a partially unrelated strain (B6SJL). Both strains of mSOD mice survived and successfully repopulated the BM after lethal irradiation. The number of GFP+ cells that penetrated the CNS by end-stage in mSOD mice was

approximately equal for both strains, suggesting that GFP+ cellular infiltration is not influenced by potential GVHD. This indicates that the progressive increase in GFP+ cell number in spinal cords of mSOD mice with age is due to mSOD over-expression and the consequent disease process.

Unlike previous studies that suggested that hematopoietic stem cells prolonged survival time of mSOD mice by creating a non-neuronal environmental change (Corti et al., 2004; Ende, et al., 2000; Garbuzova-Davis et al., 2003), we did not detect any difference in survival time between BM-transplanted and non-transplanted mSOD mice. The absence of a beneficial effect of BM transplants in our mice may result from our age of transplantation, although both we and Corti and colleagues transplanted BM into pre-symptomatic mSOD recipients. Additionally, we exposed the mice in our study to greater amounts of radiation prior to transplantation than Corti and colleagues, and the BM-transplanted mice in our study exhibited a higher percentage of circulating GFP+ leukocytes.

2.5.2 BM-derived cells enter the CNS and differentiate into microglia

Our study provides novel data on the contribution of BM-derived microglia to the CNS in this mouse model of ALS. We demonstrated that up to 83% of the BM-derived cells that enter the spinal cord are F4/80+ microglia. The absolute number of donor-derived microglia in the spinal cord progressively increases in mSOD mice beginning after 11 weeks of age. This increase was not observed in wt animals. Microglial activation and proliferation is a stereotypical response to injury in the CNS and occurs in: focal brain ischemia (Hess et al., 2004; Priller et

al., 2001); Alzheimer's disease (McGeer and McGeer, 2003); motor neuron axotomy (Kalla et al., 2001; Priller et al., 2001); in addition to ALS and in several mouse models of ALS (Boilee et al., 2001; Hall et al, 1998). Our data show that microglia increase in number in areas of the CNS that are specific to neuron degeneration, consistent with previous studies (McGeer and McGeer, 2002). It has been suggested by others that in healthy CNS tissue, microglia are normally replaced from the periphery relatively infrequently (Messengale et al., 2005), thus, one possible interpretation of these data suggests that ALS is associated with increased recruitment of BM-derived monocytes through the BBB and into the CNS.

The presence of BM-derived cells in the spinal cords of wt mice and mSOD mice prior to the development of pathological alteration suggests alternative explanations for our observations. It is known that irradiation-induced effects on the CNS include changes in the permeability of the vasculature that can result in BM-derived cellular infiltration into the brain or spinal cord (Rubin et al., 1994). Thus, in mSOD and wt mice, radiation may lead to an altered BBB permeability and subsequently the influx of GFP+ cells into the CNS. Conversely, radiation may result in increased cell death of pre-existing CNS-resident microglia which may facilitate engraftment by cells from peripheral sources, namely BM-derived monocytes. Our data strongly suggest that the increased numbers of microglia found in regions associated with neurodegeneration are due to expansion of the CNS-resident microglial pool, which at disease onset includes a limited number of donor-derived microglia.

The low percentages of GFP+ microglia compared to the total number of microglia indicate that the contribution of BM-derived microglial precursors to the microglial population is small. We have found that up to 24% of the total number of F4/80+ microglia present in the spinal cord of mSOD mice at disease end-stage were of donor BM origin. This value is consistent with previously published data on BM-derived microglia in mouse spinal cord (Corti et al., 2004; Kennedy et al., 1997; Massengale et al., 2005). However, this percentage was similar at all time points in our analysis demonstrating that the contribution of BM-derived microglia to the overall microglial population remains relatively the same throughout the disease. Our data suggest that the microgliosis present in the spinal cord of mSOD mice is primarily due to the disease-induced expansion of resident microglial cell colonies rather than the active recruitment of BM-derived monocytes from the bloodstream.

Some of the GFP+ cells failed to stain for microglial markers. Most of these cells were spherical in shape, and were not labelled by other cell markers (see above), nor did they exhibit distinctive cell-type morphology. Furthermore, the majority of GFP+ cells stained positively for CD45. These data indicate that the GFP+ cells were derived from peripheral sources and that they maintain their hematopoietic fate in the spinal cord. Failure to label some of these cells with specific markers was not due to lack of antibody penetration as 3-D confocal microscopy demonstrated adequate antibody labelling in central regions of the tissue section. The lack of labelling of GFP+ cells with microglial or other markers has been noted by others (Eglitis and Mezey, 1997; Massengale et al.,

2005; Wagers et al., 2002) and may be a consequence of the immaturity of the microglial cell, or the monocytic precursor from which it is derived. Additionally, Messengale and colleagues identified approximately 100% CD45+ immunoreactivity of BM-derived microglia, further supporting our hypothesis that the population of GFP+ cells are primarily microglia.

To evaluate the kinetics of microglia in the spinal cords of mSOD mice, we assessed the relative rate of resident and BM-derived cellular proliferation. We have demonstrated that both CD45+GFP- and CD45+GFP+ cells undergo replication, and that the rate of replication is comparable in these two populations. The majority of GFP+ cells were immunohistochemically identified as being both CD45+ and F4/80+. This suggests that the observed proliferating population of CD45+GFP+ cells are microglia. It has been previously documented that the turnover of microglia in the normal adult CNS is due to an equal contribution of proliferating CNS-resident microglia and recruitment of microlial precursors from the circulation (Lawson et al. 1992). Here we can provide additional insight, as our data suggests that not only is there entry of microglial precursors from the bloodstream, but they proliferate at a rate similar to pre-existing CNS microglia. These data further support our hypothesis that the microgliosis observed in the spinal cord of mSOD mice is most likely due to the expansion of the CNS-resident microglial population rather than active recruitment of BM-derived progenitors.

In conclusion, we observed that BM-derived cells are found in small numbers in spinal cords of control mice and in much larger numbers in mSOD

mice after 15 weeks of age, a time when mice are symptomatic. In spinal cord, BM-derived cells differentiate into microglia with no evidence for differentiation into astrocytes or neurons. Although microgliosis is seen in the CNS of mSOD mice, it appears that BM-derived cells contribute only a small fraction to the population of microglia, suggesting that blocking the entry of BM-derived monocytes into the CNS will have only limited effects on altering microglial number. The vast majority of microgliosis in the spinal cord is the result of proliferation of resident microglia.

Stem cell therapy has been proposed as an attractive strategy in the treatment of ALS (Corti et al., 2004; Mezey et al., 2000). However, our data suggest that there is restricted potential for adult BM-derived stem cells to differentiate into functional neural cells. Nonetheless, our data shows that BM-derived cells are able to penetrate the BBB, especially in mice manifesting neurological debility and are present at sites of neuron damage raising the possibility that monocytes might be able to deliver neurotrophins or other beneficial substances to localized sites of the CNS (Biffi et al., 2004).

2.6 Acknowledgements

2.7 Tables

Table 2.1 Quantification of cells expressing microglial markers.

Cells expressing the microglial markers F4/80 and CD11b were quantified in SJL control and mSOD mice (n=23) at 11 weeks (w), 15 w, and disease end-stage. Expressed as mean percentage of donor cells expressing immune label per section ± SEM.

Age at Sacrifice	Genotype	% F4/80$^+$ donor cells per section, mean ± SEM (GFP$^+$F4/80$^+$/ GFP$^+$)	% GFP$^+$ microglia per section, mean ± SEM (GFP$^+$F4/80$^+$/ F4/80$^+$)	% CD11b$^+$ donor cells per section, mean ± SEM (GFP$^+$CD11b$^+$/ GFP$^+$)	% GFP$^+$ microglia per section, mean ± SEM (GFP$^+$CD11b$^+$/ CD11b$^+$)
11 w	wt	39.1 ± 7.5 (252/575, $n = 3$)	22.3 ± 2.2 (252/1060, $n = 3$)	33.5 ± 11.9 (100/250, $n = 3$)	2.2 ± 1.0 (100/3719, $n = 3$)
	mSOD	44.6 ± 6.3 (132/296, $n = 4$)	7.9 ± 2.0 (132/1808, $n = 4$)	35.8 ± 9.8 (57/154, $n = 4$)	1.0 ± 0.4 (57/5840, $n = 4$)
15 w	wt	50.2 ± 2.2 (182/365, $n = 4$)	15.2 ± 1.3 (182/1173, $n = 4$)	18.8 ± 3.7 (49/235, $n = 4$)	1.5 ± 0.6 (49/3574, $n = 4$)
	mSOD	54.5 ± 8.3 (465/974, $n = 4$)	13.8 ± 2.4 (465/3666, $n = 4$)	22.4 ± 2.6 (130/580, $n = 4$)	2.4 ± 0.7 (130/5575, $n = 4$)
End-stage	wt	75.8 ± 4.9 (178/237, $n = 4$)	22.5 ± 6.1 (178/901, $n = 4$)	34.4 ± 3.3 (66/194, $n = 4$)	1.3 ± 0.5 (66/5743, $n = 4$)
	mSOD	85.5 ± 7.9 (767/924, $n = 4$)	15.3 ± 1.6 (767/4912, $n = 4$)	25.2 ± 6.8 (216/765, $n = 4$)	2.5 ± 1.2 (216/9113, $n = 4$)

2.8 Figures

Figure 2. 1 FACS analysis of peripheral blood leukocytes and rotorod motor function analysis of mSOD and wild type mice.

Three weeks after BM irradiation/transplantation, blood samples were analyzed for donor-derived peripheral blood leukocytes. (A) An example FACS plot demonstrating successful donor BM reengraftment. (B) Rotorod analysis for SJL mSOD and control mice and (C) C57/Bl6 mSOD and control mice; BM transplantation did not affect disease progression in mSOD mice.
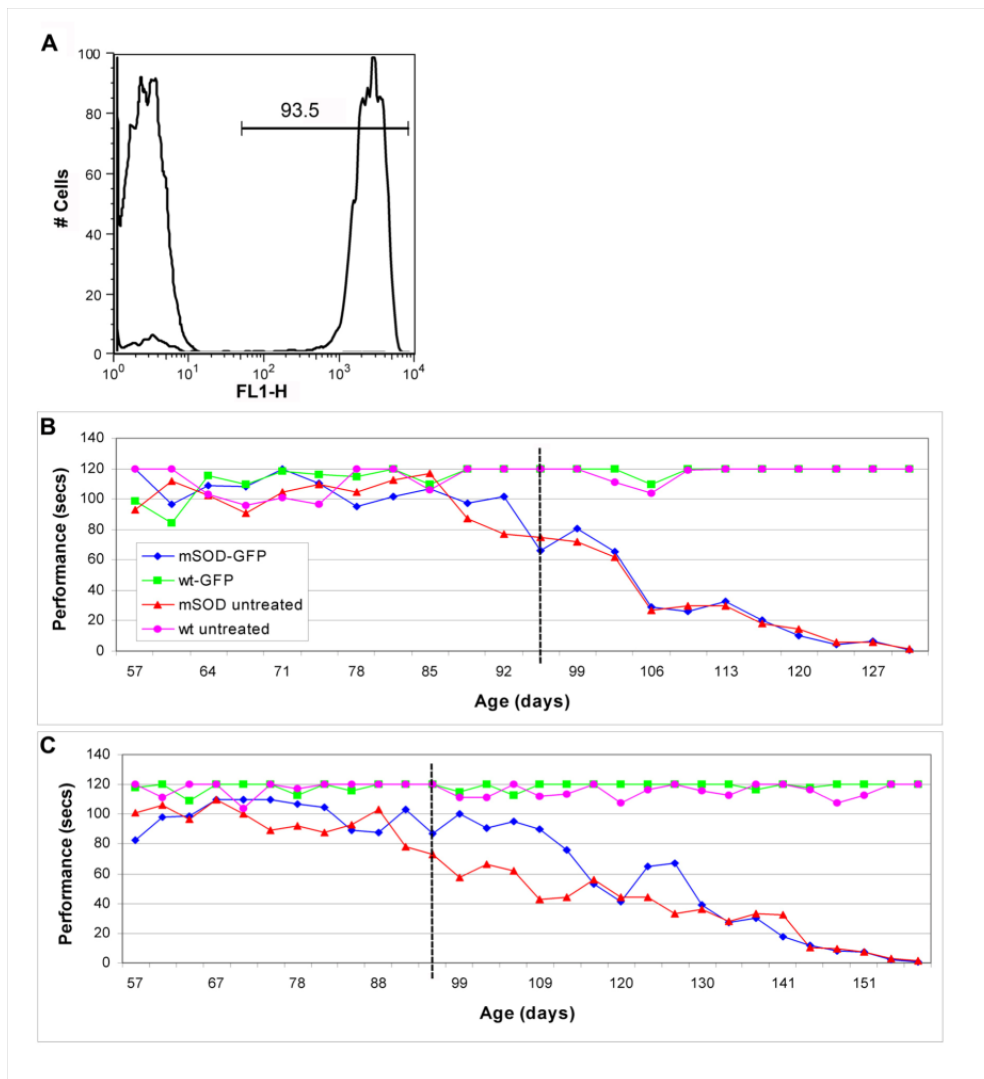
Figure 2. 2 GFP+ BM cells infiltrate the spinal cord of mSOD mice and accumulate with disease progression.

Transverse thoracic and lumbar spinal cord sections from wild type and mSOD mice at 11 w, 15 w, and disease end-stage. At 11 w, no significant differences were observed between the numbers of GFP+ BM cells in mSOD and control spinal cords. At 15 w and end-stage, significantly greater numbers of GFP+ BM cells accumulated in the spinal cords of mSOD mice at both thoracic and lumbar levels compared to control mice (p<0.001). There was a significant increase in the mean number of GFP+ BM cells in mSOD spinal cord from 11 w to disease end-stage (p<0.001). No significant differences were observed in the number of GFP+ BM cells that accumulated wild type spinal cords between 11 w, 15 w and disease-end stage.

65
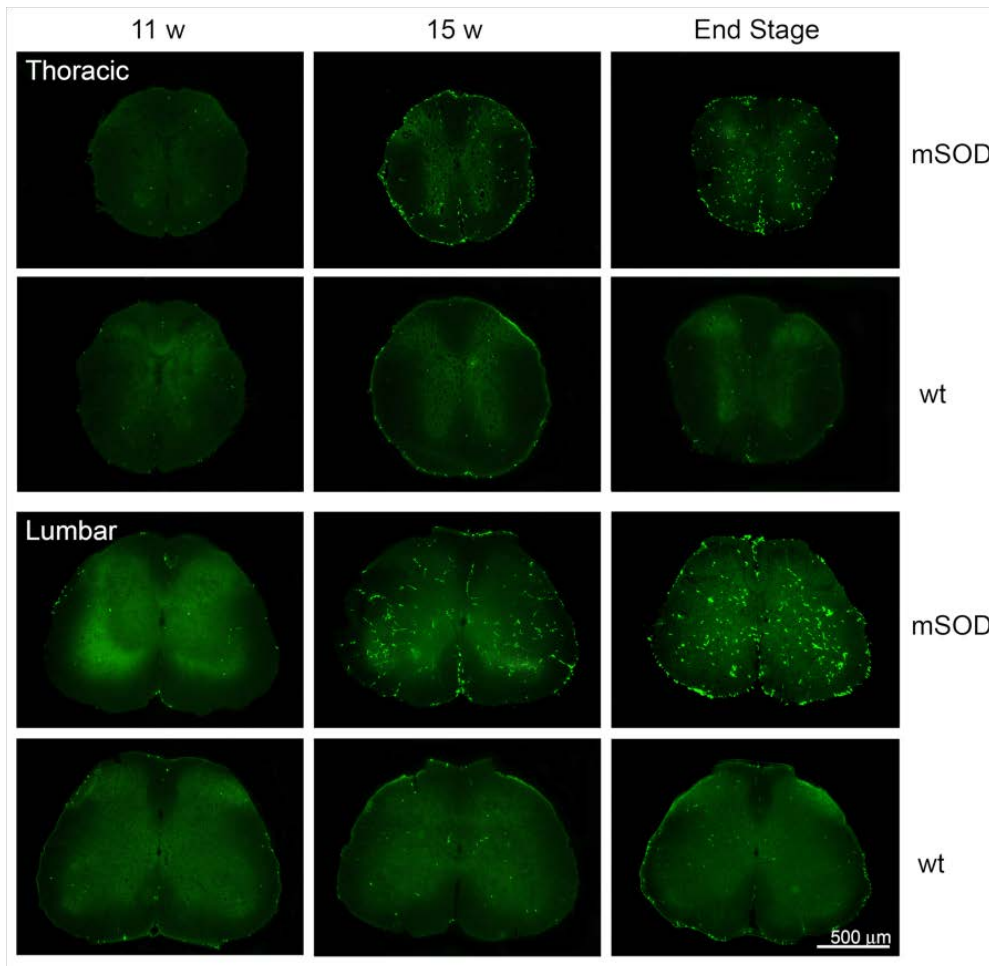
Figure 2. 3 Regional distribution of GFP+ cells in mSOD (grey bars) and wild type (black bars) at 11 w, 15 w, and disease end-stage (e.s.).

Distribution of GFP+ cells in: (A) rostral spinal cord, B6SJL mice (n=23), (B) caudal spinal cord, B6SJL mice (n=23), (C) rostral spinal cord Bl6 mice (n=23), (D) caudal spinal cord (n=23).
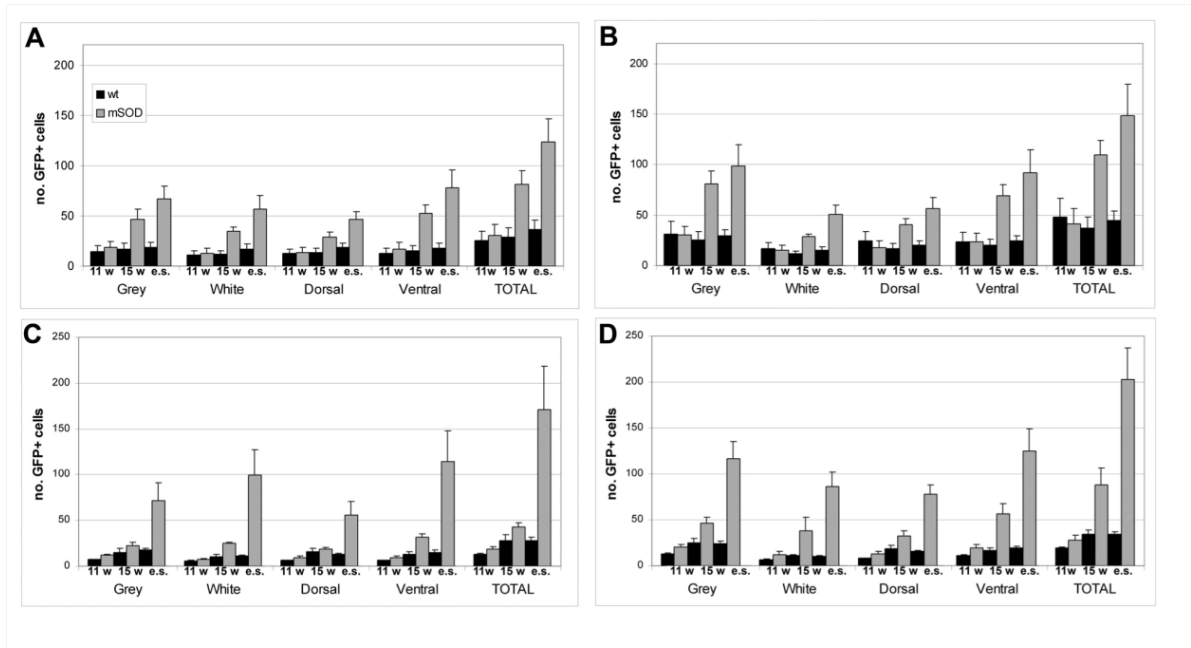
**Figure 2. 4 Immunohistochemistry labelling of GFP+ cells with the macrophage markers
F4/80 and CD11b.**

The green channel shows GFP+ cells, the red channel F4/80 or CD11b, accordingly. Merged
images demonstrate labelling of GFP+ cells with F4/80 and CD11b, respectively.
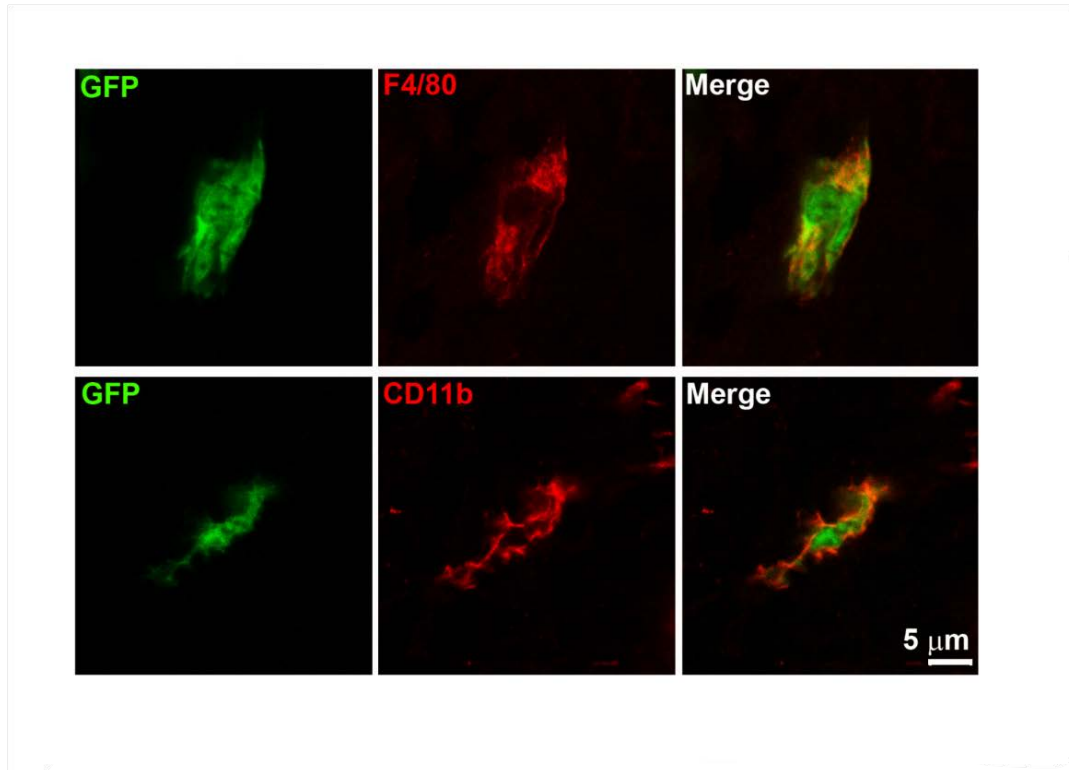
Figure 2. 5 The majority of GFP+ cells in the mSOD lumbar spinal cord express macrophage markers.

(A) Fluorescent microscopy images of mSOD spinal cord sections at 11 w, 15 w, and disease end-stage. Green channel show GFP+ cells; red channel shows immunolabelling with F4/80; merge identifies F4/80+ GFP+ cells. (B) Mean numbers of F4/80+ GFP+ cells positive in wild type (black bars) and mSOD spinal cord. (C) Mean numbers of CD11b+ GFP+ cells. (D) Percentage of F4/80+ cells that are GFP+. (E) Percentage of CD11b+ cells that are GFP+.
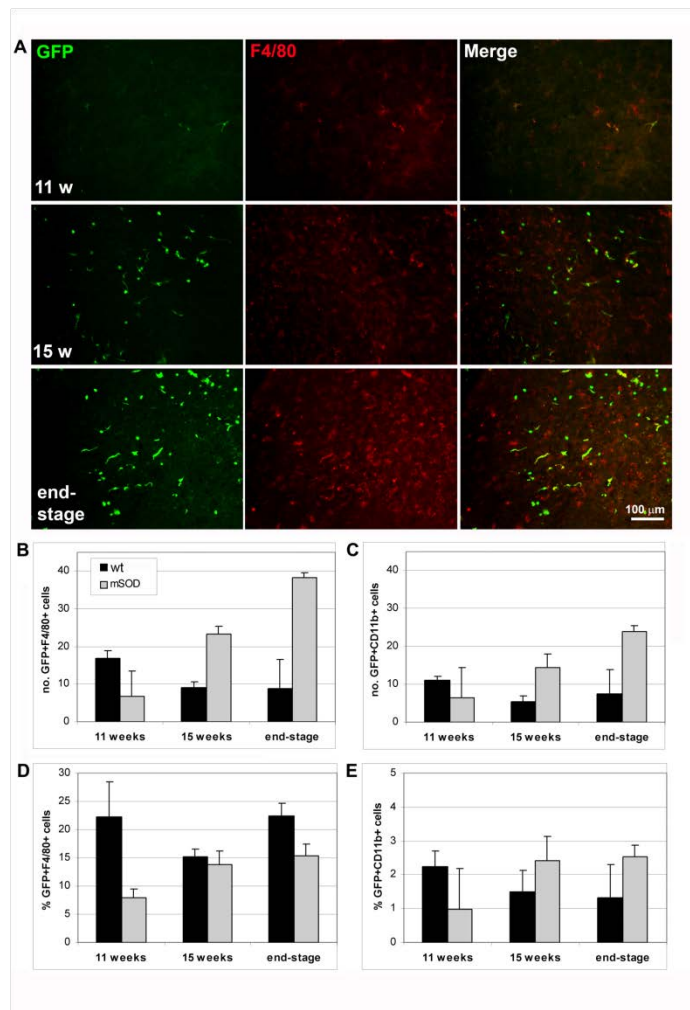
2.9 References

Alexianu ME, Kozovska M, Appel SH (2001) Immune reactivity in a mouse model of familial ALS correlates with disease progression. Neurology 57: 1282-1289.

Biffi A, De Palma M, Quattrini A, Del Carro U, Amadio S, Visigalli I (2004) Correction of metachromatic leukodystrophy in the mouse model of transplantation of genetically modified hematopoietic stem cells. J Clin Invest 113: 1118-1129.

Boillee S, Viala L, Peschanski M, Dreyfus PA (2001) Differential microglial response to the progressive neurodegeneration in the murine mutant wobbler. Glia 33: 277-287.

Clement AM, Nguyen MD, Roberts EA, Garcia ML, Boillee S, Rule M et al. (2003) Wild-type non-neuronal cells extend survival of SOD1 mutant motor neurons in ALS mice. Science 302: 113-117.

Corbel SL, Lee A, Yi L, Duenas J, Brazelton TR, Blau HM, Rossi FMV (2003) Contribution of hematopoietic stem cell to skeletal muscle. Nature Med 9: 1528-1532.

Corti S, Locatelli F, Donaoni C, Guglieri M, Papaimitriou D, Strazzer S, et al. (2004) Wild-type bone marrow cells ameliorate the phenotype of SOD1-G93A ALS mice and contribute to CNS, heart and skeletal muscle tissues. Brain 127: 2518-2532.

Dal Canto MC, Gurney ME (1995) Neuropathological changes in two lines of mice carrying a transgene for mutant human Cu, Zn SOD, and in mice over-expressing wild-type human SOD: a model of familial amyotrophic lateral sclerosis (FALS). Brain Res 676: 25- 40.

Eglitis MA & Mezey E (1997) Hematopoietic cells differentiate into both microglia and macroglia in the brains of adult mice. Proc Natl Acad Sci USA 94: 4080-4085.

Ende N, Weinstein F, Chen R, Ende M (2000) Human umbilical cord blood effect on sod mice (amyotrophic lateral sclerosis). Life Sci 67: 53-59.

Garbuzova-Davis S, Willing AE, Zigova T, Saporta S, Justen EB, Lane JC, et al. (2003) Intravenous administration of human umbilical cord blood cells in a mouse model of amyotrophic lateral sclerosis: distribution, migration and differentiation. J. Hematother. Stem Cell Res 12: 255-270.

Gurney M, Pu H, Chiu AY, Dal Canto MC, Polchow CY, et al. (1994) Motor neuron degeneration in mice that express a human Cu, Zn superoxide dismutase mutation. Science 264: 1772–1775.

Hall ED, Oostveen JA, Gurney ME (1998) Relationship of microglial and astrocyte activation to disease onset and progression in a transgenic model of familial ALS. Glia 23: 249-256.

Hamson DK, Hu JH, Krieger C, Watson NV (2002) Lumbar motor neuron fate in a mouse model of amyotrophic lateral sclerosis.   NeuroReport 13: 2291-2294.

He BP, Wen W, Strong MJ (2002) Activated microglia (BV-2) facilitation of TNF-alpha-mediated motor neuron death in vitro. J Neuroimmunol 128: 31- 38.

Hensley K, Fedynyshyn J, Ferrel S, Floyd RA, Gordon B, Grammas P, et al. 2003. Message and protein-level elevation of tumour necrosis factor (TNF alpha) and TNF alpha-modulating cytokines in the spinal cords of the G93A-SOD1 mouse model for amyotrophic lateral sclerosis. Neurobiol Dis 14: 74- 80.

Hess DC, Hill WD, Martin-Studdard A, Carroll J, Brailer J, Carothers J (2002) Bone marrow-derived cells differentiate into endothelial cells and NeuN-expressing cells after stroke. Stroke 33: 1362-1368.

Hess DC, Abe T, Hill WD, Martin-Studdard A, Carothers J, Masuya M, et al. (2004) Hematopoietic origin of microglial and perivascular cells in brain. Exp Neurol 186: 134-144.

Hu JH, Chernoff K, Pelech S, Krieger C (2003) Protein kinase and protein phosphatase expression in the central nervous system of G93A mSOD over-expressing mice. J Neurochem 85: 422-431.

Kalla R, Liu Z, Xu S (2001) Microglia and the early phase of immune surveillance in the axotomized motor nucleus. J Comp Neurol 436: 182-201.

Kennedy DW & Abkowitz JL (1997) Kinetics of central nervous system microglial and macrophage engraftment: analysis using a transgenic bone marrow transplantation model. Blood 90: 986-993.

Kreutzberg G (1996) Microglia: a sensor for pathological events in the CNS. Trends Neurosci 19: 312-318.

Lawson LJ, Perry VH, Gordon S (1992) Turnover of resident microglia in the normal adult mouse brain. Neuroscience 48: 405-415.

Lino MM, Schneider C, Caroni P (2002) Accumulation of SOD1 mutants in postnatal motor neurons does not cause motor neuron pathology or motor neuron disease. J Neurosci 22: 4825-4832.

McGeer PL, McGeer EG (2002) Inflammatory processes in amyotrophic lateral sclerosis. Muscle Nerve 26: 459-470.

McGeer PL, McGeer EG (2003) Inflammatory processes in Alzheimer's disease. Prog. Neuropyschopharmacol Biol Psychiatry 27: 741- 749.

Massengale M, Wagers AJ, Vogel H, Weissman IL (2005) Hematopoietic cells maintain hematopoietic fates upon entering the brain. J Exp Med 201: 1579- 1589.

Mezey E & Chandross KJ (2000) Bone marrow: a possible alternative source of cells in the adult nervous system. Eur J Pharmacol 405: 297- 302.

Pramatarova A, Laganiere J, Roussel J, Brisebois K, Rouleau GA (2001) Neuron-specific expression of mutant superoxide dismutase 1 in transgenic mice does not lead to motor impairment. J Neurosci 21: 3369-3374.

Priller J, Flugel A, Wehner T, Boentert M, Haas CA, Prinz M, et al. (2001) Targeting gene-modified hematopoietic cells to the central nervous system: use of green fluorescent protein uncovers microglia engraftment. Nat Med 7:1356-1361.

Rosen DR, Siddique T, Patterson D, Figlewicz DA, Sapp P, Hentati A, et al. (1993) Mutations in the Cu/Zn superoxide dismutase gene are associated with familial amyotrophic lateral sclerosis. Nature 362: 59-62.

Rubin P, Gash DM, Hansen JT, Nelson DF, Williams JP (1994) Disruption of the blood brain barrier as the primary effect of central nervous system irradiation. Radiotherapy Oncol 31: 51-60.

Streit WJ, Walter SA, Pennell NA (1999) Reactive microgliosis. Prog Neurobiol 57: 563-581.

Wagers AJ, Sherwood RI, Christensen JL, Weissman IL (2002) Little evidence for developmental plasticity of adult hematopoietic stem cells. Science 294: 2256-2259.

Watson RE, Wiegland SJ, Clough RW, Hoffman GE (1986) Use of cryoprotectant to maintain long-term peptide immunoreactivity and tissue morphology. Peptides 7: 155-159.

Wilson MB, Khabazian I, Wong MC, Seyedlikhani A, Bains JS, Pasqualotto BA, et al. (2002) Behavioural and neurological correlates of ALS-Parkinsonism dementia complex in adult mice fed washed cycad flour. Neuromolecular Med 1: 207-221.

Wright DE, Wagers AJ, Gulati AP, Johnson FL, Weissman IL (2001) Physiological migration of hematopoietic stem and progenitor cells. Science 294: 1933-1936.

3: BONE MARROW-DERIVED CELLS IN THE CENTRAL NERVOUS SYSTEM OF A MOUSE MODEL OF AMYOTROPHIC LATERAL SCLEROSIS ARE ASSOCIATED WITH BLOOD VESSELS AND EXPRESS CX$_3$CR1

3.1 Abstract

Amyotrophic lateral sclerosis (ALS) is associated with increased numbers of microglia within the CNS. However, it is unclear to what extent bone marrow (BM)-derived cells contribute to this microgliosis. We have studied the adoptive transfer of green fluorescent protein (GFP)-labeled whole BM cells and BM from mice that express GFP only in CX$_3$CR1+ cells (CX$_3$CR1$^{+/GFP}$) into the CNS of a murine model of ALS having over-expression of mutant superoxide dismutase (mSOD), and wt littermates. We find that most GFP+ and CX$_3$CR1$^{+/GFP}$ cells are found adjacent to the microvasculature within the CNS, both in mSOD and wt mice. GFP+ and CX$_3$CR1$^{+/GFP}$ cells within the CNS have a variety of morphologies, including cells with an elongated appearance, weak Iba-1 immunoreactivity, and often mannose receptor immunoreactivity, indicating that these cells are perivascular microglia. Typically, less than 10% of BM-derived cells had a stellate-shape and expressed strong Iba-1 immunoreactivity, as expected for parenchymal microglia, indicating that BM-derived cells uncommonly generate parenchymal microglia. Adoptive transfer of BM-derived cells from CX$_3$CR1$^{+/GFP}$ mice revealed that many elongated cells are GFP+,

demonstrating that some perivascular cells are derived from BM cells of the CX$_3$CR1+ lineage. The significantly greater numbers of BM cells in mSOD than in control mice indicate that the presence of these BM cells in the spinal cord is regulated by conditioning stimuli that may include irradiation and inflammatory factors within the CNS.

3.2 Introduction

Amyotrophic lateral sclerosis (ALS) is a fatal neurodegenerative disease characterized by progressive loss of motoneurons in brain stem and spinal cord, as well as neuron loss in the cerebrum. ALS pathogenesis is likely heterogeneous where a number of pathological processes have been implicated including excitotoxicity, oxidative injury, mitochondrial dysfunction, and protein aggregation, resulting in cellular dysfunction (Strong et al., 2005).

The majority of ALS cases are sporadic, however approximately 10% are familial (fALS) with autosomal dominant transmission of mutations in a variety of genes. Over 100 mutations in the gene encoding the free radical scavenger Cu,Zn- superoxide dismutase (SOD1) have been associated with ALS and mutations in this gene represent roughly 20% of fALS cases (Bruijn et al., 2004). The identification of mutant SOD1 involvement in fALS has enabled the development of transgenic mice as a model for study of ALS. The G93A mutant SOD (mSOD) transgenic mouse model over-expresses a human SOD1 missense mutation and develops progressive motoneuron degeneration and limb paralysis.

Although the nature of mSOD pathogenesis in transgenic mice has not been elucidated, studies using these models have demonstrated that restricted expression of mSOD to neurons leads to neurodegeneration (Jaarsma et al., 2008). However, other work has also demonstrated that restricted mSOD expression to neurons and some types of glia such as astrocytes and/or microglia can also influence non-cell autonomous neurodegeneration (Clement et al., 2003).

When microglial mSOD expression is reduced using a Cre-Lox system in transgenic mice, significant extensions in animal survival are observed (Boillee et al., 2006). Furthermore, when mSOD mice are crossed with PU-/- mice (a strain that does not develop macrophages or microglia), transplantation of bone marrow (BM)-derived cells from control mice differentiate into microglia and extend the survival of mSOD over-expressing mice (Beers et al., 2007). These observations indicate a detrimental role for microglia in the pathogenesis of ALS and suggest that replacement of mSOD-expressing microglia with healthy microglia might be a useful therapeutic strategy (Beers et al., 2007). For such a therapy to be effective, BM-derived cells would have to re-populate the adult CNS extensively, as has been reported following adoptive transfer of BM cells into control mice (Simard and Rivest, 2004). However, in previous work, we observed that numbers of BM-derived cells in spinal cord expressing microglial markers were limited compared to the large numbers of endogenous microglia, both in mSOD and control mice (Solomon et al., 2006).

There are several populations of CNS-associated macrophages including parenchymal microglia, perivascular microglia, and meningeal and choroid plexus macrophages, which differ from parenchymal microglia in phenotype, morphology and anatomical location (Davoust et al., 2008). Microglia are the only macrophage subtype within the CNS parenchyma; perivascular microglia are located on the abluminal surface of endothelial cells while the other macrophage subtypes are specific to the meninges and choroid plexus. Juxtavascular microglia are located adjacent to blood vessels but have a morphology distinct from perivascular microglia and are considered to be intraparenchymal (Davoust et al., 2008; Gehrmann et al., 1995). In order to differentiate BM-derived microglia from other types of CNS-associated macrophages, we examined the characteristics of BM-derived cells within the mSOD and normal CNS, as well as the cell populations within whole BM from which they may derive.

Microglia strongly express the macrophage marker Iba1 (Imai et al., 1996), and the chemokine receptor CX_3CR1, also known as the fractalkine receptor (Jung et al., 2000). Within the CNS, neurons constitutively express fractalkine (CX_3CL1), which functions as an adhesion molecule in its membrane bound form and, after proteolytic cleavage from a mucin-like stalk, as a chemoattractant (Jung et al., 2000). Experiments employing mouse models of neurodegenerative diseases have demonstrated that CX_3CR1 expression by microglia serves to control microglial neurotoxicity in the mSOD mouse model of ALS (Cardona et al., 2006) and during murine experimental autoimmune encephalitis (EAE; Huang et al., 2006).

Other cell populations that express CX_3CR1 include monocytes, dendritic cells, and subsets of natural killer and T-cells (Cardona et al., 2006). Macrophage and dendritic cells derive from monocytes, which can be divided into at least two subpopulations based on CX_3CR1 expression (Geissmann et al., 2003). CX_3CR1^{hi} monocytes migrate to tissues under homeostatic conditions and give rise to tissue-resident macrophages, while CX_3CR1^{lo} monocytes enter tissues under inflammatory conditions (Geissmann et al., 2003). Mildner and colleagues (2007) reported that within the adult murine CNS microglia are derived from the CX_3CR1^{lo} population after facial nerve axotomy and cuprizone-induced demyelination, but only after undergoing lethal irradiation and that in the absence of irradiation there is essentially no entry of BM-derived cells into the CNS.

To identify cell populations within BM that are capable of populating the mSOD CNS following irradiation, we transplanted mSOD and control mice with BM harvested from transgenic mice with a GFP knock-in at the CX_3CR1 locus (Jung et al., 2000). Mice heterozygous for this transgene ($CX_3CR1^{+/GFP}$) express functioning CX_3CR1 protein and a GFP reporter gene in CX_3CR1+ cells. We observed numerous $CX_3CR1^{+/GFP}$ cells within the spinal cord of mSOD and control mice indicating that CX_3CR1 cells or their precursors are capable of migration to the CNS, proliferation and differentiation into perivascular cells. As with ubiquitous GFP BM transplants, there were significantly greater numbers of $CX_3CR1^{+/GFP}$ cells in spinal cords of mSOD mice compared to age-matched controls.

76

Our results demonstrate that BM cells enter and/or proliferate within spinal cords of mice over-expressing mSOD and controls where BM-derived cells largely comprise perivascular cells. The present data support a model proposed previously where BM-derived cells constitute a population which does not contribute significantly to the microglial pool (Hickey et al., 1992). Although significantly greater numbers of BM-derived cells are observed in spinal cords of mSOD-over-expressing mice than wt mice, mSOD expressing mice have a distribution of BM-derived cells that is qualitatively similar to that in control animals.

3.3 Materials and Methods

3.3.1 Animals

The transgenic mouse line B6.Cg-Tg (SOD1-G93A; Jackson Laboratories, Bar Habour, ME) over-express a human SOD1 missense mutation by approximately 25-fold (Gurney et al., 1994); age-matched, non-transgenic C57BL/6 mice were used as experimental controls. The mSOD mice develop progressive motoneuron degeneration resulting in muscle atrophy and eventual paralysis. Mice were bred from progenitor stock and maintained as heterozygotes by breeding mSOD males with non-transgenic females. Mice were genotyped for the mSOD1 transgene using a protocol previously established by Gurney and colleagues (1994). Non-transgenic littermates were used as controls and sacrificed at the same time point as mSOD animals.

Mice that ubiquitously express a GFP transgene under the control of a β-actin promoter (C57BL/6; GFP/CD45.2) were obtained from Dr. I. Weissman and bred and maintained at the Biomedical Research Centre (BRC) at the University of British Columbia. $CX_3CR1^{GFP/GFP}$ mice were purchased from Jackson Laboratories (Bar Harbour, ME). Mice were bred as heterozygotes by crossing $CX_3CR1^{GFP/GFP}$ homozygotes with wild type B6 mice. Animals were provided food and water *ad libitum* and all protocols related to the use of animals at SFU and the UBC were approved by university review committees and were in compliance with guidelines from the Canadian Council on Animal Care, the NIH Guide for the Care and Use of Laboratory Animals, and the EEC Council Directive.

3.3.2 Generation of BM-chimeric mice

GFP-expressing mice were used as BM donors to mSOD and control mice, in a procedure described previously (Solomon et al., 2006). BM recipients were lethally irradiated (9-10Gy) at 6 weeks of age and each irradiated animal received tail vein injections of at least 5×10^6 GFP+ donor cells (n=8 mSOD; n=8 control). A similar protocol was used in transplanting $CX_3CR1^{+/GFP}$ BM (n=3 mSOD, n=3 control). Three weeks post BM transplantation, blood samples from transplanted animals were analyzed by fluorescence-activated cell sorting (FACS) using a FACScan (Becton Dickinson; Franklin Lakes, NJ).

3.3.3 Tissue processing

Mice receiving BM transplantations with GFP+ BM were either sacrificed at 15 weeks of age (n=4 mSOD, n=4 control) or allowed to progress to disease end-stage (n=4 mSOD, n=4 control when affected animals are unable to right themselves after 10 seconds of lateral recumbency. mSOD mice and age-matched controls that received CX$_3$CR1$^{+/GFP}$ BM were sacrificed at disease end-stage (n=3 mSOD, n=3 control). Mice were euthanized using CO$_2$ and immediately perfused transcardially with 30mL of 1% PBS (pH 7.4) followed by 30mL of 4% paraformaldehyde (PFA, w/v; pH 7.0). The spinal cord and brain were removed, fixed in 4% PFA overnight at 4°C and transferred to 20% sucrose (w/v) in PBS overnight at 4°C for cryoprotection. Tissue was then embedded in TissueTek O.C.T. and stored at -80°C until being cryosectioned (30μm) as previously described (Solomon et al., 2006).

3.3.4 Histology

Free floating spinal cord sections were permeabilized using a 0.3% Triton-X solution in PBS (PBST) at room temperature. Sections were incubated in 25% normal goat serum (v/v; NGS), 3% bovine serum albumin (w/v; BSA) in PBST blocking buffer for 1 hour at room temperature. Antibody buffer consisted of 10% NGS and 3% BSA in PBST; sections were incubated in primary antibody overnight at 4°C and secondary antibody for 2 hours at room temperature.

To identify macrophages, antibody to the ionized Ca^{++}-binding adapter molecule 1 (Iba1; 1:1000; Wako) was used; antibody to CD31 (PECAM-1; 1:800;

79

BD Pharmingen) identified vascular endothelium. Anti-alpha laminin was used to stain basal lamina and anti-alpha smooth muscle actin was used to identify pericytes. An antibody to the mannose receptor (ManR) was used to identify perivascular microglia (Galea et al, 2006; Abcam; 1:3000), antibody to CD3 (BD Pharmingen, San Diego, CA) was used to identify lymphocytes. Secondary antibodies used were either a Cy3-conjugated IgG (1:800 for Iba1) or Alexa568-conjugated IgG (1:1000 for CD31 and ManR). Stained sections were slide mounted with Vectashield mounting medium and cover-slipped.

3.3.5 Analysis

Spinal cord sections were analyzed using a Leica epi-fluorescence microscope. GFP+ cells were classified as to location in gray or white matter and by morphology based on a scheme established by Vallieres and Sawchenko (2003). Cell morphology was classified as being round (<10μm), rod-shaped (<20μm), amoeboid, stellate, or elongated

Five lumbar spinal cord sections from mSOD and control mice at 15 weeks of age and at disease end-stage were analyzed and BM cells were quantified. The relative proportion of each morphological type to the total number of GFP+ cells in lumbar spinal cord was compared between mSOD and control groups at 15 weeks and disease end-stage. To determine if the contributions of different morphologies of GFP+ cells varied significantly between spinal cord levels, five lumbar, thoracic and cervical spinal cord sections from end-stage mSOD and age-matched control mice were analyzed. The relative proportion of

each type of morphology was compared between mSOD and control mice, as well as between spinal cord levels. The number of GFP+ cells in lumbar spinal cord sections was compared between end-stage $CX_3CR1^{+/GFP}$ BM transplants in mSOD and controls. In a previous study, we quantified GFP+ cells in transverse sections of spinal cord using the mean number of GFP+ cells from approx. 60 sections/mouse (Solomon et al., 2006). From this earlier work we found that reliable cell counts could be obtained from the mean number of GFP+ cells in 5 sections, where each section was separated by > 150 µm. Reliability was evident by the low SEM values of the resulting means.

Fifty cells of each morphological class in end-stage mSOD GFP+ and $CX_3CR1^{+/GFP}$ BM chimeras were analyzed for expression of Iba1. To determine the proportion of GFP+ cells in spinal cord that were T-lymphocytes, 5 spinal cord sections from each mSOD mouse were analyzed using the pan T-lymphocyte marker CD3. Immunolabeling was evaluated using an epi-fluoresence microscope.

To determine the location of BM cells in relation to PECAM-1-labeled spinal cord blood vessels, five lumbar spinal cord sections from each end-stage mSOD and control GFP+ and $CX_3CR1^{+/GFP}$ BM chimeric mouse was analyzed using epi-fluorescence microscopy. GFP+ cells were judged to be blood vessel-associated if GFP colocalized with PECAM-1 fluorescence. BM cells from each mouse were pooled and the percentage of BM cells associated with blood vessels averaged for each experimental group.

Statistical comparison between total numbers of GFP+ cells in each group was performed using an ANOVA with a Tukey post hoc analysis. To determine if the relative proportion of GFP+ cells classified by morphology changed significantly across groups or between spinal cord levels, data was analyzed using an Aitchinson transformation. For all analyses, a p-value of less than 0.05 was taken as significant.

3.4 Results

3.4.1 BM-derived cells populate the spinal cord and are associated with blood vessels

To evaluate the presence of BM-derived cells in the CNS, we transplanted GFP+ BM into 6 week-old mSOD and age-matched controls. The effectiveness of reconstitution was determined following transplantation and all mice demonstrated successful repopulation (>80% GFP+ leukocytes in peripheral blood). Mice were sacrificed at two time points corresponding to symptoms of early disease (15 weeks) and at disease end-stage (18-21 weeks). In previous work, we established that the number of GFP+ cells in the lumbar spinal cord of pre-symptomatic (10-11 weeks) mSOD mice was not significantly different from control littermates (Solomon et al., 2006).

At 15 weeks, significantly greater numbers of GFP+ cells were observed in the lumbar spinal cord of mSOD mice compared to age-matched controls (p<0.05; Table 3.1). Spinal cord sections from mSOD mice at end-stage had significantly greater numbers of GFP+ cells within the spinal cord compared to

both age-matched controls and mSOD mice at 15 weeks (p<0.001). As shown in

Figure 3.1, GFP+ cells were observed within the gray and white matter of spinal

cord, and the leptomeninges (Figure 3.1A-B). Microgliosis was evident in mSOD

spinal cord using Iba1 immunolabelling (Figure 3.1C-D); Iba1 expression was

increased in mSOD lumbar spinal cord compared to control spinal cord.

Significantly greater numbers of GFP+ cells were observed in mSOD spinal

cords compared to age-matched controls at both the symptomatic (15 weeks)

and disease end-stage, correlating with progressive neurodegeneration and

inflammation.

3.4.2 Morphology of GFP+ cells and immunolabeling

GFP+ cells in spinal cord had a variety of morphologies and were divided

into five morphological groups using a scheme based on that of Vallieres and

Sawchenko (2003), where GFP+ cell shape was classified as round, rod-shaped,

amoeboid, stellate or elongated (Figure 3.1E-I). As reported in Table 3.1,

although significantly more GFP+ BM cells were observed in lumbar spinal cords

of mSOD mice compared to controls at 15 weeks of age, the proportion of each

morphological type to the total GFP+ cell number was similar between mSOD

and control groups. The greatest proportion of cells had a round morphology

followed by an elongated morphology. Rod-shaped and amoeboid GFP+ cells

also made appreciable contributions to the total number of GFP+ cells counted,

whereas stellate cells were the rarest GFP+ cell morphology encountered in both

15 week control and mSOD mice.

In mSOD mice, there was a significant increase (approximately 5 fold; p<0.001) in the number of GFP+ cells in the lumbar spinal cord from 15 weeks to end stage. The proportion of GFP+ cells having a round morphology was substantially reduced at end-stage and there was a concomitant increase in the proportion of GFP+ cells having either amoeboid or stellate morphologies, suggesting that round cells in the CNS altered their morphology with time. The contribution of rod and elongated cells to total GFP+ cell number at 15 weeks and end stage did not differ greatly in mSOD and control mice.

Statistical analysis of the contributions of morphological types in lumbar spinal cord revealed significant differences between mSOD and control groups at disease end-stage (p<0.001). However, within-group comparisons of GFP+ cell morphology at lumbar, thoracic and cervical levels did not reveal significant differences, suggesting the morphological contributions of GFP+ cells is relatively consistent across all levels of spinal cord. In controls, the majority of GFP+ cells were of round and elongated morphologies. In mSOD animals, the greatest proportions of cells were of amoeboid morphology, followed by elongated and round cell morphology. In both control and mSOD mice at end stage, GFP+ cells with a stellate morphology made the smallest contribution to total GFP+ cell number. However, the proportion of stellate cells to the total GFP+ cell number averaged 8.8% in lumbar spinal cord from end-stage mSOD mice whereas in age-matched control mice, the proportion of stellate cells averaged 0.6%. This observation suggests that the inflamed microenvironment of the mSOD spinal

cord either preferentially recruits precursors from the blood or influences the acquisition of a stellate morphology by BM cells within spinal cord.

Stellate cells exhibit a morphology characteristic of microglia and previous studies have demonstrated that cells of this morphology in the CNS usually express high levels of Iba1 immunoreactivity (Vallieres and Sawchenko, 2003). To determine if this was the case, Iba1 expression of fifty cells of each morphological class was evaluated in mSOD spinal cord (Table 3.2). All stellate cells strongly expressed Iba1 indicating that these cells were BM-derived microglia.

Iba1 expression in the other morphological classes ranged from 46 to 62% at end stage, with variability in expression. This is in line with our previous results in which F4/80 expression in GFP+ cells was 80% at disease end-stage (Solomon et al., 2006). Elongated cells expressed Iba1 at levels lower than stellate and amoeboid cells, consistent with the observations of Vallieres and Sawchenko (2003).

A proportion of GFP+ round cells were observed to have large nuclei with a thin rim of cytoplasm and were of a size similar to T-lymphocytes. To verify the phenotype of these cells, five sections from each mSOD mouse were analyzed and round GFP+ cells evaluated for CD3 expression. Our analysis demonstrated that $13.8 \pm 2.0\%$ (mean $\pm$ SEM) of GFP+ round cells immunolabeled with the pan-T-lymphocyte marker CD3.

3.4.3   Relationship of GFP+ cells to spinal cord microvasculature

The relation of GFP+ cells to the spinal cord vasculature was analyzed by immunolabelling spinal cord sections with an antibody to the endothelial protein PECAM-1 (Table 2). BM cells in five lumbar spinal cord sections from end-stage mSOD GFP+ BM chimeras and age-matched controls were classified by morphology and association to blood vessels. As shown in Figure 3.2: A(i-ii) and under higher power in Figure 3.2B, GFP+ cells in the spinal cord of mSOD mice were associated with PECAM1+ endothelial cells at disease end-stage. In end-stage mSOD mice, 89% of elongated cells were located along segments of the microvasculature, some with processes wrapping around the vessel. Furthermore, as illustrated in Figure 3.2: B, 79% of GFP+ cells with stellate morphologies also appear to be associated with blood vessels and their processes contact adjacent vasculature. In end-stage mSOD mice, 89% of elongated BM cells and 79% of stellate cells were associated with blood vessels.

Labeling with anti-alpha laminin, a component of the basal lamina, demonstrated that some elongated GFP+ cells contacted the vascular basal lamina, consistent with their identification as perivascular cells (data not shown). These cells were not pericytes as immunolabelling with anti-alpha smooth muscle actin did not co-localize with any GFP+ cells (data not shown). Furthermore, many elongated cells exhibited immunoreactivity to mannose receptor (ManR), a putative marker of perivascular microglia in mice (Galea et al., 2006). Expression of mannose receptors is considered to be a marker of alternatively activated (M2) macrophages having an anti-inflammatory phenotype (Komohara et al., 2008).

Our experiments show that GFP+ cells having an elongated morphology correspond to perivascular microglia having an abluminal location, weak Iba1 immunoreactivity with some cells having ManR immunoreactivity (Figure 3.3). By disease end-stage, the majority of ManR-positive cells in lumbar spinal cord sections were GFP+ and comprised BM-derived perivascular cells.

3.4.4 GFP+ perivascular cells express CX$_3$CR1

To begin to identify the lineage of those BM cells capable of migrating into the healthy and diseased adult spinal cord, we transplanted mSOD (n=3) and control mice (n=3) with BM from CX$_3$CR1$^{+/GFP}$ donors. Mice were sacrificed at disease end-stage and lumbar spinal cord sections analyzed for CX$_3$CR1$^{+/GFP}$ cells.

The morphology of CX$_3$CR1$^{+/GFP}$ cells in control and mSOD lumbar spinal cord sections were classified following the same scheme used for GFP+ cells (Table 3.3). We evaluated the proportion of each morphological cell type in these mice and found that CX$_3$CR1$^{+/GFP}$ cells contributed to each morphological class. In general, the proportions of CX$_3$CR1$^{+/GFP}$ cells in each class was similar between mSOD and control mice with the exception of stellate morphological class, which made a greater contribution in mSOD spinal cord compared to control (9.4% versus 0.4%, respectively). CX$_3$CR1$^{+/GFP}$FP cells with an elongated morphology represented the greatest contribution of cells in both mSOD and control mice. As in the ubiquitous GFP+ BM transplants, Iba1 expression was analyzed in fifty CX$_3$CR1$^{+/GFP}$ cells of each morphological class

(Table 3.2; Figure 3.4: A-D). In mSOD mice, Iba1 positivity ranged from 70% of round cells to 96% of stellate cells and approximately 80% of all $CX_3CR1^{+/GFP}$ cells in spinal cord expressed Iba1. Similar to previous results using GFP+ BM donors, $CX_3CR1^{+/GFP}$ BM cells within lumbar spinal cord were closely associated with blood vessels and differentiated into perivascular microglia, with 78% of stellate and 92% of elongated BM cells associated with blood vessels (Figure 3.4: E-G).

3.5 Discussion

During embryogenesis, microglia are derived from hematopoietic progenitors that infiltrate and colonize the developing neuroectoderm, establishing the endogenous microglial pool. There are at least two phenotypically distinct populations of microglia within the CNS; ramified, parenchymal microglia and elongated or amoeboid perivascular microglia situated between the glia limitans and the endothelial cells of the blood-brain barrier (Hickey et al, 1992; Vallieres and Sawchenko, 2003; Ascheuer, 2004). A third subset of microglia, termed juxtavascular microglia contact the parenchymal side of the vascular basal lamina and have a morphology distinct from perivascular microglia (Davoust et al., 2008; Gehrmann et al., 1995). In the normal adult CNS, the turnover of parenchymal microglia is low and maintenance of the endogenous population is maintained by the proliferation of CNS-resident microglia and possibly by the migration of BM-derived cells across the blood-

brain barrier under some conditions (Ajami et al., 2007; Messengale et al., 2005; Mildner et al., 2007).

To evaluate the presence of BM-derived cells in spinal cords of mSOD and control mice, we employed BM chimeras and transplanted BM harvested from mice that either ubiquitously express GFP, or mice with restricted GFP expression to cells of the CX_3CR1 lineage ($CX_3CR1^{+/GFP}$), into myeloablated mice. Consistent with our previous results, BM-derived cells are observed in lumbar spinal cords of control and mSOD mice where there is significantly greater cell numbers (8 to 10 fold) in mSOD mice at disease end-stage compared to age-matched controls (Solomon et al., 2006). To further characterize the phenotype of GFP+ and $CX_3CR1^{+/GFP}$ BM cells, we used immunocytochemistry in conjunction with a morphological classification scheme previously described (Vallieres and Sawchenko, 2003).

3.5.1 Identification of BM cells

Morphological analysis of GFP+ BM chimeras differed significantly between the 15 week time point and disease end-stage with a notable increase in the proportion of GFP+ stellate cells at disease end-stage. This increase may be due to changes in the mSOD spinal cord microenvironment, associated with disease progression influencing the entry and/or differentiation of BM-derived cells in the CNS. It has been suggested that BM-derived microglia may initially populate the spinal cord as perivascular microglia and then transmigrate across the glia limitans into the parenchyma, further differentiating into stellate microglia

(Guillemin and Brew, 2004). An alternative possibility is that different tissue macrophages derive from specific monocytic precursors and this may be true of perivascular and parenchymal microglia.

A proportion of perivascular microglia were immunolabeled with antibody to mannose receptor which is a membrane receptor involved in phagocytosis. Mannose receptor expression is also a marker of M2 or "alternative" macrophage activation that is associated with an anti-inflammatory phenotype (Komohara et al., 2008). No BM-derived or resident parenchymal microglia labeled with antibody to ManR, demonstrating a different phenotype and possibly activation pattern between perivascular and parenchymal microglia in the mSOD spinal cord.

In previous work, we observed a population of GFP+ round cells that did not label with the macrophage markers of CD11b or F480 (Solomon et al., 2006). These cells had large nuclei surrounded by a thin rim of cytoplasm and were of a similar size to lymphocytes. Our current work demonstrates immunolabeling of this cell type with antibody to CD3, indicating that a portion of round GFP+ BM cells in mSOD spinal cord are T-lymphocytes. This finding is in agreement with recent studies that suggest T-lymphocytes are active participants in spinal cord inflammation in the mSOD mouse (Chiu et al., 2008; Beers et al., 2008).

In $CX_3CR1^{+/GFP}$ chimeras, BM cells within the spinal cord had a variety of morphologies where nearly half of $CX_3CR1^{+/GFP}$ cells had an elongated morphology, weak Iba1 expression, and resided on the abluminal surface of

blood vessels indicating that these cells are perivascular microglia. An additional

9.4% of $CX_3CR1^{+/GFP}$ BM and 8.8% of GFP+ BM cells had a stellate morphology

and labeled strongly with Iba1, indicating these cells were likely parenchymal

microglia. The majority (~80%) of stellate cells were also associated with blood

vessels and were therefore likely juxtavascular microglia.

Within BM, monocytes can be divided into two subsets; CX_3CR1^{hi}

monocytes are believed to enter lymphoid and non-lymphoid tissues under

homeostatic conditions and CX_3CR1^{lo} cells enter tissues under conditions of

experimental inflammation (Geissmann et al., 2003). The exclusive ligand for

CX_3CR1 is CX_3CL1, also known as fractalkine, and is expressed by a variety of

cells including activated endothelial cells (Umehara et al., 2003) and neurons

(Cardona et al., 2006). CX_3CL1 is a membrane cellular adhesion molecule and,

after proteolytic cleavage of its extracellular domain, as a soluble protein which

functions as a chemoattractant for a variety of cells including monocytes (Huang

et al., 2006).

Our current results employing $CX_3CR1^{+/GFP}$ BM chimeras support the work

of Mildner and colleagues (2007) who employed irradiated $CX_3CR1^{+/GFP}$ BM

chimeric mice to demonstrate that microglia in the adult brain derive from

CX_3CR1+ monocytes. These researchers also demonstrated that this

phenomenon is enhanced in the murine cuprizone demyelination model and

facial axotomy model of neurodegeneration. We observed increased numbers of

$CX_3CR1^{+/GFP}$ cells in mSOD spinal cord compared to controls.

Although we and others have observed BM-derived stellate cells infrequently in the healthy murine CNS, other studies have reported that ramified, Iba1+ parenchymal BM cells are the most frequently observed BM-derived cell type in many regions of normal mouse brain (Simard and Rivest, 2004) and that by 1 year post-transplant, 40% (Hess et al., 2004) of parenchymal microglia in the brain are BM-derived. Our results are in line with those of Hickey and Kimura (1988), who rarely observed parenchymal BM-derived cells having a stellate morphology in wild type rats, as well as those of Vallieres and Sawchenko (2003) who demonstrated that BM-derived cells with a stellate morphology were rare in the brains of murine BM chimeras. Similarly, Kennedy and Abkowitz (1994) evaluated the presence of BM derived microglia in healthy mice 1 year post-transplant and observed that although 30% of perivascular and leptomeningeal microglia had been replaced by BM-derived cells, parenchymal BM-derived microglia were rarely seen.

These previous studies employing chimeric mice as well as our current results support the notion that microglia in the healthy CNS are capable of self-renewal with minimal to no recruitment of hematopoietic progenitors. This is also supported by recent studies using parabiotic animals, or focal BM irradiation (Ajami et al., 2007; Messengale et al., 2005; Mildner et al., 2007; Wagers et al., 2002). Studies using irradiated BM-chimeric murine models of CNS disorders including Alzheimer's disease (Stalder et al., 2005), Parkinson's disease (Rodriguez et al., 2007), facial axotomy (Flugel et al., 2001), and stroke (Priller et al., 2001) have demonstrated that there are significantly greater numbers of BM-

derived cells within the CNS in murine models of CNS disease compared to healthy controls.

A potential gradient for BM cell migration to sites of neurodegeneration may be the level of soluble CX_3CL1 in the spinal cord. Cardona and colleagues (2006) demonstrated that when mice received microinjections of V monocytes, cells migrated away from the site of injection while when non functional $CX_3CR1^{GFP/GFP}$ cells were injected cells remained located at the injection site. The CX_3CR1-CX_3CL1 signaling axis appears to be critical for the migration of CX_3CR1 BM cells within the CNS. However, a substantially larger number of GFP+ BM cells were observed in mSOD and control lumbar spinal cord of ubiquitous GFP+ BM chimeras compared to $CX_3CR1^{+/GFP}$BM chimeras, possibly suggesting other classes of BM cells that are CX_3CR1 negative also populate the spinal cord. However, because $CX_3CR1^{+/GFP}$cells have only one copy of CX_3CR1 and GFP, it cannot be ruled out that fewer cells infiltrated or were detected in the spinal cord as a result of reduced CX_3CR1 or GFP expression, respectively.

This is the first study in which the morphology of CX_3CR1-expressing BM-derived cells has been analyzed in the CNS and demonstrates that the greatest proportion of CX_3CR1+ BM cells in wild-type and mSOD spinal cord had an elongated morphology, were located along blood vessels and labeled weakly with Iba1, all characteristics of perivascular microglia. Our results further suggest that in the mSOD mouse, CX_3CR1+ BM cells differentiate into microglia in a progressive manner, initially populating the spinal cord as perivascular microglia, then crossing the glia limitans to become juxtavascular microglia, and finally

93

migrating into the parenchyma in response to progressive neurodegeneration. Alternatively, specific precursors for perivascular and parenchymal microglia may exist within BM that are recruited differentially from the circulation. The pathological conditions within mSOD spinal cord enhance the ability of CX_3CR1+ cells to populate the spinal cord and differentiate into perivascular or parenchymal microglia.

By employing myeloablated BM chimeras to study the migration of BM cells to and within the CNS, this study demonstrates that in an irradiated mSOD mouse model of ALS, CX_3CR1+ monocytes within BM populate the spinal cord and differentiate into perivascular and parenchymal microglia. Although irradiation appears to be a necessary conditioning step, if other conditioning stimuli are elucidated the ability of these BM cells to enter the spinal cord could be exploited to deliver neurotrophic substances to the CNS.

3.6 Acknowledgements

3.7 Tables

Table 3. 1 GFP+ cell counts and morphology of GFP+ cells in spinal cord at 15 weeks and end-stage in mSOD and age-matched control mice.

A significantly greater number of GFP+ cells was observed in mSOD lumbar spinal cord compared to controls at 15 weeks (a: p<0.05) and end-stage (b: p<0.0001; c: p<0.01). The distrbution of GFP+ cells by morphology was similar between mSOD and control mice at 15 weeks but was significantly different between mSOD and control mice at disease end-stage (p<0.001). The proportion of GFP+ cells with different morphology was also similar between spinal cord levels within mSOD and control groups at disease end-stage.

Genotype	Mean no. of donor cells per section mean ± SEM	% donor cells round mean ± SEM	% donor cells rod-shaped mean ± SEM	% donor cells amoeboid mean ± SEM	% donor cells stellate mean ± SEM	% donor cells elongated mean ± SEM
15 wks						
Lumbar						
con (n=4)	43.9 ± 2.3	44.0 ± 2.4	16.9 ± 2.5	9.6 ± 1.5	0.3 ± 0.2	29.3 ± 2.3
mSOD (n=4)	82.4 ± 7.5[a]	36.4 ± 1.6	15.3 ± 1.6	15.2 ± 1.8	1.3 ± 0.4	31.3 ± 1.8
End-Stage						
Lumbar						
con (n=4)	69.6 ± 6.7	46.5 ± 2.7	13.3 ± 1.5	15.4 ± 1.5	0.6 ± 0.2	24.2 ± 2.0
mSOD (n=4)	431.7 ± 42.3[b]	17.9 ± 1.0	14.1 ± 1.0	28.6 ± 1.6	8.8 ± 3.6	30.9 ± 1.1
Thoracic						
con (n=4)	35.4 ± 4.9	37.8 ± 1.2	5.23 ± 0.6	27.6 ± 0.4	2.1 ± 0.2	27.2 ± 0.6
mSOD (n=4)	284.2 ± 24.8[c]	17.2 ± 0.8	6.4 ± 0.2	33.3 ± 0.7	17.5 ± 0.3	25.5 ± 0.1
Cervical						
con (n=4)	65.7 ± 3.5	32.0 ± 0.9	7.7 ± 0.2	31.0 ± 0.2	5.0 ± 0.5	24.3 ± 0.7
mSOD (n=4)	685.2 ± 64.5[c]	31.7 ± 1.9	8.3 ± 0.2	31.2 ± 0.5	4.7 ± 1.0	24.1 ± 0.5

Table 3. 2 Percentage of GFP+ and CX$_3$CR1$^{+/GFP}$ BM cells expressing Iba1 and association of BM cells with lumbar spinal cord blood vessels as a function of cell morphology.

BM Donor	Genotype	Percentage of BM cells expressing Iba1				
		Round	Rod	Amoeboid	Stellate	Elongated
GFP+	mSOD	56	46	60	100	62
CX$_3$CR1$^{+/GFP}$	mSOD	70	72	90	96	74

		Percentage of Round GFP+ CD3+ Cells (mean ± SEM)
GFP+	mSOD	13.8 ± 2.0

BM Donor	Genotype	Association of BM cells with lumbar spinal cord blood vessels (Percentage)				
		Round mean ± SEM	Rod mean ± SEM	Amoeboid mean ± SEM	Stellate mean ± SEM	Elongated mean ± SEM
GFP+	Control	70.4 ± 4.1	84.7 ± 4.4	68.1 ± 7.1	93.3 ± 5.8	97.3 ± 1.1
	mSOD	32.2 ± 4.3	58.6 ± 12.2	49.2 ± 10.4	79.4 ± 1.0	89.2 ± 0.9
CX$_3$CR1$^{+/GFP}$	Control	65 ± 14.4	90.5 ± 12.1	82.5 ± 6.5	66.7 ± 2.5	95.6±2.7
	mSOD	55.1 ± 8.2	79.9 ± 9.5	70.9 ± 3.8	100 ± 0	92.4 ± 2.7

Table 3. 3 Morphology of CX$_3$CR1$^{+/GFP}$ cells in mSOD and control lumbar spinal cord.

Greater numbers of CX$_3$CR1$^{+/GFP}$ BM cells populate the spinal cords of mSOD mice compared to age-matched controls at disease end stage. CX$_3$CR1+ donor cells in the mSOD and control spinal cord often exhibit an elongated morphology**.**

Genotype	Mean number of donor cells per section	% donor cells round	% donor cells rod-shaped	% donor cells amoeboid	% donor cells stellate	% donor cells elongated
	mean ± SEM	mean ± SEM	mean ± SEM	mean ± SEM	mean ± SEM	mean ± SEM
Control (n=3)	12.2 ± 1.5	10.8 ± 4.2	3.8 ± 1.8	29.8 ± 5.2	0.4 ± 0.4	55.4 ± 4.4
mSOD (n=3)	87.9 ± 7.7	10.6 ± 0.9	6.8 ± 0.6	27.9 ± 1.8	9.4 ± 1.2	45.4 ± 1.7

3.8 Figures

Figure 3. 1 Increased numbers of GFP+ cells and Iba1 immunoreactivity are observed in mSOD lumbar spinal cord compared to controls.

GFP+ BM cells are present in the leptomeninges and parenchyma of control and mSOD lumbar spinal cord (green channel; A,B). Increased numbers of Iba1+ cells are seen in mSOD spinal cord compared to controls (red channel; C,D). GFP+ cells observed in lumbar spinal cord of control and mSOD mice were classified as round (E), rod-shape (F), amoeboid (G), stellate (H), or elongated (I).
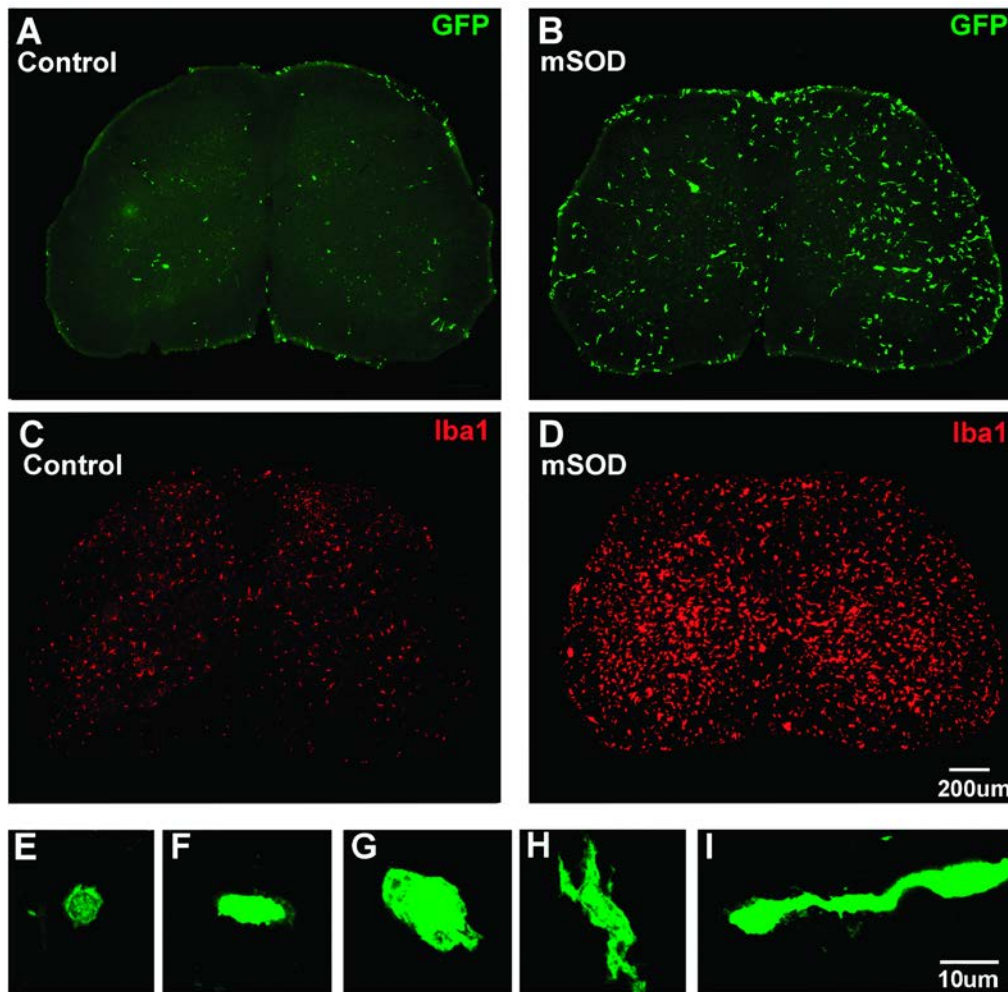
Figure 3. 2 Relation of GFP+ cells to vascular elements within the lumbar spinal cord.

(Ai) GFP+ cells (green channel) observed within lumbar spinal cord of mSOD and control mice remained associated with microvasculature immunolabelled with antibody to endothelial protein PECAM1 (Aii; green and red channel overlay). (B) GFP+ elongated cells reside along blood vessels immunolabelled with PECAM1 within spinal cord (green and red channel overlay).
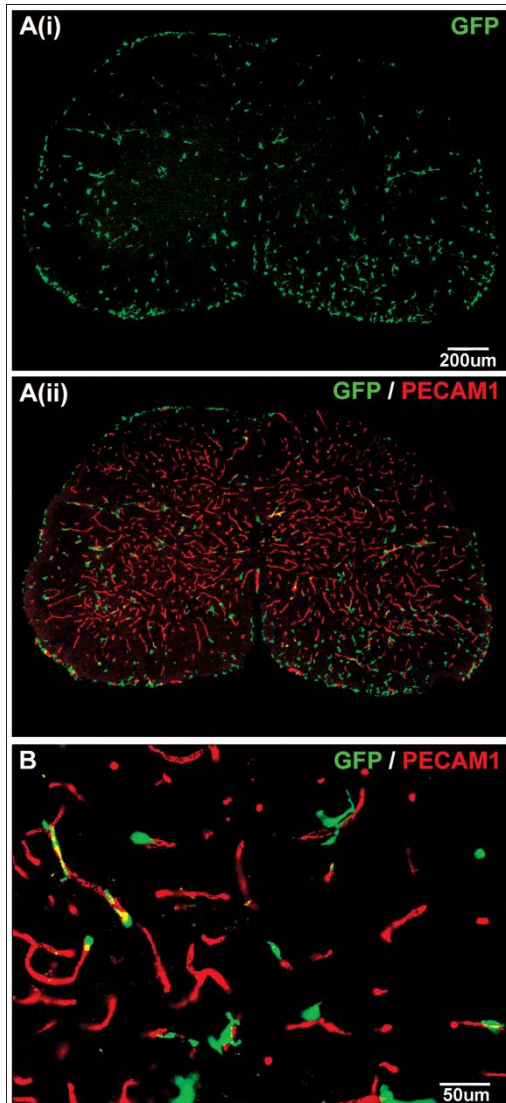
Figure 3. 3 GFP+ elongated cells express ManR.

In end stage mSOD lumbar spinal cord, elongated GFP+ cells immuno label with antibody to the perivascular macrophage marker ManR (middle panel, red channel). By disease end-stage, nearly all ManR+ cells were GFP+ (last panel; red and green channel overlay).
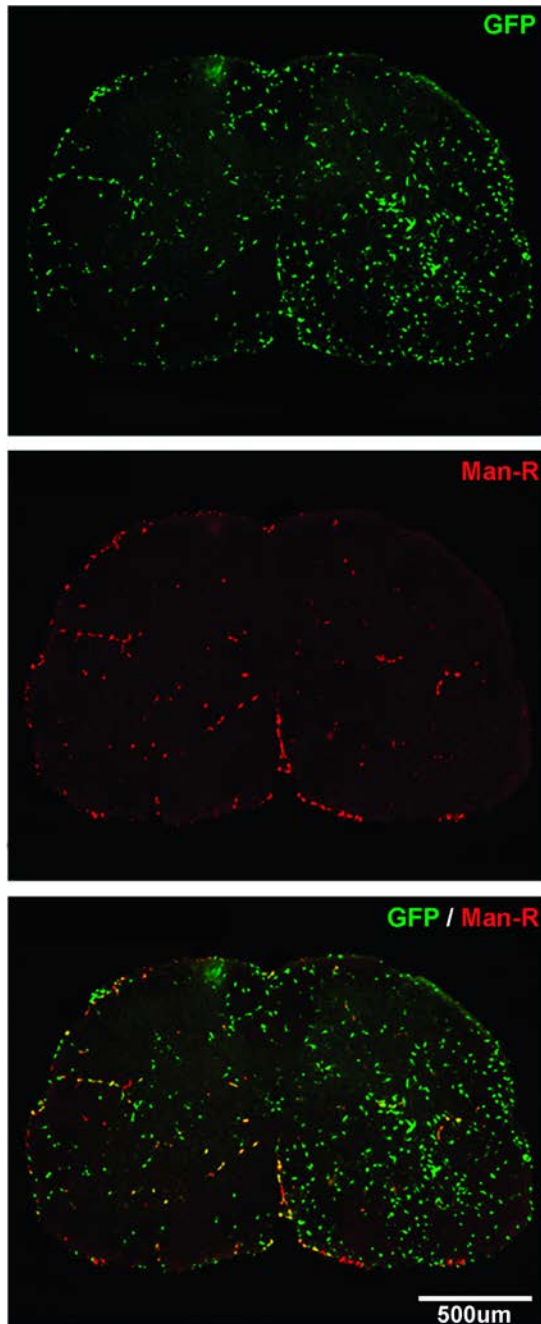
Figure 3. 4 CX3CR1+ BM cells Iba1 expression and ralation to vascular elements in mSOD lumbar spinal cord.

(A) Some CX$_3$CR1+ cells (green channel) in the mSOD spinal cord express the monocyte/macrophage marker Iba1 (B; red and green channel overlay). (C,D) Image of a stellate-shaped CX$_3$CR1+ cell immunolabelled with Iba1 at increased magnification.   (E-G) Elongated CX$_3$CR1+ cells (green channel) reside on the abluminal surface of endothelial cells immunolabelled with PECAM1 (red and green channel overlay).
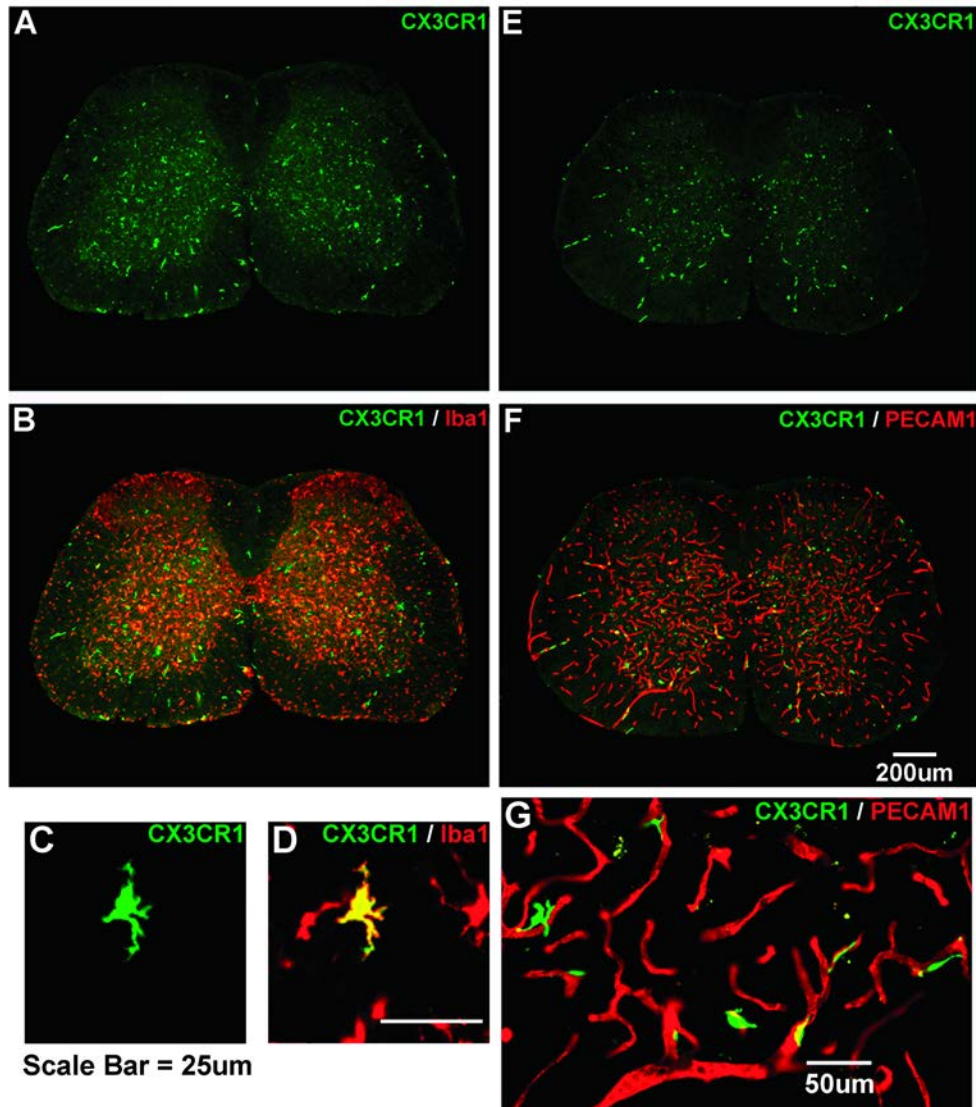
3.9 References

Ajami B, Bennett JL, Krieger C, Tetzlaff W, Rossi FM (2007) Local self-renewal can sustain CNS microglia maintenance and function throughout adult life. Nat Neurosci. 10: 1538-43.

Alexianu ME, Kozovska M, Appel SH (2001) Immune reactivity in a mouse model of familial ALS correlates with disease progression. Neurology. 57: 1282-89.

Asheuer M, Pflumio F, Benhamida S, Dubart-Kupperschmitt A, Fouquet F, Imai Y, Aubourg P, Cartier N (2004) Human CD34+ cells differentiate into microglia and express recombinant therapeutic protein. Proc Natl Acad Sci U S A. 101: 3557-62.

Beers DR, Henkel JS, Xiao Q, Zhao W, Wang J, Yen AA, Siklos L, McKercher SR, Appel SH (2006) Wild type microglia extend survival in PU.1 knockout mice with familial amyotrophic lateral sclerosis. Proc Natl Acad Sci U S A. 103: 16021-16026.

Beers DR, Henkel JS, Zhao W, Wang J, Appel SH (2008) CD4+ T cells support glial neuroprotection, slow disease progression, and modify glial morphology in an animal model of inherited ALS. Proc Natl Acad Sci U S A. 105: 15558-63.

Boillée S, Yamanaka K, Lobsiger CS, Copeland NG, Jenkins NA, Kassiotis G, Kollias G, Cleveland DW (2006) Onset and progression in inherited ALS determined by motor neurons and microglia. Science 312: 1389-92.

Bruijn LI, Miller TM, Cleveland DW (2004) Unraveling the mechanisms involved in motor neuron degeneration in ALS. Annu Rev Neurosci. 27: 723-49.

Cardona AE, Pioro EP, Sasse ME, Kostenko V, Cardona SM, Dijkstra IM, Huang D, Kidd G, Dombrowski S, Dutta R, Lee JC, Cook DN, Jung S, Lira SA, Littman DR, Ransohoff RM (2006) Control of microglial neurotoxicity by the fractalkine receptor. Nat Neurosci. 9: 917-24.

Chiu IM, Chen A, Zheng Y, Kosaras B, Tsiftsoglou SA, Vartanian TK, Brown RH Jr, Carroll MC (2008) T lymphocytes potentiate endogenous neuroprotective inflammation in a mouse model of ALS. Proc Natl Acad Sci U S A. 105: 17913-8.

Clement AM, Nguyen MD, Roberts EA, Garcia ML, Boillee S, Rule M, McMahon AP, Doucette W, Siwek D, Ferrante RJ, Brown RH Jr, Julien JP, Goldstein LS, Cleveland DW (2003) Wild-type non-neuronal cells extend survival of SOD1 mutant motor neurons in ALS mice. Science 302: 113-117.

Davis EJ, Foster TD, Thomas WE (1994) Cellular forms and functions of brain microglia. Brain Res Bull. 34:73-8.

Davoust N, Vuaillat C, Androdias G, Nataf S (2008) From bone marrow to microglia: barriers and avenues. Trends Immunol. 29: 227-34.

Flügel A, Bradl M, Kreutzberg GW, Graeber MB (2001) Transformation of donor-derived bone marrow precursors into host microglia during autoimmune CNS inflammation and during the retrograde response to axotomy. J Neurosci Res. 66: 74-82.

Galea I, Palin K, Newman TA, Van Rooijen N, Perry VH, Boche D (2005) Mannose receptor expression specifically reveals perivascular macrophages in normal, injured, and diseased mouse brain. Glia 49: 375-84.

Gehrmann J, Matsumoto Y, Kreutzberg GW (1995) Microglia: intrinsic immuneffector cell of the brain. Brain Research Reviews 20: 269-287.

Geissmann F, Jung S, Littman DR (2003) Blood monocytes consist of two principal subsets with distinct migratory properties. Immunity 19: 71-82.

Guillemin GJ, Brew BJ (2004) Microglia, macrophages, perivascular macrophages, and pericytes: a review of function and identification. J Leukoc Biol. 75; 388-97.

Gurney M., Pu H, Chiu AY, Dal Canto MC, Polchow CY, Alexander DD, Caliendo J, Hentati A, Kwon YW, Deng HX, et al. (1994) Motor neuron degeneration in mice that express a human Cu, Zn superoxide dismutase mutation. Science 264: 1772–1775.

Hess DC, Abe T, Hill WD, Martin-Studdard A, Carothers J, Masuya M, Fleming PA, Drake CJ, Ogawa M (2004) Hematopoietic origin of microglial and perivascular cells in brain. Exp. Neurol.186: 134-144.

Hickey WF, Kimura H (1988) Perivascular microglial cells of the CNS are bone marrow-derived and present antigen in vivo. Science 239: 290-2.

Hickey WF, Vass K, Lassmann H (1992) Bone marrow-derived elements in the central nervous system: an immunohistochemical and ultrastructural survey of rat chimeras. J Neuropathol Exp Neurol. 51: 246-56.

Huang D, Shi FD, Jung S, Pien GC, Wang J, Salazar-Mather TP, He TT, Weaver JT, Ljunggren HG, Biron CA, Littman DR, Ransohoff RM (2006) The neuronal chemokine CX3CL1/fractalkine selectively recruits NK cells that modify experimental autoimmune encephalomyelitis within the central nervous system. FASEB J. 20: 896-905.

Imai Y, Ibata I, Ito D, Ohsawa K, Kohsaka S (1996) A novel gene iba1 in the major histocompatibility complex class III region encoding an EF hand protein expressed in a monocytic lineage. Biochem Biophys Res Commun. 224: 855-62.

Jaarsma D, Teuling E, Haasdijk ED, De Zeeuw CI, Hoogenraad CC (2008) Neuron-specific expression of mutant superoxide dismutase is sufficient to induce amyotrophic lateral sclerosis in transgenic mice. J Neurosci. 28: 2075-88.

Jung S, Aliberti J, Graemmel P, Sunshine MJ, Kreutzberg GW, Sher A, Littman DR (2000) Analysis of fractalkine receptor CX(3)CR1 function by targeted deletion and green fluorescent protein reporter gene insertion. Mol Cell Biol. 20: 4106-14.

Kennedy DW, Abkowitz JL (1997) Kinetics of central nervous system microglial and macrophage engraftment: analysis using a transgenic bone marrow transplantation model. Blood 90: 986-993.

Komohara Y, Ohnishi K, Kuratsu J, Takeya M (2008) Possible involvement of the M2 anti-inflammatory macrophage phenotype in growth of human gliomas. J Pathol. [Epub ahead of print].

Massengale M, Wagers AJ, Vogel H, Weissman IL (2005) Hematopoietic cells maintain hematopoietic fates upon entering the brain. J Exp Med. 201: 1579-89.

Mildner A, Schmidt H, Nitsche M, Merkler D, Hanisch UK, Mack M, Heikenwalder M, Brück W, Priller J, Prinz M (2007) Microglia in the adult brain arise from Ly-6ChiCCR2+ monocytes only under defined host conditions. Nat Neurosci. 10: 1544-53.

Priller J, Flugel A, Wehner T, Boentert M, Haas CA, Prinz M, Fernández-Klett F, Prass K, Bechmann I, de Boer BA, Frotscher M, Kreutzberg GW, Persons DA, Dirnagl U (2001) Targeting gene-modified hematopoietic cells to the central nervous system: use of green fluorescent protein uncovers microglia engraftment. Nat. Med. 7: 1356-1361.

Rodriguez M, Alvarez-Erviti L, Blesa FJ, Rodríguez-Oroz MC, Arina A, Melero I, Ramos LI, Obeso JA (2007) Bone-marrow-derived cell differentiation into microglia: a study in a progressive mouse model of Parkinson's disease. Neurobiol Dis. 28: 316-25.

Simard AR & Rivest S (2004) Bone marrow stem cells have the ability to populate the entire central nervous system into fully differentiated parenchymal microglia. FASEB J. 18: 998-1000.

Solomon JN, Lewis CA, Ajami B, Corbel SY, Rossi FM, Krieger C (2006) Origin and distribution of bone marrow-derived cells in the central nervous system in a mouse model of amyotrophic lateral sclerosis. Glia 53: 744-53.

Stalder AK, Ermini F, Bondolfi L, Krenger W, Burbach GJ, Deller T, Coomaraswamy J, Staufenbiel M, Landmann R, Jucker M (2005) Invasion of hematopoietic cells into the brain of amyloid precursor protein transgenic mice. J Neurosci. 25: 11125-32.

Strong MJ, Kesavapany S, Pant HC (2005) The pathobiology of amyotrophic lateral sclerosis: a proteinopathy? J Neuropathol Exp Neurol. 64: 649-64.

Umehara H, Bloom ET, Okazaki T, Nagano Y, Yoshie O, Imai T (2004) Fractalkine in vascular biology: from basic research to clinical disease. Arterioscler Thromb Vasc Biol. 24: 34-40.

Vallières L, Sawchenko PE (2003) Bone marrow-derived cells that populate the adult mouse brain preserve their hematopoietic identity. J Neurosci. 23: 5197-207.

Wagers AJ, Sherwood RI, Christensen JL, Weissman IL (2002) Little evidence for developmental plasticity of adult hematopoietic stem cells. Science 297: 2256-9.

Xiao Q, Zhao W, Beers DR, Yen AA, Xie W, Henkel JS, Appel SH (2007) Mutant SOD1(G93A) microglia are more neurotoxic relative to wild-type microglia. J Neurochem. 102: 2008-19.

4: BONE MARROW-DERIVED CELLS ACCUMULATE IN THE SPINAL CORD IN A MOUSE MODEL OF AMYOTROPHIC LATERAL SCLEROSIS IN THE ABSENCE OF IRRADIATION

4.1 Abstract

Experimental evidence suggests that the preconditioning effects of irradiation employed to create BM chimeric rodents are requisite for bone marrow-derived cell (BMDC) accumulation in the healthy and diseased central nervous system (CNS). In order to improve the clinical potential of BMDCs as treatment vehicles for neurodegenerative diseases alternative preconditioning regimens that potentiate BMDC entry into the CNS must be elucidated. Treatment with the hyperosmolyte mannitol results in the efflux of water from endothelial cells, resulting in their shrinkage and disruption of the blood-brain barrier (BBB). We treated transgenic mice that over-express human mutant superoxide dismutase 1 (mSOD), a murine model of amyotrophic lateral sclerosis (ALS), with mannitol prior to injection of BM harvested from mice that express green fluorescent protein (GFP) to investigate whether this conditioning regimen potentiates BMDC entry into the diseased spinal cord. Analysis of spinal cord 3 days after treatment revealed an absence of BMDCs, indicating this conditioning regimen did not enable BMDC accumulation in the CNS. The chemotherapeutic

BU was employed to determine whether using myelosuppressive regimens alternative to irradiation to create GFP+ BM chimeric mice potentiate BMDC entry into the CNS of control and mSOD mice. Intraperitoneal treatment with BU at a dose of 100mg/kg followed by intravenous injection of whole GFP+ BM resulted in high levels of chimerism.   BMDCs accumulated in the spinal cords of control and mSOD mice, with a majority of BMDCs in mSOD spinal cord differentiating into CNS-associated macrophages. Cytotoxic T-cells were also observed in the spinal cords of mSOD and control mice, suggesting BU at the dose employed here has neurotoxic and neuroinflammatory effects. This was further supported by histological analysis of control spinal cord at 2 weeks post-treatment, which exhibited microglia with reactive morphology.

4.2 Introduction

Currently, a significant limitation to the treatment of neurodegenerative disorders is the inability of many pharmaceuticals to enter the central nervous system (CNS), which is surrounded by a specialized endothelial network, the blood-brain barrier (BBB) that strictly regulates the transmission of blood-borne substances and cells into the CNS. The impermeability of the BBB prevents all large molecular weight drugs and the majority of low molecular weight drugs from reaching affected areas during CNS pathology (Pardridge, 2003). Although small molecule lipid-soluble drugs can permeate the endothelial cells of the BBB, these molecules are substrates for efflux proteins belonging to the ATP-binding cassette protein family of transmembrane transporters, which effectively remove

these drugs from the CNS (Loscher and Potschka, 2005). The inefficacy of pharmaceuticals in altering the progression of neurodegenerative diseases has spurred research into alternative treatment modalities.

Clinical and experimental observations indicate that under certain conditions, bone marrow-derived cells (BMDCs) can transmigrate across the BBB and take up residence within the CNS. In patients that received gender-mismatched bone marrow (BM) transplants, limited numbers of donor-derived cells were observed in the CNS at autopsy, demonstrating that under these transplantation conditions BM cell accumulation within the CNS can occur (Unger et al., 1993; Appel et al., 2008). Studies employing BM chimeric rodents created using a myeloablative irradiation/BM transplantation paradigm have also demonstrated that BMDCs migrate to and populate the CNS (Hickey and Kimura, 1988; Hickey et al., 1993; Hess et al., 2004).   Furthermore, in BM chimeric murine models of neurodegenerative diseases including Parkinson's disease (Kokovay and Cunningham, 2005; Keshet et al., 2007; Rodriguez et al., 2007), Alzheimer's disease (Malm et al., 2005; Stalder et al., 2005), and amyotrophic lateral sclerosis (ALS; Corti et al., 2004; Solomon et al., 2006; Chiu et al., 2008; Lewis et al., 2009), the numbers of BMDCs populating the diseased CNS was significantly greater than in healthy controls, suggesting BMDCs home to and/or expand at sites of neurodegeneration. These observations underscore the potential of BMDCs to function as therapeutic vehicles for the treatment of neurodegenerative diseases.

Analysis of the phenotype of BMDCs residing in the CNS indicates that the majority of BMDCs differentiate into CNS-associated macrophages, such as perivascular cells and other cell types, with a small proportion acquiring the morphology and anatomical location of microglia (Vallieres and Sawchenko, 2003; Lewis et al., 2009). In transgenic mice overexpressing mutant superoxide dismutase (mSOD), a mouse model of ALS, increasing numbers of BMDCs were observed in the lumbar spinal cord as motoneuron degeneration progressed (Solomon et al., 2006). Although in mSOD mice the total number of BM-derived microglia increased with disease progression, the relative contribution of BMDCs to the total microglial pool remained at roughly 10 to 20% throughout the course of the disease (Solomon et al., 2006, also see Ginhoux et al., 2010). Notably, in age-matched control mice, no significant increase in the number of BMDCs accumulating in the spinal cord was observed between time points (Solomon et al., 2006).

A significant caveat to using BM chimeras to study the migration of BMDCs into the CNS is that the means by which BM chimeric mice are generated introduces two confounding variables. The first is that in order to myeloablate hosts, mice are subjected to lethal levels of irradiation, which has been shown to induce changes in BBB permeability and incite an inflammatory response (Ramanan et al., 2010).   Secondly, hosts receive intravenous injections of whole BM, which includes progenitor populations that would not otherwise be present in the circulation. Studies employing parabiosis, an experimental paradigm in which the circulations of two genetically distinct mice

are surgically joined resulting in peripheral blood cell (PBC) chimerism, have demonstrated that in the absence of irradiation, very few BMDCs are observed within the healthy CNS and in models of neurodegenerative disease (Massengale et al., 2005). However, when one parabiont was exposed to myeloablative levels of radiation while a lead shield protected the other, similarly few BMDCs were observed within the irradiated CNS even after incurring facial axotomy (Ajami et al., 2007). These results suggest that irradiation alone is insufficient for BMDC migration into the CNS and the presence of circulating BM progenitor cells is also required (Ajami et al., 2007).

The deleterious side effects associated with myeloablative levels of radiation including immunosuppression, make it an unacceptable preparative regimen to potentiate BMDC infiltration into the diseased CNS of patients and alternative conditioning regimens must be investigated. Clinical osmotherapy employs hypertonic sugar or saline solutions for the treatment of brain edema and to enhance the delivery of chemotherapeutics into the CNS. In vitro studies have demonstrated that incubating cultured monolayers of brain endothelial cells with hyperosmotic arabinose solutions results in the reversible separation of tight junctions between endothelial cells and increased barrier permeability (Dorovini-Zis et al., 1987). Similarly, intravenous injections of hypertonic mannitol solutions result in the efflux of water from endothelial cells of the BBB, resulting in their shrinkage, the transient disruption of tight junctions and an overall increase in BBB permeability (Rapoport, 2001). Studies have demonstrated that preconditioning rodents with hypertonic mannitol solutions can enhance the

transmission of viral vectors and cells into the CNS. Wu and colleagues demonstrated that preconditioning of mice with either bradykinin or 20% mannitol (w/v) followed by intracarotid or intravenous injection of monocytes increased the numbers of transferred cells that infiltrated the brain (Wu et al., 2006). Therefore, BBB disruption induced by hypertonic mannitol solutions may represent one means of enhancing the migration of BMDCs into the CNS without the deleterious effects associated with irradiation and without reconstituting recipients with genetically modified BM.

Chemotherapeutic drugs employed clinically for the treatment of hematologic cancers provide an alternative means by which to myeloablate host animals. Busulfex (BU) is a clinically well-established alkylating antineoplastic agent used to myelosuppress patients prior to receiving BM transplants. Myelosuppression using BU is an attractive alternative to irradiation as BU leaves the patient's immune system intact, while irradiation leaves patients severely immunocompromised (Yeager et al., 1993). Furthermore, BU is selectively toxic to primitive quiescent hematopoietic stem cells (HSCs), whereas other chemotherapeutics such as cyclophosphamide, 5-fluorouracil and melphalan are toxic to more mature dividing BM progenitors and as such, have only transient cytoreductive effects in BM (Nevozhay and Opolski, 2006). In mice the myeloablative dose of BU has been reported to be between 135 to 150mg/kg (Enquist et al., 2009; Hsieh et al., 2007) and studies in which mice were treated with BU doses below this obtained variable levels of BM chimerism. Intraperitoneal (IP) injection of 9 day old mice with 50mg/kg BU followed by the

IP injection of 30x10^6 BM cells and splenocytes resulted in 87.3% peripheral blood cell (PBC) chimerism (Yeager et al., 1993). Similarly reports of PBC chimerism of 20-40% at 32 weeks post-transplant has been reported after a single IP treatment of 20mg/kg BU and intravenous injection of 15x10^6 BM cells (Andersson et al., 2003).

Yeager and colleagues (1993) used the twitcher mouse, a model of demyelinating sphingolipid storage disease caused by a genetic galactosylceramidase deficiency, to demonstrate that treatment of mice with BU followed by BM transplantation increased galactosylceramidase activity in the brain; the authors inferred this increase was due to donor-derived mononuclear cells infiltrating the brains of the twitcher mice (Yeager et al., 1993). Although this was not verified histologically, Espejel and colleagues (2008) did observe BMDCs in the cerebellum of murine neonates that received BU during gestation. In line with these observations, recent work suggests that BU damages endothelium, as indicated by the presence of increased numbers of circulating endothelial cells and their progenitors after BU treatment (Zeng et al., 2010). BU-induced disruption of the BBB may therefore enable BMDC infiltration into the CNS.

Here we employ the mSOD mouse model of ALS to investigate the efficacy of preconditioning with hypertonic solutions of mannitol prior to BM transfer at enhancing the migration of BMDCs to the diseased spinal cord. We will also determine whether irradiation is requisite for BMDC migration into the CNS of BM chimeras created by myelosuppressing mice using BU rather than

radiation, followed by BM injection. The results of these studies may present alternative treatment regimens to irradiation that enhance the migration of BMDCs into the diseased CNS thereby improving the clinical potential of BMDCs as treatment vehicles in neurodegenerative diseases.

4.3 Methods

4.3.1 Animals:

Transgenic SJL.B6 mice that over-express human SOD1 (G93A) missense mutation (mSOD) were bred from progenitor stock obtained from Jackson Laboratories (Bar Harbour, ME) and were maintained as heterozygotes by breeding mSOD males with non-transgenic females. Mouse progeny were genotyped for mSOD transgene using a protocol established by Gurney and colleagues (Gurney et al., 1994). The mSOD mice develop progressive motoneuron degeneration, culminating in muscle atrophy and eventually hind limb paralysis (Gurney et al., 1994).   Age-matched, non-transgenic mice were used as controls and sacrificed at the same time point as mSOD animals.

Mice that ubiquitously express green fluorescent protein (GFP) under the control of the B-actin promoter (C57BL/6; GFP/CD45.2) were obtained from Dr. I. Weissmann via Dr. F. Rossi and were bred and maintained as heterozygotes at the Animal Research Facility (ARC) at Simon Fraser University (SFU). GFP-expressing mice aged 8 weeks to 6 months served as BM donors and BM was harvested by flushing fermurs and tibiae with sterile PBS using a syringe. Male

BM recipients received only male BM while female recipients received either male or female BM to avoid any graft-versus-host effects.

Animals were provided food and water ad libitum; all protocols related to the use of animals were approved by the SFU Animal care committee and were in compliance with the Canadian Council on Animal Care, the NIH Guide for the Care and Use of Laboratory Animals, and the EEC Council Directive.

4.3.2 Mannitol Treatment

A hypertonic solution of 20% mannitol in PBS was prepared and passed through a filter to remove any undissolved particles.   Advanced mSOD mice were treated with 0.5g/kg of mannitol by lateral tail vein injection. As per a protocols established by Wu and colleagues (2006), twenty minutes after mannitol injection 30×10^6 BM cells harvested from GFP-expressing mice were transferred into hosts via tail vein injections. Three days after treatment, mice were sacrificed at which time spinal cord and brain were collected and analyzed for the presence of GFP+ BMDCs.

4.3.3 Nonirradiative myeloablation

Control and presymptomatic mSOD mice aged 9 weeks were used for the following experiments. The chemotherapeutic drug BU for injection (Otsuka Pharmaceuticals, Japan) was diluted from the pharmaceutical stock solution to a concentration of 3mg/mL using sterile PBS. Three different treatment regimens were employed:

Group 1: Control (n=3) and mSOD (n=1) mice received 80 mg/kg BU delivered in 4 fractionated doses of 20mg/kg a day via IP injection for 4 days followed by intravenous (IV) injection of 5.0×10^5 enriched GFP+ BM cells 24 hours after the last BU treatment. This protocol was based on unpublished work by Berry carried out under the supervision of Dr. Keith Humphries (Berry, 2003). GFP+ BM donors were treated with 150mg/kg of 5-fluorouracil (5FU; Hospira, USA) 4 days before BM harvest in order to increase the number of cycling HSCs. 5FU is selectively toxic to rapidly dividing cells and induces the cycling of quiescent HSCs within the BM. Treating donors with 5FU destroys more mature cycling progenitors within BM, thereby increasing the frequency of HSCs in BM from 1/10,000 to 1/3000 cells (Szilvassy et al., 1999), while another study equated the transplantation of 5×10^5 enriched BM cells with 5×10^6 whole BM cells (Enquist et al., 2009). Blood samples from treated mice were taken beginning at 3 weeks post-transplant and analyzed via flow cytometry using a BD Aria FACS machine (Becton-Dickenson, NJ, USA) to determine the proportion of donor-derived PBCs, as described previously (Solomon et al., 2006).

Group 2: Control (n=13) and mSOD (n=12) received 100 mg/kg BU treatment delivered in 5 fractionated IP doses of 20mg/kg a day for 5 days; this dose is still below the reported myeloablative dose of 150mg/kg. Twenty-four hours after the final BU treatment, mice received 30×10^6 GFP+ whole BM cells and PBC chimerism was analyzed beginning at 3 weeks post-transplant

Group 3: Control mice (n=6) were treated with daily IP injections of freshly diluted BU at a dose of 20mg/kg for 5 days (total dose 100mg/kg). Twenty-four

hours after the final BU treatment mice received 30x10^6 GFP+ whole BM cells via tail vein injection. Blood samples were collected beginning at 1 week post-transplant and labeled with lymphoid (CD3 for T-cells, B220 for B-cells; conjugated to PeCy7 fluorophore) and myeloid (Gr1 for granulocytes, CD11b for MO; conjugated to APC fluorophore) lineage markers to analyze PBC chimerism. Mice were sacrificed at 2 (n=3) and 4 (n=3) weeks post-transplant to analyze the kinetics of GFP+ BMDC entry into the spinal cord.

4.3.4 Tissue Processing

Mice in groups 1 and 2 were sacrificed once mSOD mice had progressed to advanced disease stages, as defined as mice exhibiting a severe rolling gait, dragging hind limbs, or being unable to right themselves after lateral recumbency. Mice were euthanized using CO_2 and immediately transcardially perfused with 30 mL of 1xPBS followed by 30 mL of 4% paraformaldehyde (w/v; PFA).   The spinal cord was dissected out, post-fixed in 4% PFA overnight at 4°C, and then immersed in 20% sucrose (w/v) in PBS at 4°C overnight for cryoprotection. After cryoprotection, tissue was embedded in TissueTek O.C.T. (Sakura Finetek, USA) and stored at -80°C until being cryosectioned at 30 μm as previously described (Solomon et al., 2006).

4.3.5 Immunohistochemistry

Free floating spinal cord sections underwent immunohistochemical analysis as previously described (Lewis et al., 2009). To identify macrophages, antibody to the ionized Ca2+ -binding adapter (Iba1; Wako, VA, USA) was used;

vascular endothelium was labeled using antibody to CD31 (PECAM1; BD

Pharmingen). Monocytes were identified using antibody to CD11b (Serotec,

Raleigh, NC) and antibodies to CD3 and CD8 (BD Pharmingen, San Diego, CA)

were used to identify and classify T-lymphocytes. Secondary antibodies used

were either anti-rabbit Cy3-conjugated IgG (Iba1 visualization; Jackson

Immunoresearch) or anti-rat Alexa568-conjugated IgG (CD3, CD8, CD31

visualization; Molecular Probes). Immunolabeled sections were slide mounted

and coverslipped using Vectashield mounting medium.

4.3.6 Analysis

Spinal cord sections were analyzed using a Leica epifluorescence

microscope and a Nikon laser scanning confocol microscope. GFP+ cells from

each mSOD and control mouse were quantified over 15 lumbar spinal cord

sections separated by at least 150 µm and were classified according to

morphology as previously described (Lewis et al., 2009).   The phenotypes of

GFP+ BMDCs were analyzed using immunohistochemistry, and the numbers of

Iba1+ and CD3+ BMDCs were quantified over 5 lumbar spinal cord sections from

each experimental animal. Quantitative assessment of GFP+ cells within the

spinal cords of mSOD and control mice was statistically evaluated using SPSS

software using a Student's t-test; significance was taken at $p < 0.05$.

4.4 Results:

4.4.1 Mannitol does not enhance the infiltration of BMDCs into the mSOD spinal cord

Three days after receiving GFP+ BM, nonirradiated mSOD mice with advanced disease were sacrificed and blood and spinal cord were collected. Less than 1% of circulating cells were GFP+ (figure 4.1A) and in lumbar spinal cord sections no GFP+ BMDCs were observed, indicating preconditioning with mannitol does not effectively enhance the migration of BMDCs to the spinal cord in the mSOD mouse.

4.4.2 BU myeloablation and BM reconstitution

Three weeks post-transplant, a time point past reported BU-induced nadirs in blood counts (Hsieh et al., 2007), blood samples were analyzed for the percent donor contribution to PBCs. Group 1 (n=4) treated with 80mg/kg and provided 5×10^5 enriched BM cells did not exhibit successful reengraftment as indicated by the absence of GFP+ PBCs.

Successful BM rengraftment is dependent on the extent of myeloablation, which increases both the available niches within BM for donor HSCs to engraft in and the production of proliferative factors within the BM compartment, and the number of HSCs recipients are transplanted with (Nevozhay and Opolski, 2006). As such, for group 2, the BU dose was raised to 100 mg/kg to increase myelosuppression followed by injection of 30×10^6 GFP+ whole BM cells, given our previous success in creating BM chimeric mice by transplanting whole BM following myeloablative irradiation (Solomon et al., 2006; Lewis et al., 2009).

Under this protocol, effective BM reengraftment was obtained in a portion of mice (n=3 control, n= 3 mSOD), with successful transplants exhibiting 75.7 ± 9.7% (mean ± standard deviation (s.d.); averaged over mSOD and control groups) donor chimerism in PBCs at 3 weeks post-transplant which increased to 84.4 ± 7.3% by 5 weeks post-transplant (figure 4.1B). PBC chimerism levels in successfully reengrafted mice were stable over the course of disease progression in mSOD mice (figure 4.2) and analysis of BM indicated that 71.2 ± 7.3% of BM cells were donor derived at 9 weeks post-transplant.

Repeated trials using this protocol yielded highly variable results with some mice exhibiting high levels of donor reengraftment and others none at all; interestingly, intermediate levels of chimersim were not observed at 3 weeks post-transplant. Out of 25 mice treated, only 6 demonstrated successful BM reengraftment. Investigation into factors that might contribute to the high number of unsuccessful transplants suggested that the stability of BU once mixed with sterile PBS is limited to 8 hours (United States Food and Drug Administration).

To determine if using freshly diluted BU improved the frequency of successful BM reengraftment, group 3 (n=6 control mice) was treated with freshly diluted BU rather than that which had been diluted and stored for a period of days at 4°C. Levels of PBC chimersim were analyzed beginning at 1 week post-BM transplant and rates of myeloid and lymphoid PBC reconstitution was analyzed by immunolabelling PBCs with antibodies to Gr-1 and CD11b for myeloid cells, and CD3 and B220 for lymphoid cells. Given that in the previous trial either high levels or absent PBC chimersim was observed in mice, blood samples were

collected starting at 1 week post-transplant to investigate whether some mice obtained transient levels of chimerism that subsided by 3 weeks post-transplant.

By using freshly diluted BU, five out of six treated mice exhibited successful donor reengraftment as indicated by GFP+ donor-derived PBCs. At one week post-transplant, levels of GFP+ PBCs were highly variable and ranged from 7.9 to 52.0% and averaged 32.8 ± 19.9%. Myelomonocytic cells were rapidly reconstituted with donor cells (65.5 ± 24.7% GFP+) owing to their short half-life within the circulation, while lymphoid cell reconstitution (13.8 ± 7.8% GFP+) lagged behind, indicative of the minimal immunosuppressive effect of BU (figure 4.3).   Blood analysis at 2 weeks post-transplant indicated that one mouse that had exhibited ~10% PBC chimerism at 1 week post-transplant was not successfully reconstituted with donor BM, as indicated by the absence of GFP+ PBCs; for all other mice, PBC chimerism was increased over previous values (figure 4.3).

The reason for unsuccessful BM reconstitution may be due to problems arising with IV injection of BM although no obvious difficulties were encountered with BM cell preparation or injection; however, incidents of unsuccessful BM reengraftment after treatment with high doses of BU have been reported elsewhere (Berry, 2003, unpublished work). In successfully transplanted mice, high levels of PBC chimerism averaging 97.1 ± 0.3% were observed at 4 weeks post transplant.   Analysis of BM reconstitution indicated that an average of 57.8 ± 28.0% of BM cells were GFP+ at 2 weeks post-transplant and by 4 weeks post-transplant donor BM reconstitution averaged 88.4± 11.1%; in the mouse that

exhibited only transient PBC chimerism, 0.4% of BM cells were GFP+ at 2 weeks post-transplant. The results of this trial indicate that employing freshly diluted BU increased the frequency of successful BM transplants and high levels (>80%) of donor BM reengraftment were observed in mice at both 2 and 4 weeks post-transplant.

4.4.3 GFP+ BMDCs Accumulate in Control and mSOD Spinal Cords:

After BM transplantation, mSOD mice were allowed to progress to advanced stages of disease at which time spinal cords were harvested and processed. Lumbar spinal cord sections were analyzed for the presence of GFP+ BMDCs. For mice in group 1 which did not exhibit successful donor BM reengraftment, no GFP+ cells were observed within the spinal cord. Mice in group 2 that were successfully reconstituted with donor BM were observed to have GFP+ BMDCs in the lumbar spinal cord, while unsuccessfully transplanted control and mSOD mice had no GFP+ cells in the spinal cord. GFP+ cells were located throughout the grey and white matter of lumbar spinal cord sections, with large numbers of GFP+ cells observed in the leptomeninges surrounding the spinal cord (Figure 4.4A).   These observations are similar to those obtained using irradiated BM chimeric mice in which it is observed the rate of turnover and contribution of BMDCs to leptomeningeal macrophage pools is greater than that to parenchymal microglia within the spinal cord (Hickey et al., 1992; Chinnery et al., 2010).

Quantitative analysis of spinal cord sections demonstrated that numerically greater numbers of GFP+ BMDCs accumulate in the spinal cords of mSOD mice compared to age-matched controls (Figure 4.4B). However, because of the high degree of variability in the number of BMDCs observed in the spinal cords of mice within control and mSOD groups, a statistically significant difference between control and mSOD mice was not obtained ($p > 0.5$).

4.4.4 Analysis of BMDC morphology and immunophenotype:

BMDCs were observed to possess a variety of morphologies and were categorized as being round, rod, amoeboid, stellate or elongated in shape, as described in previous work (table 4.1A; Vallieres and Sawchenko, 2003; Lewis et al., 2009). Elongated BMDCs were often found in association with spinal blood vessels in a perivascular location, exhibiting low levels of Iba1 expression, indicating that these BMDCs acquired the phenotype of perivascular macrophages (Figure 4.5). In control mice, the majority of GFP+ cells were of a round morphology, followed by elongated and rod-shaped cells, while GFP+ cells with stellate and rod-shaped morphologies made the smallest contributions. Comparatively, the majority of GFP+ cells in mSOD mice were observed to have a stellate morphology, followed by rod and elongated cells; round and amoeboid-shaped cells made modest contributions. The differential frequencies of morphological classes between control and mSOD mice likely reflect differences in the spinal cord microenvironments. In mSOD mice, advanced disease stages are associated with widespread microgliosis within the spinal cord and increased

expression of inflammatory mediators (Philips and Robberechts, 2011) which likely influence the differentiation of BMDCs that accumulate within the spinal cord.

Immunolabelling of lumbar spinal cords sections with antibody to Iba1 demonstrated widespread microgliosis in the lumbar spinal cord of mSOD mice, as indicated by an overt increase in the number of Iba1+ cells and an increase in labeling intensity compared to control mice (Figure 4.6). The proportion of GFP+ BMDCs that express Iba1 as a function of cell morphology was quantified and averaged over 5 lumbar spinal cord sections from each mouse; these values were then averaged over mSOD and control groups (table 4.1B). Averaged across all morphological classes, the proportion of BMDCs that expressed Iba1 was 60.2 ± 9.3% and 25.1 ± 1.3% (mean ± s.d.) in mSOD and control lumbar spinal cord sections, respectively. These numbers likely under represent Iba1+ BMDCs as immunohistochemical analyses are often limited by a lack of sensitivity in labeling low-level antigen expression. Furthermore, given that the majority of GPF+ cells in control spinal cords had round, rod and elongated morphologies, the low proportion of Iba1+ GFP+ cells in control mice is not unexpected, as previous studies have demonstrated that BMDCs of these morphological classes in the healthy CNS do not express Iba1 or do so only weakly (Vallieres and Sawchenko, 2003). In control and mSOD spinal cords, the majority (73.9 ± 16.1% and 87.0 ± 10.6%, respectively) of stellate-shaped cells expressed Iba1; the morphology and immunolabelling of these cells with Iba1 together identify these cells as BM-derived microglia.

Five lumbar sections from each treated mouse were immunolabeled with antibody to CD3 to identify and quantify the number of T-cells within spinal cord sections. The numbers of T-cells within mSOD and control lumbar spinal cords was highly variable between mice and when averaged over experimental groups, a substantial difference was observed, with 14.8 ± 15.2 (s.d.) and 60.4 ± 60.2 T-cells per section observed in control and mSOD mice, respectively; the high degree of variability within groups abrogated a statistically significant difference between groups. Although previous studies have observed increased numbers of T-cells in the spinal cords of mSOD mice (Chiu et al., 2008), typically only a few T-cells are observed in age-matched control spinal cords (unpublished data). There was also considerable variability in the origin of T-cells, with some mice primarily exhibiting donor-derived T-cell populations within the spinal cord while in others T-cells were primarily of host origin.

Sections were double immunolabeled with CD3 and CD8 antibodies in order to classify the types of T-cells populating the spinal cord. The majority of T-cells ($88.8 \pm 5.1\%$ in mSOD, $97.2 \pm 2.5\%$ in control mice) were CD8+ identifying these cells as cytotoxic T-cells. The presence of CD8+ T-cells within the CNS is often observed in association with a variety of types of encephalitis, ischemic lesions, and neurodegenerative diseases including ALS, as well as in the CNS of the mSOD mouse; however, they are usually only rarely observed in the healthy CNS (Neumann et al., 2002). BU readily crosses the BBB and clinical side effects associated with treatment includes seizures and deleterious effects on mental development in children (Hassan et al., 1996). The presence of CD8+ T-

124

cells within the spinal cord of control mice treated with BU suggests that treatment with BU at the dose I employed has neurotoxic effects that may induce a neuroinflammatory response, inciting T-cell infiltration into the spinal cord

4.4.5 Kinetics of cell entry into the spinal cord

To analyze the kinetics of BM cell accumulation in the spinal cord, BM chimeric control mice were sacrificed at 2 and 4 weeks post-BM transplant. Mice sacrificed a 2 weeks post-transplant (n=2; 1 mouse omitted due to unsuccessful BM reengraftment) exhibited variable numbers of GFP+ cells in the lumbar spinal cord sections that ranged from an average 3.4 cells per section in one mouse and 13.8 cells per section in another. The vast majority (88.2 ± 0.1%) of GFP+ cells observed in the spinal cord were rod-shaped in morphology and were found in association with blood vessels (figure 4.7A); these cells did not immunolabel with Iba1 and only a portion (32.4 ± 12.4%) immunolabelled with the monocyte marker CD11b. It is possible that some of the rod-shaped cells observed were granulocytes, as reported by Audoy-Remus and colleagues (2008), and additional immunohistochemical studies are underway to identify these cells. T-cells were also observed within spinal cord sections at an average 3.0 ± 0.3 cells per section; these numbers are similar to that observed in control mice not treated with BU (unpublished data). Notably, microglia within the spinal cord of treated mice exhibited a reactive morphology, with slightly thickened processes and increased intensity of Iba1 immunolabelling (figure 4.7B). Analysis of BMDC accumulation in the spinal cords of mice at 4 weeks (n=3) is

currently underway and due to time constraints relating to submission of this thesis, data on the accumulation of BMDCs in the spinal cords of this group will not be included.

4.5   Discussion

Using the clinically well-established chemotherapeutic BU, we have demonstrated that both high levels of BM chimerism and BMDC migration into the CNS can be achieved in the absence of irradiation.

4.5.1   Mannitol treatment does not enhance the migration of BM cells into the mSOD spinal cord

Although preconditioning regimens employing mannitol have been successful at enhancing the migration of PBCs into the CNS in previous studies (Wu et al., 2006; Seyfried et al., 2008), this treatment did not lead to GFP+ BM cell entry into the spinal cord of mSOD mice at advanced stages of disease. One problem that may account for the absence of GFP+ cells into the CNS of mSOD mice is that in both previous studies, BMDC migration into the brain rather than the spinal cord was assessed. Therefore, the protocol I followed may not be optimal for enhancing the migration of BMDCs into the spinal cord, although I did analyze brain tissue and no GFP+ cells were seen in brain in treated mice.   In future experiments, I will reevaluate the efficacy of mannitol treatment at enhancing the migration of BMDCs into the CNS by using BM chimeric animals and compare the accumulation of BMDCs in mannitol treated and untreated BM chimeras.

4.5.2 Creation of BM chimeras

In previous studies, treatment with BU at a variety of doses has been used to obtain variable levels of BM chimerism. IP injections of 20mg/kg of BU followed by injection of 1.5×10^7 whole BM cells resulted in 20 to 40% PBC chimerism in mice at 32 to 62 weeks post-transplant but with lower levels of chimerism observed up to 10 weeks post-transplant (Andersson et al., 2003). Similarly, Hsieh and colleagues (2007) observed high levels of leukocyte chimerism (~80%) following treatment with 40mg/kg BU and injection of 20×10^6 BM cells at 12 to 13 weeks post-transplant. There is a dose-dependent effect of chemotherapeutic agents on levels of myeloablation, which in turn determines levels of BM reconstitution (Nevozhay and Opolski, 2006). Because the lifespan of mSOD mice (approx. 17-19 weeks; Solomon et al., 2006) limits the length of time over which BM reconstitution can be assessed, in my first experimental trial, I used a higher dose of BU following a protocol employed by Barry (2003, unpublished data). Following this protocol, mice received 80mg/kg BU in 4 daily doses of 20mg/kg followed by the transplantation of enriched BM cells. Subsequent blood analysis of transplanted mice at 3 weeks post-transplant revealed that BM reengraftment had been unsuccessful, as indicated by an absence of GFP+ PBCs.

In the following trial, I increased the dose of BU to 100mg/kg delivered in 5 20mg/kg daily doses followed by the injection of 30×10^6 BM cells. Although a BU dose of 100mg/kg is higher than that used in some studies (Yeager et al., 1993; Andersson et al., 2003), it is below the maximum tolerated dose of

150mg/kg reported for mice (Hsieh et al., 2007), and on a dose per surface area basis, it is equivalent to 70% of the usual high dose patients would receive clinically (Andersson et al., 2003). The BM cell dose of 30x10^6 used is comparable to that of the studies cited above. Employing this protocol, I obtained successful BM reengraftment in only a portion of treated mice. Investigations into factors contributing to this lack of efficacy suggested that BU should be diluted in PBS immediately before injection rather than being diluted and stored for a period of days, as the reported stability of the diluted drug is limited to 8 hours (U.S. Food and Drug Administration).

Therefore, in the next experimental trial, mice were treated with BU immediately after it was diluted in PBS. This amendment to my protocol increased the frequency of successfully transplanted mice and 5 out of 6 mice exhibited successful BM reconstitution. Blood samples from these mice were collected weekly from 1 to 4 weeks post-transplant and the chimersm of myelomonocytic and lymphoid lineages were analyzed. In line with previous reports (Hsieh et al., 2007), chimerism in lymphoid PBCs lagged behind that of myelomonoytic cells owing to the nonimmunosuppressive properties of BU and the short half-life of myeloid cells in the circulation. At 2 and 4 weeks post-transplant, high levels of donor reengraftment in BM were observed and averaged ~60% and ~90%, respectively.

It should be noted that with the exception of one mouse that had to be euthanized after receiving an errant injection of BU into the liver, treatment with

BU in all trials was not fatal and was tolerated by mice well, as indicated by the maintenance of body weight over the course of treatment.

4.5.3 BMDCs accumulate in the spinal cords of control and mSOD BM chimeric mice

As in previous work employing irradiated BM chimeras (Solomon et al., 2006; Lewis et al., 2009), I observed that substantially greater numbers of BMDCs accumulate in the spinal cords of mSOD mice compared to controls. However, a high degree of variability in the numbers of GFP+ cells observed in both mSOD and control mice prevented statistical significance from being reached. The degree of variability I observed in the numbers of BMDCs that accumulated in the spinal cord may be a consequence of treating mice with BU that had been diluted and stored for a period of days, rather than with freshly diluted BU.

Although the accumulation of BMDCs in the CNS following BU treatment and BM transplantation in adult mice has been inferred from previous studies (Yeager et al., 1993) and demonstrated in neonates (Espejel et al., 2008), this is the first study in which BMDC accumulation in the CNS of adult mice has been specifically analyzed.   Clinical side effects associated with conditioning regimens that employ BU for HSC transplant are often related to vascular damage and include microangiopathy (Martinez et al., 2005) and capillary leak syndrome (Nurnberger et al., 1997). A recent study by Zeng and colleagues (2010) demonstrated that intragastric administration of BU at 4mg/kg per day for 4 days resulted damage to vascular endothelium, as indicated by increased levels of

circulating endothelial cells and analysis of endothelium using transmission

electron microscopy.   It is therefore plausible that treatment with BU at the dose I

employed results in disruption to the BBB and enhances the migration of BMDCs

into the CNS. Although it is possible that BMDCs might accumulate in the CNS

of mice exhibiting transient chimerism (< 3 weeks of GFP+ cells in the

circulation), my experience to date does not suggest this finding.

4.5.4   BMDC morphology and immunophenotype

GFP+ cells were observed throughout the grey and white matter of the

spinal cord and were classified according to round, rod, amoeboid, stellate, or

elongated morphology. Categorizing GFP+ cells by their morphology provides

insight into the identity and function of these cells. The stellate morphology is

characteristic of parenchymal microglia, while elongated morophology is

associated with perivascular macrophages that reside between the basal lamina

of blood vessels and the glia limitans (Vallieres and Sawchenko, 2003; Hess et

al., 2004). An amoeboid morphology is associated with microglia that have

acquired a phagocytic phenotype (Kreutzberg, 1996), as well as with perivascular

macrophages (Vallieres and Sawchenko, 2003). Rod-shaped cells have been

described as resident monocytes or granulocytes that reside within the lumen of

blood vessels where they function to patrol the vasculature (Audoy-Remus et al.,

2008). Round cells may be intravascular GFP+ cells that were ineffectively

cleared during perfusion, intraparenchymal T-cells (Lewis et al., 2009) or

intraparenchymal cells that exhibit differential Iba1 expression (Vallieres and Sawchenko, 2003).

As in my previous studies (Solomon et al., 2006; Lewis et al., 2009), increased numbers of GFP+ cells were observed in the leptomeninges surrounding the spinal cord and recent studies have indicated that this population of macrophages is maintained by circulating progenitors (Chinnery et al., 2010). It has been suggested that this population of CNS-associated macrophages may be completely reconstituted as early as 4 weeks post-BM transplant in chimeric mice (Chinnery et al., 2010), however, other studies have suggested the complete turnover of this population takes longer and occurs between 6 months and 1 year (Vallieres and Sawchenko, 2003).

Iba1 expression by GFP+ cells was variable across morphological classes but when averaged across all morphological classes, a substantially greater proportion of GFP+ cells in mSOD spinal cord expressed Iba1 compared to control spinal cord. Part of this disparity between groups may be due to the fact that at advanced disease stages, the mSOD spinal cord is associated with a substantial neuroinflammatory response, which likely activates and upregulates the expression of Iba1. Comparatively, Iba1 expression by GFP+ cells within control lumbar spinal cord may be too low to detect with immunohistochemistry. Notably, in both control and mSOD spinal cords, the vast majority (~80%) GFP+ cells with stellate morphology were also observed to express Iba1, indicative of these cells differentiating into parenchymal microglia.

Immunolabeling with CD3 and CD8 antibodies indicated that cytotoxic T-cells accumulate in the spinal cords of control and mSOD mice after treatment with BU. Although CD8+ T-cells have been observed in the mSOD spinal cord by other groups (Chiu et al., 2008), they are only rarely observed in the healthy CNS (Neumann et al., 2002). Therefore, the presence of CD8+ T-cells in control spinal cord suggests that treatment with BU may elicit a neuroinflammatory response. This is supported by the qualitative observation of reactive microgliosis occurring in the spinal cord of control mice treated with BU at 2 weeks-post treatment. BU readily crosses the BBB and is associated with neurotoxicity that clinically presents as seizures (Hassan et al., 1996). Given the high degree of BM chimerism I observed using BU at a dose of 100mg/kg, future experiments will test the efficacy of lower doses of BM in creating BM chimeras and enhancing the accumulation of BMDCs into the spinal cord of mSOD and control mice.

4.5.5 Kinetics of BMDC entry into the control spinal cord

At 2 weeks post-transplant, limited numbers of rod-shaped GFP+ cells were observed in the lumbar spinal cord of control mice. These cells resembled those previously described by Audoy-Remus and colleagues (2008), which reside within the lumen of blood vessels and express CD11b or Gr-1. A portion of these cells labeled with antibody to the monocytic marker CD11b and further immunohistochemical analyses to identify the remainder of these cells are

underway, as is the analysis of BMDC accumulation in spinal cord at 4 weeks post-transplant.

4.5.6 Conclusion

Previous studies of BM chimeric rodents created using myeloablative radiation have demonstrated that under some conditions, BMDCs migrate to and reside within the CNS. However, substantial evidence from studies employing parabiosis suggests that the ability of BMDCs to accumulate within the CNS is dependent in part on the conditioning effects elicited by exposure to radiation. These include the widespread up-regulated expression of inflammatory cytokines (Ramanan et al., 2010), disruptions in cerebral vasculature, and increased endothelial cell expression of adhesion molecules (Gavins et al., 2007). As such, it is apparent that in the steady state, microglial populations are maintained primarily through self-renewal with exceedingly limited contributions from circulating progenitors (Ajami et al., 2007).

It is becoming increasingly apparent that in order to for BMDCs to traverse the BBB and accumulate within the CNS, preconditioning of recipient mice is required. Given the deleterious side effects associated with irradiation, alternative conditioning regimens that similarly enhance the migration of BMDCs into the diseased CNS must be investigated. The results of this study improve the clinical potential for BMDCs to function as treatment vehicles in neurodegenerative disease by demonstrating that conditioning regimens alternative to irradiation potentiate BMDC accumulation in the CNS.

Furthermore, the ability to obtain high level of BM chimerism using BU increases the feasibility of using BM chimeric models experimentally, as an irradiation device such as a gamma cell is not required to myeloablate rodents. A caveat to the results presented here is that treatment with BU at the dose employed in this study appears to incite a neuroinflammatory response, likely attributable to its neurotoxic effects within the CNS. Currently, experiments exploring the efficacy of lower doses of BU at enhancing BMDC accumulation in the CNS are underway.

4.6 Figures

Figure 4. 1 Sample FACS plots indicating GFP- (A) and GFP+ (B) peripheral blood cells (PBCs).

Blood samples were analyzed using FACS analysis; the x-axis indicates fluorescence intensity in arbitrary units while the y-axis measures frequency of cells. (A) Blood samples collected from mice treated with 80mg/BU and transplanted with 5x10^5 enriched GFP+ BM cells revealed an absence of GFP+ PBCs. (B) Blood samples collected from mice treated with 100mg/kg BU and transplanted with 30x10^6 whole GFP+ BM cells exhibited successful chimerism and ~80% of PBCs were GFP+.
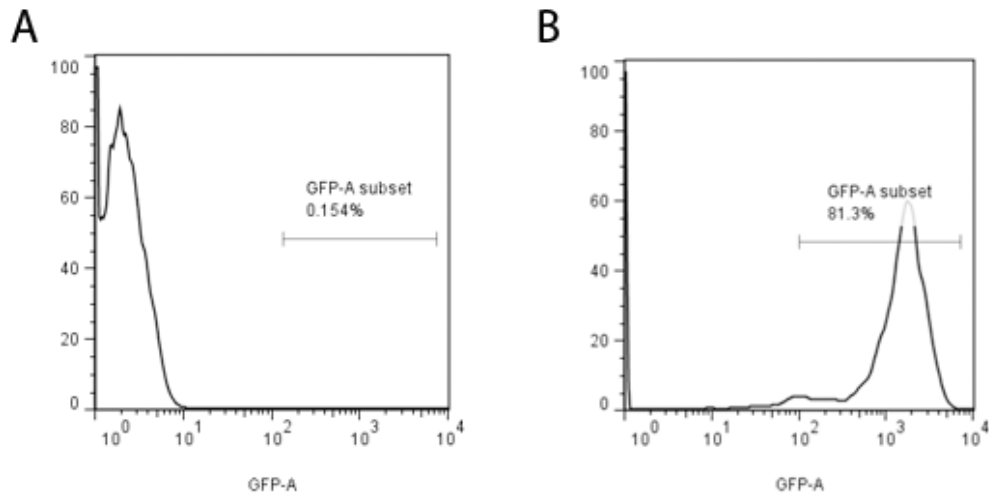
Figure 4. 2 Levels of GFP+ PBCs from 3 weeks post-transplant to disease end-stage in mSOD and control mice.

Weekly blood samples taken from successfully transplanted mice indicated that levels of PBC chimerism increased and remained stable over the course of disease progression in mSOD mice; y-axis indicates percentage of PBC chimerism and x-axis indicates weeks post-BM transplant.
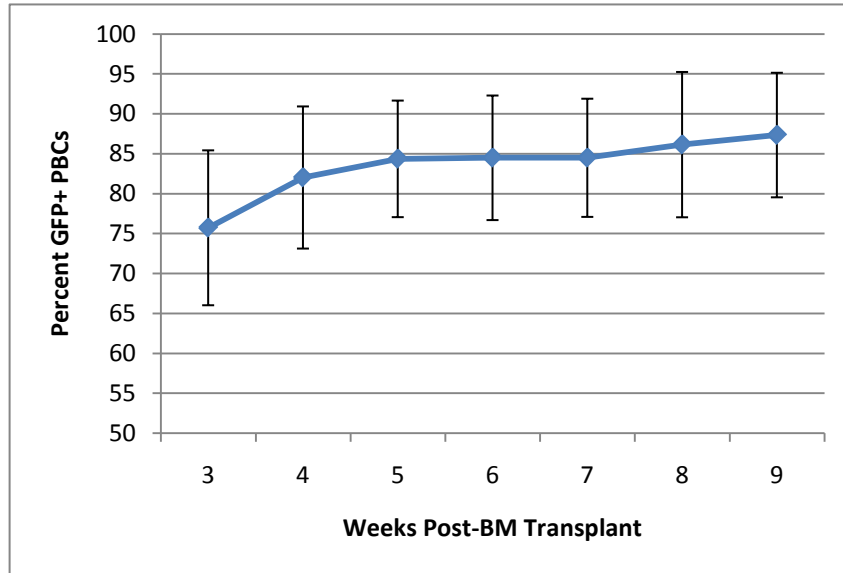
Figure 4. 3 Kinetics of PBC chimerism following treatment with freshly diluted BU; comparison of myeloid and lymphoid PBC reconstitution.

PBC chimerism was variable at 1 week post-treatment; myeloid cells were reconstituted rapidly owing to the short half-life of these cells in the circulation. Reconstituion of lymphoid cells (green line) lagged behind that of myeloid cells (red line), indicative of BU's nonimmunosuppressive effects.
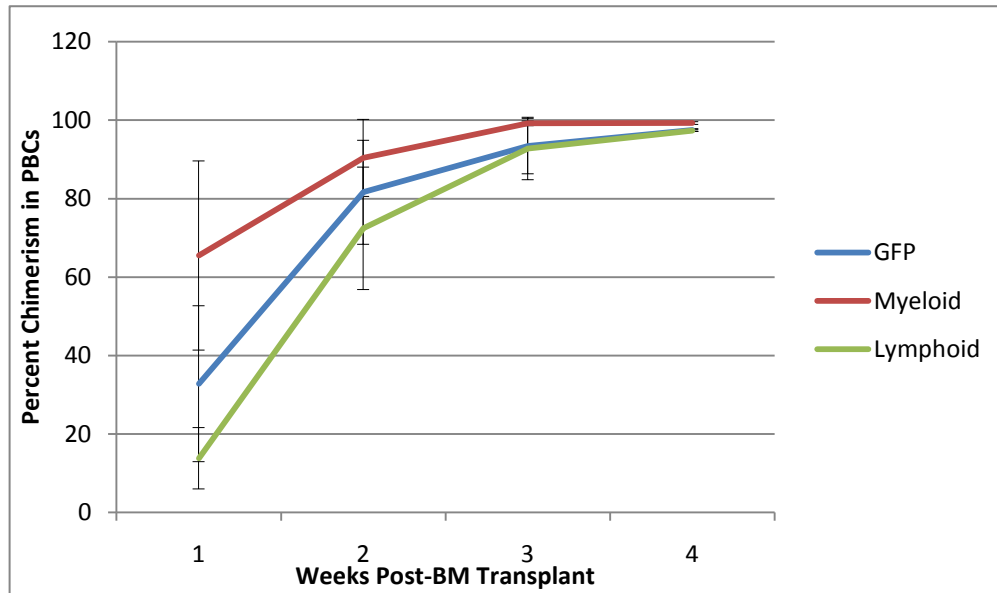
Figure 4. 4 GFP+ cells accumulate in the spinal cords of control and mSOD mice treated with BU and transplanted with GFP+ BM.

(A) GFP+ cells (green labelling) were observed in the grey and white matter of control and mSOD lumbar spinal cord sections; increased numbers of GFP+ cells were observed in the meninges surrounding the spinal cord. (B) Numerically greater numbers of GFP+ cells were observed in mSOD spinal cord compared to control spinal cord but a high degree of variability in the numbers of GFP+ cells observed between mSOD mice, a statistically significant difference between mSOD and control mice was not obtained.

(A)
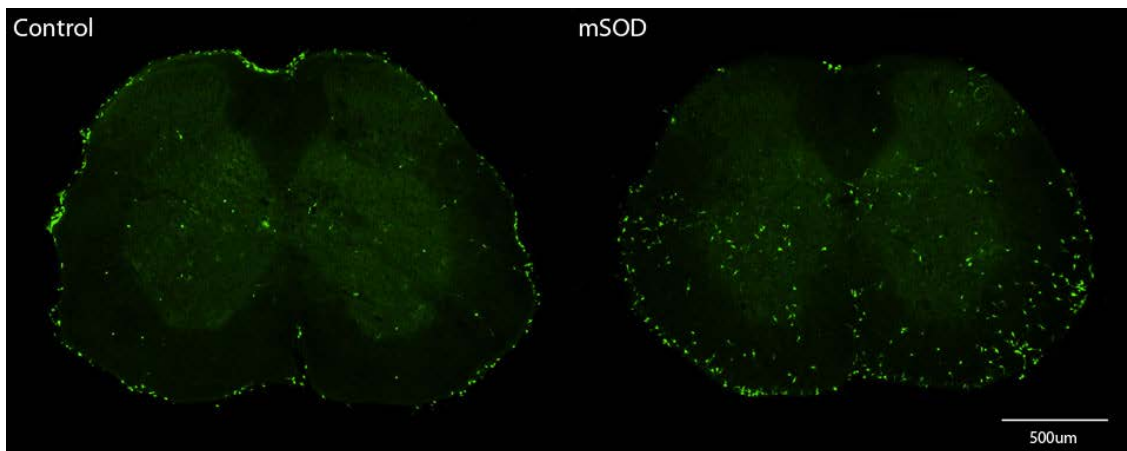
(B)
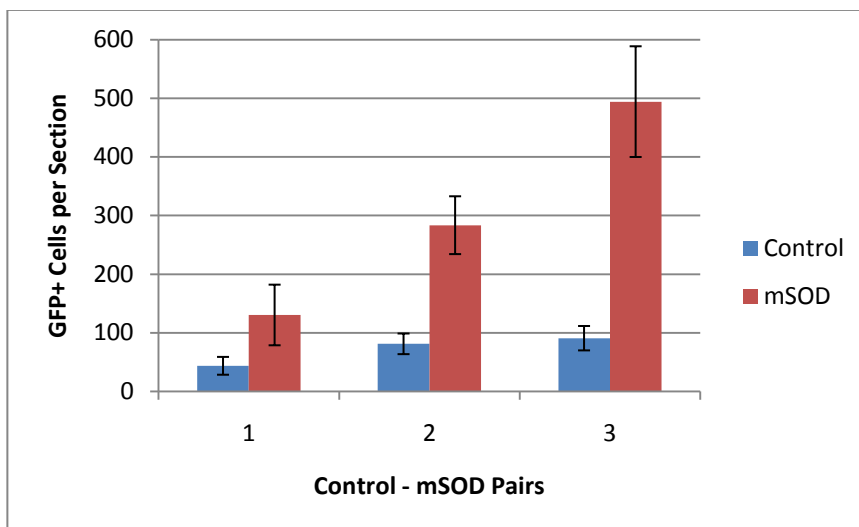
Figure 4. 5 Elongated GFP+ cells reside along spinal cord blood vessels labelled with CD31 (PECAM1).

GFP+ cells (in green) with an elongated morphology were often observed in close approximation with spinal cord blood vessels (immunolabelled with antibody to CD31; in red) in combination with low-levels of Iba1 expression, indicative of these cells being perivascular macrophages.

.
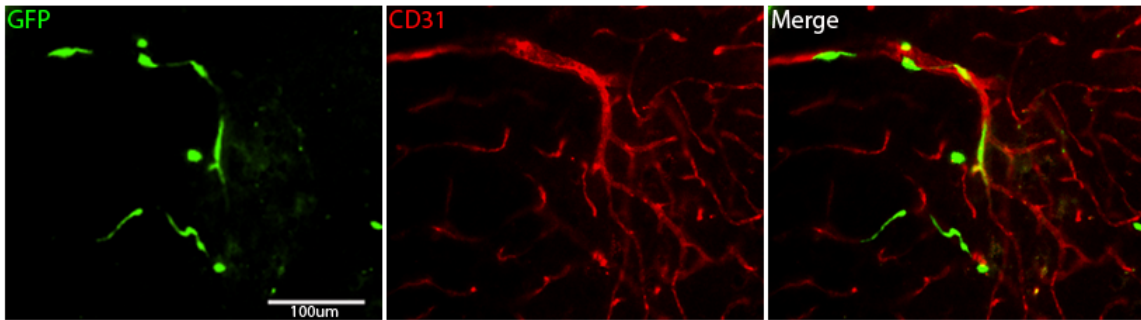
Figure 4. 6 A portion of GFP+ cells within spinal cord express the macrophage marker Iba1.

Top panel: increased numbers of Iba1+ cells and Iba1 labelling intensity (in red) is observed in the spinal cords of mSOD mice compared to controls, indicative of the microgliosis observed in mSOD spinal cord. Bottom panel: GFP+ cells (in green) within mSOD spinal cord immunolabel with Iba1 indicating these cells differentiated into CNS-associated macrophages.
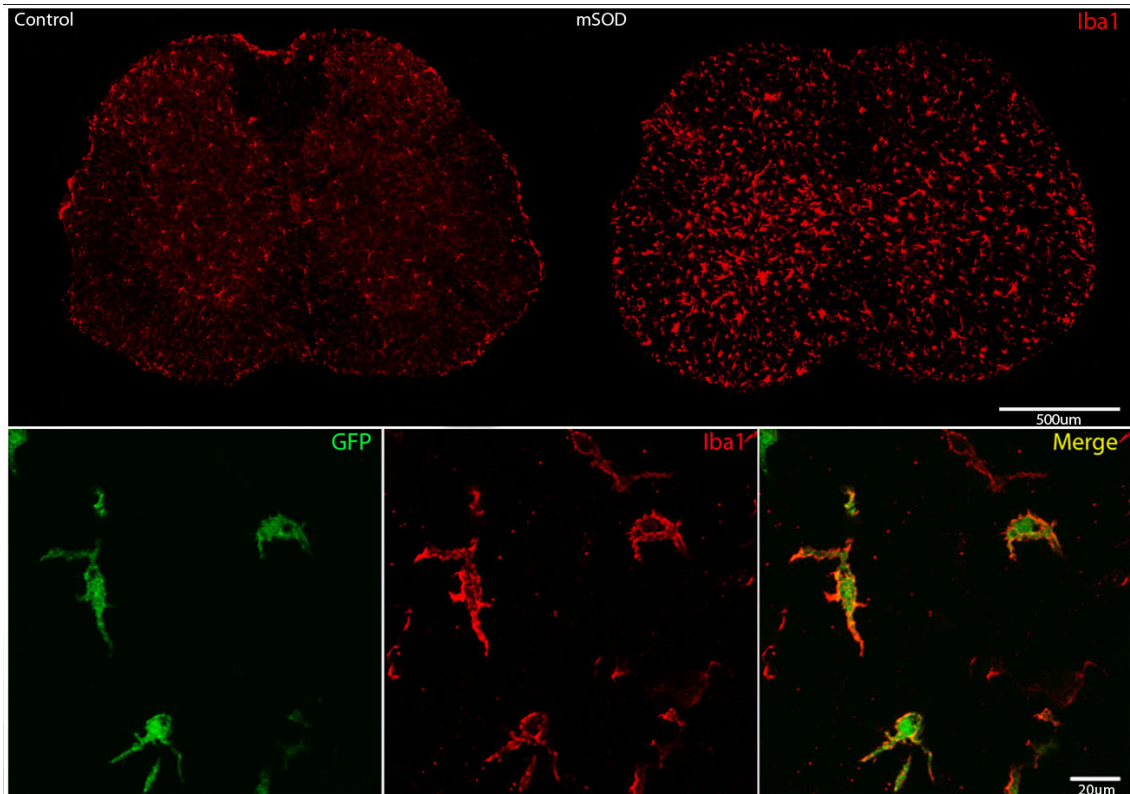
Figure 4. 7 At 2 weeks post-transplant, variable numbers of rod-shaped GFP+ cells are observed in control lumbar spinal cord sections.

(A) The vast majority (~90%) of GFP+ cells (in green) observed in control lumbar spinal cord at 2 weeks post-treatment had a rod-shaped morphology and were found in association with blood vessels (in red, labelled with antibody to CD31). (B) Microglia within the spinal cord of control mice exhibited a reactive morphology, as indicated by thickened processes, cell body hypertrophy and increased Iba1 immunolabelling intensity.

(A)
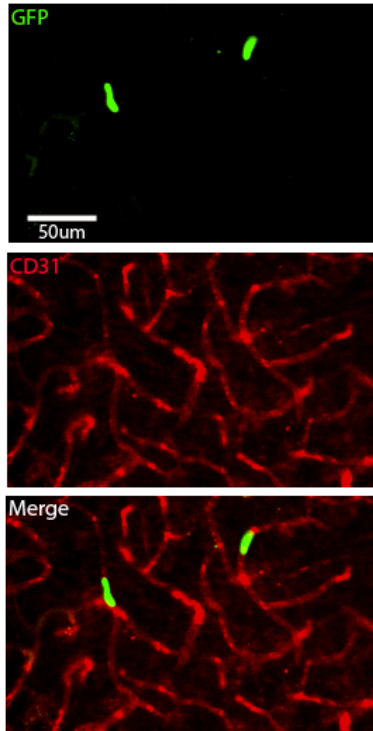
(B)
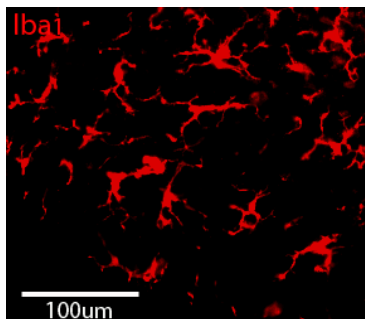
Table 4. 1 Proportional morphology and expression of Iba1 by GFP+ that accumulated in control and mSOD spinal cords.

(A GFP+ cells were quantified and classified according to morphology; an incresed proportion of GFP+ cells in mSOD spinal cord were observed to have the stellate morphology associated with parenchymal microglia compared to controls. (B) An increased proportion of GFP+ cells within the mSOD spinal cord expressed the macrophage marker Iba1 compared to controls; in both mSOD and control spinal cords, the majority of stellate-shaped GFP+ cells expressed Iba1 suggesting these cells differentiated into BM-derived microglia.

(A) Morphology of GFP+ Cells in Lumbar Spinal Cord Section

	% GFP+ Cells Round (mean ± st.dev.)	% GFP+ Cells Rod (mean ± st.dev.)	% GFP+ Cells Amoeboid (mean ± st.dev.)	% GFP+ Cells Stellate (mean ± st.dev.)	% GFP+ Cells Elongated (mean ± st.dev.)
Control (n=3)	29.7 ± 19.7	15.7 ± 13.0	3.4 ± 1.8	7.8 ± 2.0	18.4 ± 10.6
mSOD (n=3)	13.1 ± 11.9	24.8 ± 1.7	9.6 ± 2.2	32.5 ± 8.4	19.9 ± 8.6

(B) Proportion of Iba1+ GFP+ Cells by Morphology

	Round (mean ± st.dev.)	Rod (mean ± st.dev.)	Amoeboid (mean ± st.dev.)	Stellate (mean ± st.dev.)	Elongated (mean ± st.dev.)
Control (n=3)	1.4 ± 2.5	16.1 ± 8.2	18.4 ± 11.1	73.9 ± 16.1	15.6 ± 12.5
mSOD (n=3)	5.4 ± 3.1	70.0 ± 12.2	78.5 ± 9.6	87.0 ± 10.6	60.3 ± 16.4

4.7 References

Ajami B, Bennett JL, Krieger C, Tetzlaff W, Rossi FM (2007) Local self-renewal can sustain CNS microglia maintenance and function throughout adult life. *Nature Neuroscience, 10*(12), 1538-1543.

Andersson G, Illigens BM, Johnson KW, Calderhead D, LeGuern C, Benichou G, et al. (2003) Nonmyeloablative conditioning is sufficient to allow engraftment of EGFP-expressing bone marrow and subsequent acceptance of EGFP-transgenic skin grafts in mice. *Blood, 101*(11), 4305-4312.

Appel SH, Engelhardt JI, Henkel JS, Siklos L, Beers DR, Yen AA, et al. (2008) Hematopoietic stem cell transplantation in patients with sporadic amyotrophic lateral sclerosis. *Neurology, 71*(17), 1326-1334.

Audoy-Remus J, Richard JF, Soulet D, Zhou H, Kubes P, Vallieres L (2008) Rod-shaped monocytes patrol the brain vasculature and give rise to perivascular macrophages under the influence of proinflammatory cytokines and angiopoietin-2. *The Journal of Neuroscience : The Official Journal of the Society for Neuroscience, 28*(41), 10187-10199.

Chinnery HR, Ruitenberg MJ, McMenamin PG (2010) Novel characterization of monocyte-derived cell populations in the meninges and choroid plexus and their rates of replenishment in bone marrow chimeric mice. *Journal of Neuropathology and Experimental Neurology, 69*(9), 896-909.

Chiu IM, Chen A, Zheng Y, Kosaras B, Tsiftsoglou SA, Vartanian TK, et al. (2008) T lymphocytes potentiate endogenous neuroprotective inflammation in a mouse model of ALS. *Proceedings of the National Academy of Sciences of the United States of America, 105*(46), 17913-17918.

Corti S, Locatelli F, Donadoni C, Guglieri M, Papadimitriou D, Strazzer S, et al. (2004) Wild-type bone marrow cells ameliorate the phenotype of SOD1-G93A ALS mice and contribute to CNS, heart and skeletal muscle tissues. *Brain : A Journal of Neurology, 127*(Pt 11), 2518-2532.

Dorovini-Zis K, Bowman PD, Betz AL, Goldstein GW (1987) Formation of a barrier by brain microvessel endothelial cells in culture. *Federation Proceedings,* 46(8):2521-2.

Enquist IB, Nilsson E, Mansson JE, Ehinger M, Richter J, Karlsson S (2009) Successful low-risk hematopoietic cell therapy in a mouse model of type 1 gaucher disease. *Stem Cells (Dayton, Ohio), 27*(3), 744-752.

Espejel S, Romero R, Alvarez-Buylla A (2009) Radiation damage increases purkinje neuron heterokaryons in neonatal cerebellum. *Annals of Neurology, 66*(1), 100-109.

Gavins F, Yilmaz G, Granger DN (2007) The evolving paradigm for blood cell-endothelial cell interactions in the cerebral microcirculation. *Microcirculation (New York, N.Y.: 1994), 14*(7), 667-681.

Ginhoux F, Greter M, Leboeuf M, Nandi S, See P, Gokhan S, et al. (2010) Fate mapping analysis reveals that adult microglia derive from primitive macrophages. *Science (New York, N.Y.), 330*(6005), 841-845.

Gurney ME, Pu H, Chiu AY, Dal Canto MC, Polchow CY, Alexander DD, et al. (1994) Motor neuron degeneration in mice that express a human cu,zn superoxide dismutase mutation. *Science (New York, N.Y.), 264*(5166), 1772-1775.

Hassan M, Ehrsson H, Ljungman P (1996) Aspects concerning busulfan pharmacokinetics and bioavailability. *Leukemia & Lymphoma, 22*(5-6), 395-407.

Hess DC, Abe T, Hill WD, Studdard AM, Carothers J, Masuya M, et al. (2004) Hematopoietic origin of microglial and perivascular cells in brain. *Experimental Neurology, 186*(2), 134-144.

Hickey WF & Kimura H (1988) Perivascular microglial cells of the CNS are bone marrow-derived and present antigen in vivo. *Science (New York, N.Y.), 239*(4837), 290-292.

Hickey WF, Vass K, Lassmann H (1992) Bone marrow-derived elements in the central nervous system: An immunohistochemical and ultrastructural survey of rat chimeras. *Journal of Neuropathology and Experimental Neurology, 51*(3), 246-256.

Hsieh MM, Langemeijer S, Wynter A, Phang OA, Kang EM, Tisdale JF (2007) Low-dose parenteral busulfan provides an extended window for the infusion of hematopoietic stem cells in murine hosts. *Experimental Hematology, 35*(9), 1415-1420.

Keshet GI, Tolwani RJ, Trejo A, Kraft P, Doyonnas R, Clayberger C, et al. (2007) Increased host neuronal survival and motor function in BMT parkinsonian mice: Involvement of immunosuppression. *The Journal of Comparative Neurology, 504*(6), 690-701.

Kokovay E & Cunningham LA (2005) Bone marrow-derived microglia contribute to the neuroinflammatory response and express iNOS in the MPTP mouse model of parkinson's disease. *Neurobiology of Disease, 19*(3), 471-478.

Kreutzberg GW (1996) Microglia: a sensor for pathological events in the CNS. *Trends in Neuroscience,* 19(8): 312-8.

Lewis CA, Solomon JN, Rossi FM, Krieger C (2009) Bone marrow-derived cells in the central nervous system of a mouse model of amyotrophic lateral sclerosis are associated with blood vessels and express CX(3)CR1. *Glia,* 57(13):1410-1419.

Loscher W & Potschka H (2005) Role of drug efflux transporters in the brain for drug disposition and treatment of brain diseases. *Progress in Neurobiology*, 76(1):22-76.

Malm T, Koistinaho M, Muona A, Magga J, Koistinaho J (2010) The role and therapeutic potential of monocytic cells in alzheimer's disease. *Glia, 58*(8), 889-900.

Martinez MT, Bucher C, Stussi G, et al. (2005) Transplant-associated microangiopathy (TAM) in recipients of allongeneic hematopoietic stem cell transplants. *Bone Marrow Transplant,* 36:993-1000.

Massengale M, Wagers AJ, Vogel H, Weissman IL (2005) Hematopoietic cells maintain hematopoietic fates upon entering the brain. *The Journal of Experimental Medicine, 201*(10), 1579-1589.

Neumann H, Medana IM, Bauer J, Lassmann H (2002) Cytotoxic T lymphocytes in autoimmune and degenerative CNS diseases. *Trends in Neurosciences, 25*(6), 313-319.

Nevozhay D & Opolski A (2006) Key factors in experimental mouse hematopoietic stem cell transplantation. *Archivum Immunologiae Et Therapiae Experimentalis, 54*(4), 253-269. doi:10.1007/s00005-006-0030-2

Nurnberger W, Heying R, Burdach S, Gobel U (1997) C1 esterase inhibitor concentrate for capillary leakage syndrome following bone marrow transplantation. *Annals of Hematology, 75*(3), 95-101.

Pardridge WM (2003) Blood-brain barrier drug targeting: The future of brain drug development. *Molecular Interventions, 3*(2), 90-105, 51.

Philips T & Robberecht W (2011) Neuroinflammation in amyotrophic lateral sclerosis: Role of glial activation in motor neuron disease. *Lancet Neurology, 10*(3), 253-263.

Ramanan S, Zhao W, Riddle DR, Robbins ME (2010) Role of PPARs in radiation-induced brain injury. *PPAR Research, 2010*, 234975.

Rapoport SI (2001) Advances in osmotic opening of the blood-brain barrier to enhance CNS chemotherapy. *Expert Opinion on Investigational Drugs, 10*(10), 1809-1818.

Rodriguez M, Alvarez-Erviti L, Blesa FJ, Rodríguez-Oroz MC, Arina A, Melero I, Ramos LI, Obeso JA (2007) Bone-marrow-derived cell differentiation into microglia: a study in a progressive mouse model of Parkinson's disease. *Neurobiology of Disease,* 28(3): 316-325.

Seyfried DM, Han Y, Yang D, Ding J, Savant-Bhonsale S, Shukairy MS, et al. (2008) Mannitol enhances delivery of marrow stromal cells to the brain after experimental intracerebral hemorrhage. *Brain Research, 1224*, 12-19.

Solomon JN, Lewis CA, Ajami B, Corbel SY, Rossi FM, Krieger C (2006) Origin and distribution of bone marrow-derived cells in the central nervous system in a mouse model of amyotrophic lateral sclerosis. *Glia, 53*(7): 744-753.

Stalder AK, Ermini F, Bondolfi L, Krenger W, Burbach GJ, Deller T, et al. (2005) Invasion of hematopoietic cells into the brain of amyloid precursor protein transgenic mice. *The Journal of Neuroscience : The Official Journal of the Society for Neuroscience, 25*(48): 11125-11132.

Szilvassy SJ, Bass MJ, Van Zant G, Grimes B (1999) Organ-selective homing defines engraftment kinetics of murine hematopoietic stem cells and is compromised by ex vivo expansion. *Blood, 93*(5), 1557-1566.

Unger ER, Sung JH, Manivel JC, Chenggis ML, Blazar BR, Krivit W (1993) Male donor-derived cells in the brains of female sex-mismatched bone marrow transplant recipients: A Y-chromosome specific in situ hybridization study. *Journal of Neuropathology and Experimental Neurology, 52*(5), 460-470.

Vallières L & Sawchenko PE (2003) Bone marrow-derived cells that populate the adult mouse brain preserve their hematopoietic identity. J Neurosci. 23: 5197-207.

Wu J, Yang S, Luo H, Zeng L, Ye L, Lu Y (2006) Quantitative evaluation of monocyte transmigration into the brain following chemical opening of the blood-brain barrier in mice. *Brain Research, 1098*(1), 79-85.

Yeager AM, Shinn C, Shinohara M, Pardoll DM (1993) Hematopoietic stem cell transplantation in the twticher mouse. The effects of pretransplant conditioning with graded doses of busulfan. *Transplantation,* 56(1):185-90.

Zeng L, Jia L, Xu S, Yan Z, Ding S, Xu K (2010) Vascular endothelium changes after conditioning in hematopoietic stem cell transplantation: Role of cyclophosphamide and busulfan. *Transplantation Proceedings, 42*(7), 2720-2724.

5: ACCUMULATION OF CX$_3$CR1$^{+/GFP}$ BM CELLS AND CELLS DERIVED FROM DEFINITIVE HEMATOPOIESIS IN THE SPINAL CORD IN A MOUSE MODEL OF AMYOTROPHIC LATERAL SCLEROSIS

5.1 Abstract

Previous studies have demonstrated that under some circumstances, bone marrow-derived cells (BMDCs) accumulate in the central nervous system (CNS) of mice and increased numbers are recruited to the CNS in a variety of models of neurodegenerative disease. The majority of BMDCs observed within the CNS differentiate into CNS-associated macrophages, suggesting that monocytic cells and/or their progenitors within bone marrow (BM) accumulate within the CNS of BM chimeric mice. Within whole BM, the macrophage-dendritic cell precursor (MDP), developing monocytes (MOs) and MOs are identified by the expression of CX$_3$CR1. Using transgenic mice that express a green fluorescent protein (GFP) cDNA at the CX$_3$CR1 locus, the CX$_3$CR1+ fraction of cells was collected using fluorescence activated cell sorting (FACS). To assess the accumulation of cells from the CX$_3$CR1 fraction of BM and cells derived from definitive hematopoiesis, the CX$_3$CR1$^{+/GFP}$ fraction of BM cells along with c-Kit+Lin-Sca1+ BM cells collected from transgenic mice that ubiquitously express red fluorescent protein (RFP) were transplanted into irradiated control mice and a transgenic mouse model of amyotrophic lateral sclerosis (ALS).

Analysis peripheral blood cells indicated that $CX_3CR1^{+/GFP}$ cells persisted within the circulation of mice up to and over 6 weeks post-transplant. Examination of control and mSOD spinal cords indicated that $CX_3CR1^{+/GFP}$ cells and RFP+ cells derived from definitive hematopoiesis accumulate in the spinal cords of mSOD and control mice. In future experiments, the purity of the $CX_3CR1^{+/GFP}$ fraction and RFP+ KLS cells transplanted will be increased in order to confirm these results.

5.2 Introduction

Studies employing bone marrow (BM) chimeric animals have demonstrated that under some conditions bone marrow-derived cells (BMDCs) are capable of traversing the blood-brain barrier (BBB) and accumulating within the central nervous system (CNS; Hickey and Kimura, 1988; Vallieres and Sawchenko, 2003). The number of BM cells accumulating in the CNS is increased in affected areas in a variety of models of neurodegenerative disease including Parkinson's disease, Alzheimer's disease, and amyotrophic lateral sclerosis (ALS; Solomon et al., 2006), compared to healthy controls. Typically, these studies have employed BM chimeric rodents generated by using myeloablative irradiation and thus introduce the confounding effects of total body irradiation (TBI) on BM migration into the CNS.

Experiments employing parabiosis, a technique in which the circulations of mice are joined surgically, demonstrate that in the absence of irradiation, few, if any BMDCs are observed in either the healthy or diseased/injured CNS

148

(Massengale et al., 2005; Ajami et al., 2007; Ginhoux et al., 2010). Although

these results suggest that the effects of irradiation are requisite for the migration

of BMDCs into the CNS, Ajami and colleagues created parabiotic pairs of GFP+

and GFP- mice and subjected the GFP- parabiont to myeloablative doses of

radiation while protecting the GFP+ mouse from radiation exposure by using a

lead shield. Five weeks after irradiation, when approx. 80% of peripheral blood

cells (PBCs) were GFP+, the irradiated mouse was subjected to facial nerve

axotomy (Ajami et al. 2007). However, similar to results from non-irradiated

parabionts, very few GFP+ cells were observed near the inured facial nucleus

and those cells that were observed in this region appeared to be intravascular

(Ajami et al. 2007). The results of this study suggest that not only is radiation

necessary for BMDC engraftment into the CNS but so too is the presence of

circulating BM progenitors that in that absence of whole BM transplantation,

would not normally enter the blood stream (Ajami et al. 2007). Therefore, along

with identifying factors that facilitate BMDC migration into the CNS, the cell

populations within BM capable of migration to the CNS should also be identified.

The majority of BMDCs observed within the CNS acquire macrophage

phenotypes (Vallieres and Sawchenko, 2003; Lewis et al., 2009), making it highly

probably that monocytic cells and their progenitors within BM migrate to the CNS.

Monocytes (MOs) are the circulating precursors of tissue macrophages that

migrate into tissue during inflammation and may enter to some extent in the

steady state (Geissmann et al., 2003).

There is uncertainty as to whether BMDCs can contribute to the pool of microglia within the CNS parenchyma (Ransohoff and Cardona, 2010). Recently, Ginhoux and colleagues (2010) demonstrated that microglia in adult mice derive from primitive myeloid progenitors that migrate from the yolk sac to the developing ectoderm between embryonic days 8.5 and 9.5, rather than through the continuous recruitment of myeloid progenitors derived from definitive hematopoiesis. However, this does not resolve the issue as to whether BMDC could contribute to the microglial population during post-natal life, especially during conditions where disease is present (Wirenfeldt et al., 2011).

In mice, two different populations of MO can be identified based on the expression of the chemokine receptor CX_3CR1; CX_3CR1^{lo} "inflammatory" MO and CX_3CR1^{hi} "resident" MO (Auffray et al., 2009; Robbins and Swirski, 2010; Yona and Jung, 2010). Within BM, the earliest cell population to express CX3CR1 is the clonogenic macrophage-dendritic cell precursor (MDP), the upstream progenitor to MOs, as well as a dendritic cell population within the spleen (Fogg et al., 2000; refer to figure 1.1 "Hematopoietic Hierarchy within BM").

Using transgenic mice that are heterozygous for a green fluorescent protein (GFP) cDNA insertion at the CX_3CR1 locus (Jung et al., 2000), the CX_3CR1 fraction of BM cells which includes the MDP, developing MOs and MOs, can be collected on the basis of GFP expression using fluorescence activated cell sorting (FACS). Co-transplanting lethally irradiated mice with $CX_3CR1^{+/GFP}$ cells and hematopoietic stem cells (cKit+, Lin-, Sca1+) harvested from transgenic

mice that ubiquitously expresses red fluorescent protein (RFP) will enable investigation into the differential migration and accumulation of $CX_3CR1^{+/GFP}$ BM cells and RFP+ cells derived from definitive hematopoiesis in the CNS. Furthermore, because $CX_3CR1^{+/GFP}$ cells will not contribute to long-term BM rengraftment (Kondo et al., 2003), the clearance of $CX_3CR1^{+/GFP}$ cells from the circulation will provide a timeline of $CX_3CR1^{+/GFP}$ BM cell entry into the spinal cord and facilitate the analysis of BMDC proliferation once in the spinal cord. The accumulation of BMDCs in the spinal cord will be compared between control mice and the transgenic mSOD mouse model of ALS.

5.3 Methods

5.3.1 Animals:

Transgenic SJL.B6 mice that over-express the human SOD1 (G93A) missense mutation (mSOD) were bred from progenitor stock obtained from Jackson Laboratories (Bar Harbour, ME) and were maintained as heterozygotes by breeding mSOD males with non-transgenic females. Mouse progeny were genotyped for the mSOD transgene using a protocol established by Gurney and colleagues (Gurney et al., 1994). The mSOD mice develop progressive motoneuron degeneration, culminating in muscle atrophy and eventually hind limb paralysis (Gurney et al., 1994). Age-matched, non-transgenic SJL.B6 mice were used as controls and sacrificed at the same time point as mSOD animals.

BM donor strains of mice including $CX_3CR1^{GFP/GFP}$ mice and transgenic mice that express red fluorescent protein (RFP) driven by the β actin promoter,

resulting in near ubiquitous RFP expression (see Vintersten et al., 2004), were purchased from Jackson Laboratories (Bar Harbour, ME). $CX_3CR1^{GFP/GFP}$ mice were bred to heterozygotes by crossing $CX_3CR1^{GFP/GFP}$ mice with wild type B6 mice; RFP mice were initially maintained as homozygotes and later bred to heterozygotes by crossing RFP homozygotes with wild type B6 mice.

Animals were provided food and water *ad libitum*; all protocols related to the use of animals were approved by the SFU Animal care committee and were in compliance with the Canadian Council on Animal Care, the NIH Guide for the Care and Use of Laboratory Animals, and the EEC Council Directive.

5.3.2 BM Fractionation

BM was flushed from the femurs and tibiae of donor mice following a protocol described previously (Solomon et al., 2006). The age at which BM was harvested from donor mice was variable but mice were at least 8 weeks old and no older than 6 months in age. Male recipients received only male BM while females received either male or female BM to avoid any potential graft-versus-host effects. RFP+ BM was immunolabelled with antibodies to c-Kit, Sca1, and lineage markers (Ter119, CD11b, B220, CD3, Gr-1); the c-Kit+, Sca1+ and Lin- fraction of cells was collected using an Influx FACS machine (Becton-Dickenson, NJ, USA). $CX_3CR1^{+/GFP}$ BM cells were sorted based on the expression of GFP using the Influx and Aria FACS machines (Becton-Dickenson, NJ, USA). Recipient mice were exposed to 10Gy of ionizing radiation at 10 or 12 weeks of age and received BM transplants via tail vein injection. Weekly blood samples

were taken beginning at 3 weeks-post transplant until mSOD mice reached

advanced/end-stages of disease, and peripheral blood cells (PBCs) were

analyzed using an Aria FACS machine to determine the levels of RFP+ and

$CX_3CR1^{+/GFP}$ cells.

5.3.3 Tissue Processing

Control and mSOD mice were euthanized using CO2 and immediately

transcardially perfused with 30 mL of 1xPBS followed by 30 mL of 4%

paraformaldehyde (w/v; PFA); before perfusion with PFA, a femur was dissected

out of each mouse and BM harvested for analysis by flow cytometry. The spinal

cord was dissected out, post-fixed in 4% PFA overnight at 4°C, and then

immersed in 20% sucrose (w/v) in PBS at 4°C overnight for cryoprotection. After

cryoprotection, tissue was embedded in TissueTek O.C.T. (Sakura Finetek, USA)

and stored at -80°C until being cryosectioned at 30 ɥm as previously described

(Solomon et al., 2006).

5.3.4 Histology

Free floating spinal cord sections were permeabilized using a 0.3% Triton-X

solution in PBS (PBST) at room temperature. Sections were incubated in 25% normal

goat serum (v/v; NGS), 3% bovine serum albumin (w/v; BSA) in PBST blocking buffer for

1 hour at room temperature. Antibody buffer consisted of 10% NGS and 3% BSA in

PBST; sections were incubated in primary antibody overnight at 4°C and secondary

antibody for 2 hours at room temperature. To identify macrophages, antibody to the

ionized Ca++-binding adapter molecule 1 (Iba1; 1:1000; Wako) was used.

5.3.5 Analysis

Spinal cord sections were analyzed using a Leica epifluorescence microscope and a Nikon laser scanning confocol microscope. RFP+ and CX$_3$CR1$^{+/GFP}$ cells from each mSOD and control mouse were quantified over 5 lumbar spinal cord sections separated by at least 150 µm (Lewis et al., 2009). The phenotypes of GFP+ BMDCs were analyzed using immunohistochemistry, and the proportion of RFP+ and CX$_3$CR1$^{+/GFP}$ cells immunolabelling with Iba1+ were quantified over 5 lumbar spinal cord sections from each experimental animal. Quantitative assessment of CX$_3$CR1$^{+/GFP}$ and RFP+ cells within the spinal cords of mSOD and control mice was statistically evaluated using SPSS software using a Student's t-test; significance was taken at $p < 0.05$.

5.4 Results

5.4.1 Creation of BM chimeric mice

In initial experimental trials, twelve, 12 week-old mice were given fractionated BM and no successful re-engrafment was detected, as defined by the absence of donor-derived RFP+ or GFP+ PBCs. I believed the absence of detectable, labelled BM cells was due to insufficient radiation dosimetery, which resulted in unsuccessful BM reengraftment presumably related to inadequate myeloablation. To rectify this issue, the dosimetry of the gamma cell was re-evaluated and it was established that in order to achieve a radiation dose of 10Gy, 16 minutes of exposure at 68Gy/minute was required. Because of the

length of the exposure time, the treatment was split into two consecutive 8 minute sessions to ensure mice were adequately oxygenated while in the gamma cell.

Initially, there was difficulty in obtaining pure populations of RFP+ KLS cells for these experiments as the RFP signal was very bright when using BM cells from RFP+ homozygous mice and the intensity of the fluorescence interfered with other fluorescent channels being used to discriminate cells based on lineage, c-kit, and Sca1 labelling. To rectify these issues, RFP mice were bred to heterozygotes in an attempt to reduce the RFP signal after consultation with Jackson Laboratories (supplier of this mouse strain), and Dr. Andras Nagy, in whose laboratory this mouse strain was engineered, to ensure that this breeding would not deleteriously effect the expression of RFP. The revised duration of irradiation resolved the issue of myeloablation, while the new heterozygote RFP donors improved the discrimination between fluorophores when using FACS, as indicated by the ability to distinguish cells labelled with antibody-fluorophore conjugates from those that were unlabelled

5.4.2 Establishing sorting conditions for fractionation

For the collection of RFP+ KLS cells, a population representing roughly 0.3% of BM cells was collected; this value is higher than the frequency of KLS cells within BM, which is reported to be approximately 0.05% of BM cells (Seita and Weissman, 2010). The purity of the $CX_3CR1^{+/GFP}$ cell fraction collected was 98% and 92% for the Aria and Influx FACS machines, respectively, as

determined by running samples of sorted cells through the FACS machine and analyzing the proportion of cells expressing GFP.

Twelve week-old control (n=2) and mSOD (n=4) mice were subjected to 10Gy of irradiation and each host received 2x10^3 RFP+ KLS cells and 2x10^6 $CX_3CR1^{+/GFP}$ cells. Of the six mice treated, three mice were omitted from the study; one mouse was euthanized due to an intestinal obstruction, another developed dermatitis presumably related to the irradiation, and one was not successfully reconstituted with donor BM but did not succumb to radiation sickness.

For the remaining mice in the study (n=3), blood analysis at 3 weeks post-transplant revealed that an average of 48.5± 7.7% (mean ± standard deviation (s.d.))   of PBCs were RFP+ and increased to levels averaging 77.7 ± 8.0% by 5 weeks post-transplant (figure 5.1A, figure 5.2A). Data from mSOD and wt mice were pooled as these experiments were primarily aimed at assessing reconstitution. At three weeks post-transplant, variable levels of $CX_3CR1^{+/GFP}$ PBCs were observed ranging from 12.8-28.2% and averaging 18.4 ± 8.5% (figure 5.1B, figure 5.2B).   By 5 weeks post-BM transplant, mSOD mice reached disease end-stage and were euthanized; however, the final blood analysis indicated that there were still levels of circulating $CX_3CR1^{+/GFP}$ PBCs that ranged from 0.6-3.3% of PBCs. Analysis of BM by flow cytometry demonstrated RFP+ BM re-engraftment levels averaging 67.3 ± 11.1%. $CX_3CR1^{+/GFP}$ cells were also detected in BM at levels averaging 0.5 ± 0.4% suggesting ineffective clearance of blood from blood vessels within the BM compartment during tissue perfusion, or

impurities within the $CX_3CR1^{+/GFP}$ sort resulting in HSCs from $CX_3CR1^{+/GFP}$

donors engrafting within the BM compartment of the host.

Initially, I expected that $CX_3CR1^{+/GFP}$ PBCs would clear the circulation of

recipient mice before mSOD mice reached disease end-stage. This finding

would provide two important pieces of information: it would establish a timeframe

during which $CX_3CR1^{+/GFP}$ cells migrate from the circulation into the spinal cord

and enable us to then analyze the proliferation of $CX_3CR1^{+/GFP}$ cells once they

accumulated in the spinal cord. Once $CX_3CR1^{+/GFP}$ PBCs have cleared the

circulation, mice can be treated with intraperitoneal injections of the thymidine

analogue 5-ethynyl-2'deoxyuridine (EdU) which is incorporated into dividing cells

(Zeng et al., 2010).

As such, in the subsequent trial, mice (n=2 mSOD, n=2 control) received

BM transplants at 10 weeks of age rather than at 12 weeks of age, so as to

increase the period of evaluation post-transplant, as mSOD mice typically reach

disease end-stage at 17 to 20 weeks of age (Solomon et al., 2006). One mSOD

mouse developed dermatitis and was omitted from the study. Data from the

mSOD and wt mice were pooled (n=3) to assess reconstitution. Mice exhibited

levels of RFP+ PBCs at 3 weeks post-transplant averaging 45.3 ± 11.2% ranging

from 32.8% to 54.6% chimerism (figure 5.3A). By six weeks post-transplant, this

average increased to 53.8 ± 23.3% with the high level of variability due to one

mouse which exhibited reduction to 24.7% RFP+ PBC chimerism which

stabilized after 4 weeks post-transplant (figure 5.3A). Levels of $CX_3CR1^{+/GFP}$

PBCs averaged 2.6 ± 1.4% and ranged from 1.2 to 4% at 3 weeks post-

transplant (figure 5.3B). However, analysis of blood at 4 weeks post-transplant indicated that the levels of $CX_3CR1^{+/GFP}$ PBCs were increasing to an average of 4.6 ± 2.1% (figure 5.3B), which may be the result of the clonogenic expansion of GFP+ MDPs producing of GFP+ MOs (Fogg et al., 2006). Alternatively, the transplanted $CX_3CR1^{+/GFP}$ cell population may have included some HSCs as a result of impurities in the $CX_3CR1^{+/GFP}$ sort, resulting in HSCs from the $CX_3CR1^{+/GFP}$ donors being reengrafted in the BM compartment of myeloablated recipients. This latter view was supported by the analysis of recipient BM, which indicated an average of 2.9 ± 2.1% of BM cells were GFP+ when analyzed at 6 weeks post-transplant, suggesting that GFP+ cells were being generated by GFP- HSCs that were included in the $CX_3CR1^{+/GFP}$ sort; 40.8 ± 17.1% of BM cells were RFP+. To address this issue, in future trials, $CX_3CR1^{+/GFP}$ cells will be sorted twice to increase the purity of $CX_3CR1^{+/GFP}$ cells to be transplanted; repeated sorting will result in >99% purity in the GFP+ fraction of cells collected (personal communication with F. Rossi).

5.4.3 RFP+ and CX₃CR1+ BMDCs accumulate in the spinal cords of irradiated mice

Five lumbar spinal cord sections from each successfully transplanted mouse (n=3 control, n=3 mSOD; pooled over groups 1 and 2) were analyzed, and RFP+ and $CX_3CR1^{+/GFP}$ cells were quantified, pooled and averaged over mSOD and control groups. RFP+ and $CX_3CR1^{+/GFP}$ cells were observed throughout the grey and white matter (figure 5.4) and substantially greater numbers of RFP+ and $CX_3CR1^{+/GFP}$ cells were observed in the lumbar

spinal cords of mSOD mice compared to control mice (table 5.1). In mSOD mice, numbers of $CX_3CR1^{+/GFP}$ and RFP+ cells averaged 152.5 ± 44.8 and 120.4 ± 49.4 respectively, while in control mice an average of 36.6 ± 25.8 CX_3CR1 cells and 42.9 ± 27.6 RFP+ cells were observed per lumbar spinal cord section. Although numbers of RFP+ and $CX_3CR1^{+/GFP}$ cells were numerically higher in the spinal cord of mSOD mice, because of a high degree of variability between control mice, statistical significance was not achieved.

In control mice, 43.1 ± 13.31% of RFP+ cells and 46.1 ± 12.2% of $CX_3CR1^{+/GFP}$ cells expressed the macrophage marker Iba1 (figure 4.5). Comparatively, in mSOD mice 67.4 ± 22.1% of RFP+ cells and 75.4 ± 7.8% of $CX_3CR1^{+/GFP}$ cells expressed Iba1. In both cases, these values likely under-represent the numbers of Iba1+ RFP+ and $CX_3CR1^{+/GFP}$ cells, as in control mice, as Iba1 is expressed at lower levels due to an absence of inflammation and in both control and mSOD mice, perivascular macrophages express Iba1 at lower levels than parenchymal microglia (Vallieres and Sawchenko, 2003). In future trials, the relative contributions of RFP+ and CX_3CR1+ cells to perivascular macrophages in the CNS will be evaluated and compared.

5.5 Discussion

The results of this study demonstrate that circulating $CX_3CR1^{+/GFP}$ BM cells as well as cells derived from definitive hematopoiesis (i.e. RFP+ cells) can be detected in the peripheral blood of transplanted mice and that both GFP+ and RFP+ cells accumulate in the spinal cords of irradiated control and mSOD mice.

5.5.1 Establishing BM chimeric mice

In studies of mice transplanted at 12 weeks of age, I found that levels of RFP+ PBC chimerism following transplantion exhibited a progressive increase consistent with BM reconstitution (i.e. 80%). The levels of reconstitution achieved with mice transplanted at 12 weeks of age were similar to PBC chimerism achieved in previous studies (>80%; see Vallieres and Sawchenko, 2003; Stalder et al., 2005; Solomon et al., 2006). However, chimerism in the present experiment was achieved with 2 x10^3 KLS cells, rather than 5x10^6 whole BM cells in the studies referenced above. The rate and extent of BM reengraftment with donor cells is dependent on the initial number of HSCs transplanted (Nevozhay and Opolski, 2006). Given that chimerism levels reached ~80% at 5 weeks post-transplant in RFP+ KLS transplanted mice while similar levels of chimerism were observed at 3 weeks post-transplant in mice that received 5x10^6 whole BM cells (Solomon et al., 2006), suggests that fewer HSCs were present in the injected RFP+ KLS cells than in the 5x10^6 GFP+ whole BM cell injection. The frequency of HSCs in whole BM has been reported to be 1/10000 cells; therefore, 5x10^6 whole BM cells would be anticipated to contain 500 HSCs (Szilvassy et al., 1999). It has been reported that 20% of cells within the KLS fraction are HSCs (Hexner and Emerson, 2007); therefore, it can be deduced that mice transplanted with 2x10^3 RFP+ KLS cells received roughly 400 HSCs. Furthermore, a population of 0.3% of RFP+ BM cells was collected, while the KLS fraction is reported to constitute only 0.05% of BM cells, suggesting that some of the RFP+ cells collected may not have been within the

KLS fraction (Seita and Weismann, 2010). Therefore, recipients receiving RFP+

KLS cells most likely received reduced numbers of HSCs compared to those

receiving 5x10^6 whole BM cells. As the rate of BM reengraftment is dependent

on the number of HSCs transplanted (Nevozhay and Opolski, 2006), this could

account for the delay in achieving the levels of chimerism that I observed in

previous studies (see Solomon et al., 2006; Lewis et al., 2009).

Analysis of the GFP+ CX_3CR1 lineage population in mice transplanted at

12 weeks of age revealed that approx. 17% of PBC were GFP+ at three weeks

after transplant. This value is much greater than the 'physiological' level of

monocyte lineage cells in peripheral blood, which is generally reported to be 4%

(Auffray et al., 2009). However, the elevated level of GFP+ cells is a function of

the large numbers of $CX_3CR1^{+/GFP}$ MO-lineage cells that were injected into the

recipient mice. GFP+ cell number progressively fell in 12 week-old transplanted

mice to 2.9% at 4 weeks after transplant, and 1.8% at 5 weeks post-transplant.

Given the half-life of circulating MOs is ~24 hours (Yona and Jung, 2010), the fall

in GFP+ cell number was expected. However, cell numbers appeared to

asymptote at approx. 2% at 5 weeks and did not drop to zero, suggesting that

GFP+ MO-lineage cells were still in the circulation.

To address this issue, in the subsequent experimental trial, mice were

transplanted at 10 weeks of age rather than 12 weeks of age, increasing the time

span between transplantation and disease end-stage in mSOD mice. It was

hoped that in doing so, I would observe the clearance of GFP+ PBCs from the

circulation and mice could then be treated with EdU to analyze the proliferation of

$CX_3CR1^{+/GFP}$ cells within the spinal cord. Although given the same dose of radiation and transplanted with the same number of RFP+ KLS cells as mice in the previous trial, the percent of RFP+ PBCs at 3 weeks post-transplant was highly variable ranging from 32.3% to 54.6% and averaging 45.3 ± 11.2%. This average is lower than that achieved in the previous trial but did increase to 53.8 ± 23.3% at 6 weeks post-transplant; the high level of variability was due to one mouse which exhibited only 23% PBC chimerism at 6 weeks post-transplant. Lower levels of GFP+ PBCs at 3 weeks post-transplant were also observed in this group compared to the 12 week transplantation group and averaged 2.6 %. However, levels of GFP+ PBCs increased to 4.6 % upon subsequent analysis at 4 weeks post-transplant and remained at relatively consistent levels over 5 to 6 weeks post-transplant at which point mSOD mice reached disease end-stage.

The CX_3CR1+ fraction of BM cells includes MOs and their direct upstream progenitor, the MDP. The half-life of circulating MOs is approximately 24 hours (Yona and Jung, 2010); however, because I transplanted myeloblasts (developing MOs) and immature MOs that were within the BM compartment, the GFP+ MO half-life within the circulation was likely increased. Fogg and colleagues (2006) transplanted irradiated mice with 10^4 MDPs and observed F4/80+CD11b+ (MOs) and CD11c+ (DCs) donor-derived cells in the spleens of recipients beginning at 2 days post-transplant. Although the persistence of the clonogenic MDP in the spleen has not been explicitly reported, levels of MDP-derived DCs in the spleens of recipient mice peaked at 6 to 7 days post-

transplant (Fogg et al., 2006), suggesting that this time corresponds to the turnover of MDPs in the spleen.

Therefore, given that the inferred turnover time for the MDP is ~7 days, the most parsimonious explanation for the persistence of CX$_3$CR1$^{+/GFP}$ PBCs at 6 weeks post-transplant and the presence of CX$_3$CR1$^{+/GFP}$ cells in the BM of recipients is that an undetermined number of HSC from the CX$_3$CR1$^{+/GFP}$ mice, that were GFP-, were included in the sort. The GFP- HSC will progressively manifest a GFP+ signal as the HSC differentiates into a MO lineage and exhibits CX$_3$CR1 (Jung et al., 2000). Inclusion of GFP- HSC is possible in these experiments in that although FACS sorting was restricted to GFP+ cells, it is possible that rare GFP- cells could have crept through the sort.

5.5.2 RFP+ and CX$_3$CR1$^{+/GFP}$ cells accumulate in the spinal cords of mSOD and control mice

I observed that RFP+ and CX$_3$CR1$^{+/GFP}$ BMDCs accumulated in the spinal cords of control and mSOD mice, in line with expectations based on previous experiments (Solomon et al., 2006; Lewis et al., 2009). Although numerically higher numbers of RFP+ and CX$_3$CR1$^{+/GFP}$ cells were observed in the lumbar spinal cord of mSOD mice compared to controls, because of a high degree of variability between the numbers of BMDCs observed in the spinal cords of control mice statistical significance was not obtained. An average of ~43 RFP+ and ~37 CX$_3$CR1$^{+/GFP}$ cells were observed in the spinal cords of control mice compared to ~120 RFP+ and ~153 CX$_3$CR1$^{+/GFP}$ cells in the mSOD spinal cord. The majority of RFP+ and CX$_3$CR1$^{+/GFP}$ cells labelled with antibody to Iba1, indicating that

many BMDCs in the spinal cord differentiated into CNS-associated macrophages, as has been reported previously (Solomon et al., 2006; Lewis et al., 2009; Vallieres and Sawcheko, 2003).

The results of previous studies suggest that irradiation (Mildner et al., 2007) and the presence of circulating BM progenitor cells are requisite for the migration of BMDCs into the CNS (Ajami et al., 2007). Although I employed irradiation to create BM chimeric mice, the accumulation of RFP+ cells within the spinal cords of mSOD and control mice suggests that cells derived from definitive hematopoiesis also contribute to BMDC populations within the CNS of chimeric mice, although the purity of the KLS fraction of RFP+ cells transplanted is questionable and may have contained downstream BM progenitor populations.

5.5.3 Future Directions

In order to address the issues related to the persistence of $CX_3CR1^{+/GFP}$ cells in the circulation of mSOD mice at disease end-stage, in future trials mice will be treated at 10 rather than 12 weeks of age, increasing the time between BM injection and disease end-stage. After observing $CX_3CR1^{+/GFP}$ cells in the BM of transplanted mice, the numbers of $CX_3CR1^{+/GFP}$ BM cells transplanted will be reduced by half to 1x10^6 and will be sorted twice via FACS. In previous trials, recipients received 2x10^6 $CX_3CR1^{+/GFP}$ cells which typically required 4 to 5 hours of FACS to obtain, depending on the number of recipients. By reducing the number of cells by half, the sort time will also be significantly reduced providing time to sort the cells twice. This will increase the purity of $CX_3CR1^{+/GFP}$

cells injected, reducing the chances that HSCs will be included in this fraction and engraft within the recipient's BM compartment.

Once CX$_3$CR1$^{+/GFP}$ BM cells clear the circulation, I will analyze the proliferation of CX$_3$CR1$^{+/GFP}$ BMDCs within the spinal cord and compare it to that of endogenous microglia. This is of particular interest, as in previous experiments we have been unable to ascertain whether the increasing accumulation of BMDCs in the spinal cord of mSOD mice observed at advancing stages of disease is due to a continued influx of cells from the circulation or from a transient infiltration of BMDCs that then proliferate within the CNS.

Although RFP+ cells were also observed within the spinal cords of mSOD and control mice, the purity of the RFP+ KLS population transplanted into mice is also questionable. A population of 0.3% of RFP+ BM cells were collected which is substantially greater than reported 0.05% of BM cells within the KLS fraction (Seita and Weissman, 2010), and thus may have included downstream progenitor cells. To confirm that cells derived from definitive hematopoiesis also migrate into the spinal cord of irradiated chimeras, the purity of the RFP+ HSCs transplanted into recipient mice should also be improved. This can be achieved through immunolabelling with additional markers for HSCs such as the signalling lymphocyte activation molecule (SLAM) receptors CD150, CD48 and CD244 and endothelial protein C receptor (EPCR). HSCs are identified by the expression of CD150 and EPCR, and by a lack of CD244 and CD48 expression (Kiel et al., 2005; Balazs et al., 2006).

The contribution of subpopulations of CX_3CR1+ BM cells to the accumulation of BMDCs in the CNS should also be investigated and is possible by fractionating $CX_3CR1^{+/GFP}$ cells based on the expression of lineage markers. The MDP represents approximately 0.5% of BM cells and is identified by $CD117+CX_3CR1+Lin-$ expression, while the monocyte fraction is identified by CD11b expression (del Rio et al., 2006). The differential recruitment of MO subsets has been investigated by several groups. Mildner and colleagues (2007) demonstrated that inflammatory CX_3CR1^{lo} MOs are preferentially recruited to lesioned sites in the brain, while Audoy-Remus and colleagues (2008) demonstrated that resident CX_3CR1^{hi} MOs acquire a rod-shaped morphology, are recruited to patrol blood vessels in an angiopoiten II-dependent fashion and differentiate into perivascular macrophages. After transplantation of 2x10^4 MDPs, Fogg and colleagues (2006) observed GFP+ microglia in the CNS of mice transplanted with 2x10^4 MDP cells, although it is uncertain whether the MDP or its downstream progeny that accumulates in the CNS. Given the results of these studies, analysing the differential migration patterns and accumulation of CX_3CR1 BM subsets in control and mSOD mice will provide information on factors dictating the migration of BMDCs to the CNS.

5.5.4 Conclusion

In order to improve the clinical potential of BMDCs as treatment vehicles for neurodegenerative disease, the conditions under which BMDC migration into the CNS occurs and the cell populations within BM capable of this migration must

be identified. Here I demonstrate that the $CX_3CR1^{+/GFP}$ fraction of BM cells can migrate into the spinal cord of irradiated mice and contribute to populations of CNS-associated macrophages. Studies employing BMDCs as treatment vehicles in mouse models of neurodegenerative disease provide proof of principle that these cells can have a therapeutic effect in the diseased CNS. Recently Biju and colleagues (2009) transplanted lethally irradiated mice with HSCs that had been transfected with a cDNA for glial cell-derived neurotrophic factor (GDNF) under the control of a macrophage-specific promoter, thereby restricting the expression of the transgene to cells that differentiate into macrophages. Transplanted mice were then treated with MPTP to induce dopaminergic (DA) neurodegeneration, a protocol used to model Parkinson's disease in rodents.   Mice that received GDNF-transfected HSCs exhibited substantial reductions in DA neuron loss compared to non-transfected BM chimeric MPTP treated controls. Furthermore, this reduction in DA degeneration translated to a reduced decline in physical activity levels compared to sham-treated mice. A limitation to this study is that the entire BM compartment of hosts was replaced with genetically modified BM, which would not be ideal in the clinical setting and underscores the importance of demonstrating that the CX_3CR1+ BMDCs accumulate within the CNS without reconstituting the BM of recipients.

By further refining the protocol used to create RFP+ KLS and $CX_3CR1^{+/GFP}$ fraction BM chimeras, the levels of BMDC proliferation within the spinal cord and the contribution of cells derived from definitive hematopoiesis to the accumulation of BDMCs within the spinal cord of mSOD mice will be evaluated. However,

although irradiation is employed clinically for a plethora of medical conditions, it is also associated with deleterious side effects including immunosuppression and an acute inflammatory response (Ramanan et al., 2010). Therefore, further investigation into alternative conditioning methods that enhance the migration of CX_3CR1+ BMDCs into the diseased CNS without prior irradiation of hosts must also be undertaken to improve the clinical potential of these cells.

5.6 Figures

Figure 5. 1 Sample FACS plots from CX$_3$CR1$^{+/GFP}$ BM fraction and RFP+ KLS BM cell transplants.

Sample FACS plot analyzing levels of (A) RFP+ PBCs and CX$_3$CR1$^{+/GFP}$ PBCs; variable levels of RFP+ and CX$_3$CR1$^{+/GFP}$ PBCs were observed in recipient mice at 3 weeks post-transplant. The x-axis of the plots represents fluorescence intensity while the y-axis represents cellular granularity.
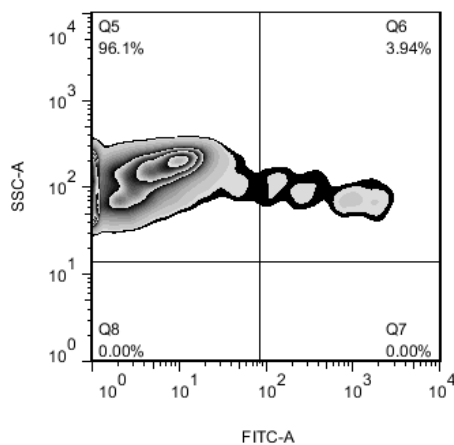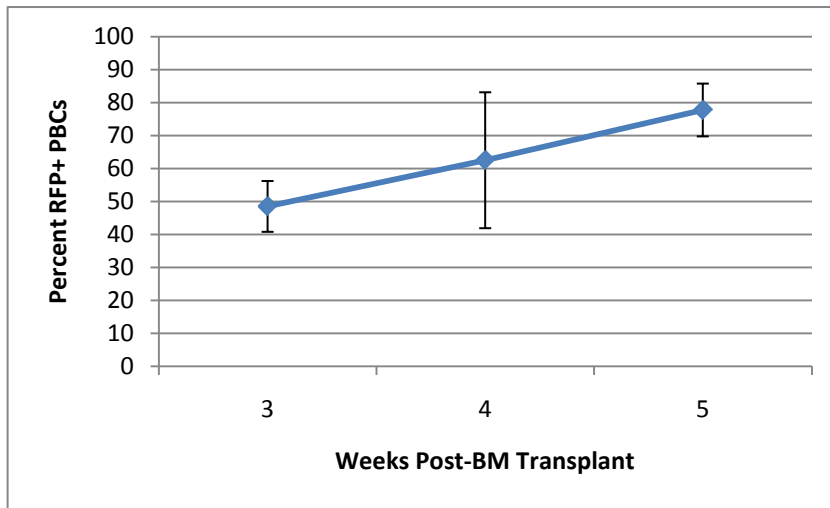
(A)
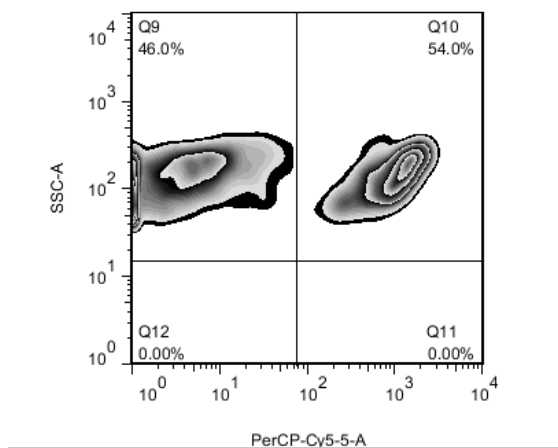
(B)

Figure 5. 2 Analysis of RFP+ and CX$_3$CR1$^{+/GFP}$ PBCs in mice transplanted with BM at 12 weeks of age.

(A) Levels of RFP+ PBCs steadily increased over the period of observation, while (B) levels of CX$_3$CR1$^{+/GFP}$ PBCs decreased but were still present in the circulation when mSOD mice reached disease end-stage.

(A)

(B)
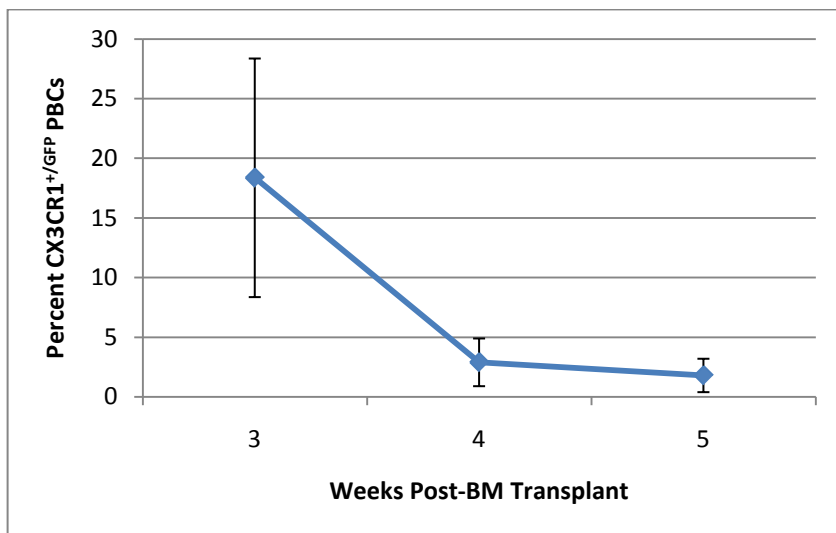
Figure 5. 3 Analysis of RFP+ and CX$_3$CR1$^{+/GFP}$ PBCs in mice transplanted at 10 weeks of age.

(A) RFP+ reconstitution of PBCs was variable but increased over the period of observation. (B) CX$_3$CR1$^{+/GFP}$ PBCs levels were highly variable between mice and increased from 3 to 4 weeks post-transplant, afterwhich levels of CX$_3$CR1$^{+/GFP}$ PBCs remained relatively consistent.

(A)
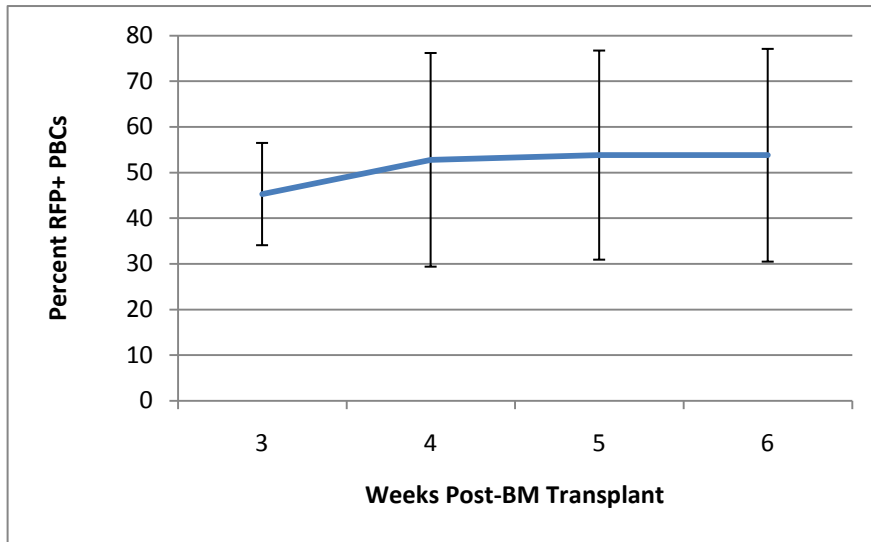
(B)
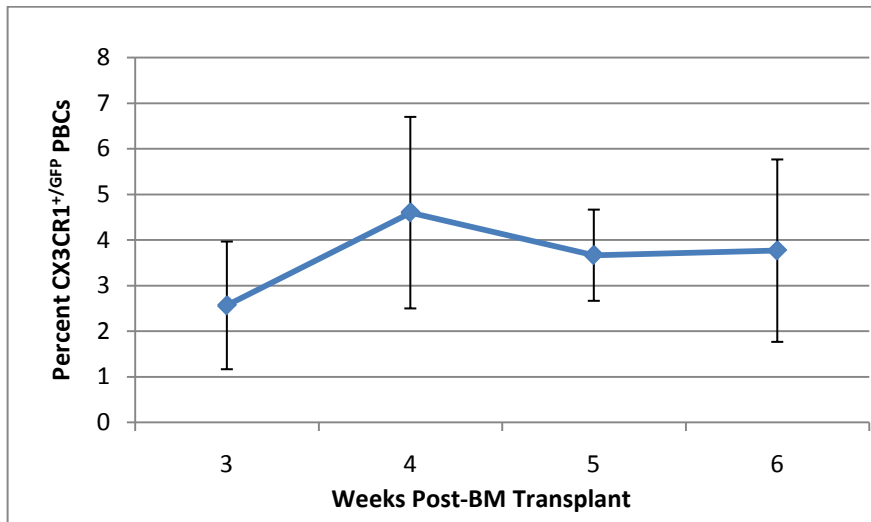
Figure 5. 4 RFP+ and CX$_3$CR1$^{+/GFP}$ cells accumulate in the spinal cords of control and mSOD mice.

Substantially greater numbers of CX$_3$CR1$^{+/GFP}$ (in green) and RFP+ (in red) BMDCs were observed in the spinal cords of mSOD mice compared to age-matched controls. Scale bar: 500um.
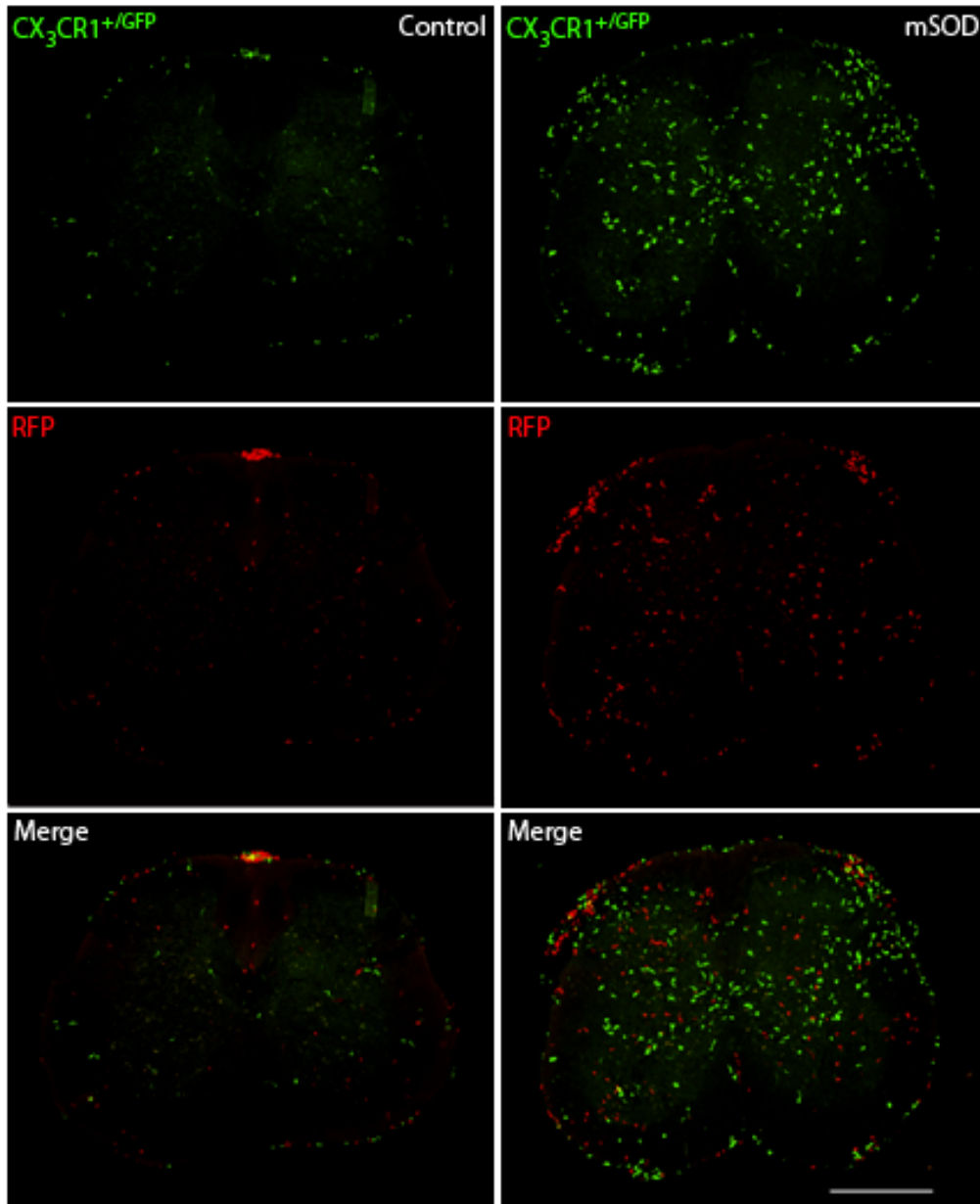
Figure 5. 5 CX$_3$CR1$^{+/GFP}$ and RFP+ cells accumulate in the spinal cords of mSOD and control mice and express Iba1.

Confocal images taken of a lumbar spinal cord section from an mSOD mouse at 20x (A) and 40x (B) magnification; portions of RFP+ (in red) and CX$_3$CR1$^{+/GFP}$ (in green) that accumulate in the mSOD spinal cord immunolabel with the macrophage marker Iba1 (in blue). Scale bar: A= 100um, B=10um

(A)   (B)
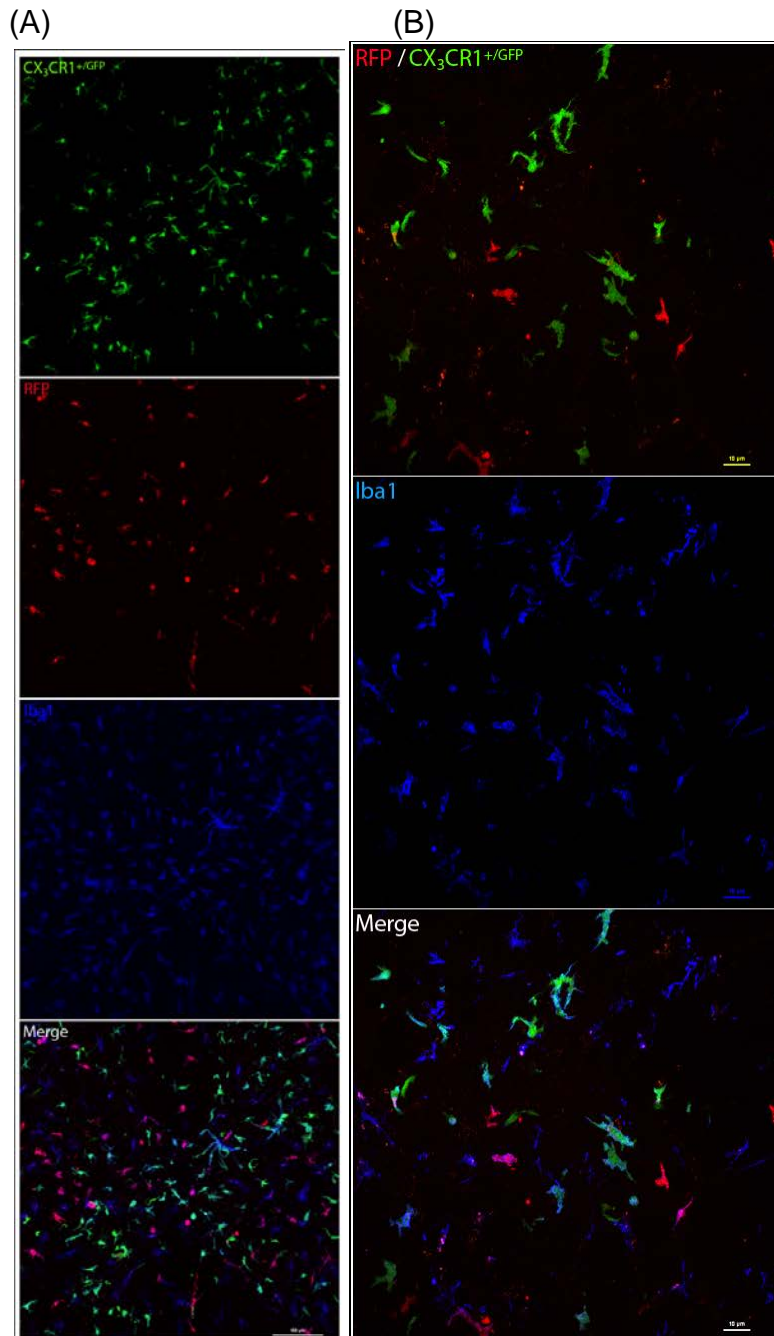
5.7 Tables

Table 5. 1 Mean BMDCs per Lumbar Spinal Cord Section (Mean ± st.dev.)
Substantially greater numbers of RFP+ and $CX_3CR1^{+/GFP}$ BMDCs accumulate in the lumbar spinal cord of mSOD mice compared to age matched controls; statistical significance was not achieved as a result of the high level of variability in the number of BMDCs observed between mice. Values were pooled over mice transplanted at 12 weeks and 10 weeks of age.

	RFP+	CX3CR1+/GFP	Total
mSOD	120.4 ± 49.4	152.5 ± 44.8	272.9 ± 20.5
Control	42.9 ± 27.6	36.6 ± 28.5	79.5 ± 49.7

5.8 References

Ajami B, Bennett JL, Krieger C, Tetzlaff W, Rossi FM (2007) Local self-renewal can sustain CNS microglia maintenance and function throughout adult life. *Nature Neuroscience, 10*(12), 1538-1543.

Audoy-Remus J, Richard JF, Soulet D, Zhou H, Kubes P, Vallieres L (2008) Rod-shaped monocytes patrol the brain vasculature and give rise to perivascular macrophages under the influence of proinflammatory cytokines and angiopoietin-2. *The Journal of Neuroscience : The Official Journal of the Society for Neuroscience, 28*(41), 10187-10199.

Auffray C, Sieweke MH, Geissmann F (2009) Blood monocytes: development, heterogeneity, and relationship with dendritic cells. *Annual Review of Immunology,* 27:669-92.

Balazs AB, Fabian AJ, Esmon CT, Mulligan RC (2006) Endothelial protein C receptor (CD201) explicitly identifies hematopoietic stem cells in murine bone marrow. Blood, 107(6): 2317-21.

Biju K, Zhou Q, Li G, Imam SZ, Roberts JL, Morgan WW, et al. (2010) Macrophage-mediated GDNF delivery protects against dopaminergic neurodegeneration: A therapeutic strategy for parkinson's disease. *Molecular Therapy : The Journal of the American Society of Gene Therapy, 18*(8), 1536-1544.

del Rio ML, Rodriguez-Barbosa JI, Bolter J, Ballmaier M, Dittrich-Breiholz O, Kracht M, Jung S, Forster R (2008) CX3CR1+c-kit+ bone marrow cells give rise to CD103+ and CD103- dendritic cells with distinct functional properties. *The Journal of Immunology,* 181:6178-88.

Fogg DK, Sibon C, Miled C, Jung S, Aucouturier P, Littman DR, et al. (2006) A clonogenic bone marrow progenitor specific for macrophages and dendritic cells. *Science (New York, N.Y.), 311*(5757), 83-87.

Geissmann F, Jung S, Littman DR (2003) Blood monocytes consist of two principal subsets with distinct migratory properties. *Immunity, 19*(1), 71-82.

Ginhoux F, Greter M, Leboeuf M, Nandi S, See P, Gokhan S, et al. (2010) Fate mapping analysis reveals that adult microglia derive from primitive macrophages. *Science (New York, N.Y.), 330*(6005), 841-845.

Gurney ME, Pu H, Chiu AY, Dal Canto MC, Polchow CY, Alexander DD, et al. (1994) Motor neuron degeneration in mice that express a human cu,zn superoxide dismutase mutation. *Science (New York, N.Y.), 264*(5166), 1772-1775.

Hexner EO & Emerson SG (2008) Stem Cell Biology. In JE Karp (Ed) Hematopoietic Stem Cell Transplantation (pp. 3-18). New Jersey: Humana Press.

Hickey WF & Kimura H (1988) Perivascular microglial cells of the CNS are bone marrow-derived and present antigen in vivo. *Science (New York, N.Y.), 239*(4837), 290-292.

Jung S, Aliberti J, Graemmel P, Sunshine MJ, Kreutzberg GW, Sher A, et al. (2000) Analysis of fractalkine receptor CX(3)CR1 function by targeted deletion and green fluorescent protein reporter gene insertion. *Molecular and Cellular Biology, 20*(11), 4106-4114.

Kiel MJ, Yilmaz OH, Iwashita T, Yilmaz OH, Terhorst C, Morrison SJ (2005) SLAM family receptors distinguish hematopoietic stem and progenitor cells and reveal endothelial niches for stem cells. *Cell,* 7:1109-21.

Kondo M, Wagers AJ, Manz MG, Prohaska SS, Scherer DC, Beilhack GF, et al. (2003) Biology of hematopoietic stem cells and progenitors: Implications for clinical application. *Annual Review of Immunology, 21*, 759-806.

Lewis CA, Solomon JN, Rossi FM, Krieger, C (2009) Bone marrow-derived cells in the central nervous system of a mouse model of amyotrophic lateral sclerosis are associated with blood vessels and express CX(3)CR1. *Glia, 57*(13), 1410-1419.

Massengale M, Wagers AJ, Vogel H, Weissman IL (2005) Hematopoietic cells maintain hematopoietic fates upon entering the brain. *The Journal of Experimental Medicine, 201*(10), 1579-1589.

Mildner A, Schmidt H, Nitsche M, Merkler D, Hanisch UK, Mack M, et al. (2007) Microglia in the adult brain arise from ly-6ChiCCR2+ monocytes only under defined host conditions. *Nature Neuroscience, 10*(12), 1544-1553.

Nevozhay D & Opolski A (2006) Key factors in experimental mouse hematopoietic stem cell transplantation. *Archivum Immunologiae Et Therapiae Experimentalis, 54*(4), 253-269.

Ramanan S, Zhao W, Riddle DR, Robbins ME (2010) Role of PPARs in radiation-induced brain injury. *PPAR Research, 2010*, 234975.

Ransohoff RM & Cardona AE (2010) The myeloid cells of teh central nervous system parenchyma. *Nature,* 468:253-62.

Robbins CS & Swirski FK (2010) The multiple roles of monocyte subsets in steady state and inflammation. *Cellular and Molecular Life Sciences : CMLS, 67*(16), 2685-2693.

Seita J & Weissman IL (2010) Hematopoietic stem cell: Self-renewal versus differentiation. *Wiley Interdisciplinary Reviews.Systems Biology and Medicine, 2*(6), 640-653.

Solomon JN, Lewis CA, Ajami B, Corbel SY, Rossi FM, Krieger C (2006) Origin and distribution of bone marrow-derived cells in the central nervous system in a mouse model of amyotrophic lateral sclerosis. *Glia, 53*(7), 744-753.

Stalder AK, Ermini F, Bondolfi L, Krenger W, Burbach GJ, Deller T, et al. (2005) Invasion of hematopoietic cells into the brain of amyloid precursor protein transgenic mice. *The Journal of Neuroscience : The Official Journal of the Society for Neuroscience, 25*(48), 11125-11132.

Szilvassy SJ, Bass MJ, Van Zant G, Grimes B (1999) Organ-selective homing defines engraftment kinetics of murine hematopoietic stem cells and is compromised by ex vivo expansion. *Blood, 93*(5), 1557-1566.

Vallieres L & Sawchenko PE (2003) Bone marrow-derived cells that populate the adult mouse brain preserve their hematopoietic identity. *The Journal of Neuroscience : The Official Journal of the Society for Neuroscience, 23*(12), 5197-5207.

Vintersten K, Monetti , Gertsenstein M, Zhang P, Laszlo L, Biechele S, Nagy A (2004) Mouse in red: Red fluorescent protein expression in mouse ES cells, embryos and adult animals. *Genesis*, 40(4):241-6.Yona, S., & Jung, S. (2010). Monocytes: Subsets, origins, fates and functions. Current Opinion in Hematology, 17(1), 53-59.

Wirenfeldt M, Babcock AA, Vinters HV (2011) Microglia – insights into immune system structure, function, and reactivity in the central nervous system. *Histology and Histopathology* 26(4):519-30.

Yona S & Jung S (2010) Monocytes: Subsets, origins, fates and functions. *Current Opinion in Hematology, 17*(1): 53-59.

Zeng C, Pan F, Jones LA, Lim MM, Griffin EA, Sheline YI, et al. (2010) Evaluation of 5-ethynyl-2'-deoxyuridine staining as a sensitive and reliable method for studying cell proliferation in the adult nervous system. *Brain Research, 1319*, 21-32.

6: GENERAL DISCUSSION

Substantial research has demonstrated that under some circumstances, bone marrow-derived cells (BMDCs) can migrate to and accumulate within the central nervous system (CNS). In a variety of rodent models of neurological disease, the accumulated BMDCs are increased in affected regions suggesting that these cells could 'home' to sites of CNS damage and function as vehicles to deliver therapeutic substances into the CNS. However, in order to exploit the clinical potential of BDMCs, we must improve our understanding of factors that govern BMDC recruitment into the CNS and determine which cell populations within whole BM are capable of this migration.

In Chapter 2, in collaboration with Jennifer Solomon, I assessed the accumulation of BMDCs in spinal cords of transgenic mice that overexpress human mutant superoxide dismutase 1 (mSOD), a murine model of amyotrophic lateral sclerosis (ALS), and control mice. BM chimeric mSOD and control mice were created by lethally irradiating and transplanting mice with whole BM harvested from mice that ubiquitously express green fluorescent protein (GFP). Using this model, we established that significantly greater numbers of BMDCs accumulate in the spinal cords of symptomatic and end-stage mSOD mice compared to nontransgenic controls. Analysis of the phenotype of BDMCs in the mSOD and control spinal cords revealed that a portion of these cells contributed

to populations of CNS-associated macrophages, as indicated by immunolabelling with antibodies to the monocyte/macrophage-associated antigens CD11b and F4/80; notably, we did not observe any instances of BMDC transdifferentiation. Expansion in the number of microglia, as determined by the quantification of CD11b+/F4/80+ cells within the mSOD spinal cord, paralleled disease progression, as did the accumulation of GFP+ BMDCs; however, the contribution of CD11b/F4/80+ BMDCs to the total microglial pool within the spinal cord remained relatively consistent at ~10-20%. This finding suggested that the expansion of microglia populations observed in the mSOD spinal cord was due primarily to the proliferation of endogenous microglia rather than the recruitment of progenitors from the circulation.   This result has been supported by recent studies that similarly observed 10-20% BMDC contributions to microglial populations in the control CNS of BM-chimeric mice at 10 to 21 months post-transplant (Ginhoux et al., 2010).

A limitation associated with the study in Chapter 2 is that within the CNS, there are several distinct CNS-associated macrophage populations that label with CD11b and F4/80 other than microglia. These populations can be distinguished based on their morphology and location within the CNS. For example, perivascular macrophages reside between the basal lamina of blood vessels and the glia limitans, leptomeningeal macrophages are located in the meninges surrounding the CNS, while microglia reside within the parenchyma of the CNS and possess a stereotypic stellate morphology. In order to clarify the identity of

BM-derived microglia, the morphology, anatomical location within the spinal cord, and the expression of macrophage markers could be analyzed.

Therefore, in my next study I described in detail the immunophenotype, morphology and location of BMDCs in relation to blood vessels within the mSOD spinal cord. BMDCs were classified as being round, rod, amoeboid, stellate, or elongated in morphology. Statistical analysis of the contributions of morphological types in lumbar spinal cord revealed significant differences between mSOD and control groups at disease end-stage, most notably in the proportions of round, stellate and amoeboid BDMCs. The majority of BMDCs in both mSOD and control spinal cord immunolabelled with the macrophage marker Iba1, indicating that a portion of BMDCs had differentiated into CNS-associated macrophages. A fraction of BMDCs exhibited the stellate morphology characteristic of microglia and labelled with Iba1, indicating these cells were likely BM-derived microglia.

Spinal cord blood vessels were immunolabelled with antibody to the endothelial protein CD31 (PECAM1) and analysis indicated that a substantial proportion of BMDCs remained associated with blood vessels, although there was a trend for a greater proportion of BDMCs in the end-stage mSOD spinal cord to reside within the parenchyma compared to controls. Overall, the results of these analyses demonstrated that only a minority of BMDCs possessed the stellate morphology, parenchymal location and Iba1 expression associated with microglia. Notably, in end-stage mSOD spinal cord, the proportion of BMDCs with a stellate morphology was increased over that of age-matched controls,

suggesting that the inflamed microenvironment of the mSOD spinal cord either preferentially recruits microglial precursors from the blood or influences the migration of BMDCs into the parenchyma and their differentiation into microglia-like cells.

To begin to identify which populations of cells within whole BM accumulate with the spinal cord, control and mSOD mice were transplanted with BM from transgenic mice in which GFP expression is limited to cells that express the chemokine receptor CX_3CR1+. Cells within BM that express CX_3CR1 include the macrophage dendritic cell precursor (MDP), developing monocytes (MOs) and MOs (Fogg et al., 2006), and within the CNS, microglia constituitively express CX_3CR1 (Cardona et al., 2006) Similar to results obtained using GFP+ BM, significantly greater numbers of $CX_3CR1^{+/GFP}$ BMDCs accumulated in the spinal cord of mSOD mice compared to control mice at disease end-stage; however, a limitation to this experiment is the possibility that populations of CX_3CR1- BM cells migrated into the spinal cord and subsequently acquired CX_3CR1 expression.

A caveat to the results of studies employing irradiated/whole BM chimeras is that the means by which BM chimeras are created introduces two confounding variables to the study of BMDC accumulation in the CNS. Firstly, irradiative treatments have been demonstrated to induce inflammatory responses and damage vasculature (Gavins et al., 2007). Secondly, intravenous injection of whole BM includes progenitor cells, which would not otherwise enter the circulation of recipient mice. Several studies employing parabiosis, an

experimental model in which the circulations of genetically distinct mice are surgically joined resulting in partial peripheral blood cells chimerism (PBC), have demonstrated that conditioning effects elicited by irradiation are requisite for the migration of BMDCs into the healthy and diseased/injured CNS (Massengale et al., 2005; Ajami et al., 2007). Ajami and colleagues (2007) created parabiotic pairs consisting of ubiquitous GFP-expressing mice and mSOD mice. Once mSOD mice reached symptomatic stages of disease, the parabionts were separated and subsequent analysis of mSOD spinal cord demonstrated an absence of GFP+ cells. However, when one parabiont was irradiated and the other protected by a lead shield, a similar absence of GFP+ cells was observed in both the healthy CNS and following facial axotomy (Ajami et al., 2007). Together these results suggest that BMDC accumulation in the CNS is dependent on the conditioning effects of irradiation and the novel presence of BM progenitors in the circulation. As well, in line with the observations made in Chapter 2, these results indicate that microglial populations are maintained primarily through self-renewal in both healthy and diseased states (Solomon et al., 2006; Ajami et al., 2007).

Although radiation treatments are used clinically for a variety of maladies, the deleterious effects associated with this treatment for the purpose of potentiating BMDC migration into the CNS currently limit the clinical potential of BMDCs as treatment vehicles for neurodegenerative disease. As such, I investigated whether alternative preconditioning regimens result in BMDCs accumulation in the spinal cords of mSOD and control mice. I created BM

chimeric mSOD and control mice using the chemotherapeutic agent Busulfex

(BU), rather than irradiation, to myelosuppress recipient mice prior to BM

transplantation. I chose this particular pharmaceutical agent because unlike

alternative chemotherapeutics, it specifically targets quiescent HSCs within BM,

and unlike irradiation leaves the immune system intact. In line with my results

obtained using myeloablative irradiation, I obtained both high levels of BM

chimerism and BMDC accumulation in the spinal cord. GFP+ cells were

quantified and classified according to morphology in the lumbar spinal cords of

control and mSOD mice at advanced disease stages. Immunolabelling with Iba1

indicated that a portion of GFP+ differentiated into CNS-associated macrophages

and a high proportion of BMDCs with stellate morphology also expressed Iba1,

suggesting these BMDCs had differentiated into microglia . There were also

variable numbers of T-lymphocytes, the majority of which immunolabelled with

antibody to CD8, indicating these were cytotoxic T-lymphocytes.   Although

cytotoxic T-cells are observed in the spinal cord of mSOD mice, they are typically

only very rarely observed in the healthy CNS (Neumann et al., 2002).

The kinetics of BMDC entry into the spinal cord of control mice was

investigated and variable numbers of donor-derived cells were observed in spinal

cord 2 weeks after BM transplant. The vast majority of these cells had a rod-

shaped morphology and were located in association with blood vessels.

Immunohistochemical analyses indicated that BMDCs accumulating in the spinal

cord at 2 weeks post-transplant did not express the macrophage antigen Iba1,

and only a minority immunolabelled with the monocyte marker CD11b; future

work should be directed to identify these cells using immunohistochemistry. I expect that these rod shaped cells correspond to the intralumenal rod-shaped BMDCs described by Vallieres and Sawchenko (2003) and Audoy-Remus and colleagues (2008), specifically MOs and granulocytes that patrol blood vessels

At 2 weeks post-transplant, I qualitatively observed that microglia had a reactive phenotype, as indicated by thickened cellular process, cell body hypertrophy and increased Iba1 immunoreactivity. BU readily crosses the BBB and is associated with neurotoxicity that presents as seizures clinically (Hassan et al., 1996). Therefore, given the observed reactive state of microglia and the presence of CD8+ cytotoxic T-cells in the spinal cord of control mice, it seems likely that treatment with BU at the dose of 100mg/kg I employed is associated with a neuroinflammatory response. Furthermore, I suspect the BMDCs observed in control spinal cord at 2 weeks post-transplant are likely patrolling MO and Gr-1+ polymorphonuclear cells that are responding to the inflammatory response elicited by the BU treatment. Although we failed to find any reports in which treatment with solely BU caused encephalitis, there have been clinical studies on the incidence of encephalitis in patients treated with BU in concert with other immunosuppressive drugs (Barba et al., 2009). In future experimental trials, mice will be treated with lower doses of BU in attempts to minimize the neuroinflammatory response. The efficacy of lower doses of BU in obtaining levels BM chimerism and BMDC accumulation in the spinal cord of mSOD and control mice will be evaluated.

In addition to identifying the conditioning factors that enhance BMDC migration into the CNS, which cells within BM capable of this migration should also be identified. In the clinical setting, reconstituting patients' BM with that which has been engineered to over-express neurotrophic factors is not ideal as these factors have mitogenic properties. Therefore, if populations of BM cells downstream of HSCs that capable of accumulating in the CNS were identified, it would enable BMDC-mediated delivery of therapeutic substances into the CNS in the absence of BM replacement and improve the clinical potential of BMDCs.

In Chapter 3, I demonstrated that CX_3CR1+ BM cells populate the spinal cords of control and mSOD BM chimeric mice; however, it could not be distinguished whether CX_3CR1+ BM cells migrated into the spinal cord or CX_3CR1- BM cells migrated in and then acquired CX_3CR1 expression. Within BM, the CX_3CR1+ fraction of cells includes the MDP, myeloblasts (i.e. developing MOs) and MOs (Fogg et al., 2006). In Chapter 5, in order distinguish the contribution of CX_3CR1+ BM cells and cells derived from definitive hematopoiesis to the accumulation of BMDCs in spinal cord, I harvested BM from $CX_3CR1^{+/GFP}$ donor mice and collected the $CX_3CR1^{+/GFP}$ fraction of BM cells using fluorescence-activated cell sorting (FACS). HSCs are contained within the c-kit+Lin-Sca1+ (KLS) fraction of BM and this fraction of cells was collected from BM harvested from donor mice that ubiquitously express red fluorescent protein (RFP) using FACS; long-term HSCs contained within this fraction will reconstitute the BM of recipient mice. The $CX_3CR1^{+/GFP}$ fraction of BM cells and RFP+ KLS cells were transplanted into irradiated control and mSOD mice.

Because the $CX_3CR1^{+/GFP}$ fraction of cells will not contribute to long-term BM reconstitution of hosts, it was anticipated that $CX_3CR1^{+/GFP}$ cells would clear the circulation of recipients, enabling the analysis of the proliferation of $CX_3CR1^{+/GFP}$ cells that accumulate in the spinal cord. Furthermore, this experimental paradigm enabled investigation into the differential accumulation of $CX_3CR1^{+/GFP}$ cells in the CNS of recipient compared to RFP+ cells derived from definitive hematopoiesis. One issue encountered during repeated experimental trials was the persistence of $CX_3CR1^{+/GFP}$ cells in the circulation of recipients up to the time mSOD mice reached disease end-stage. Assessment of factors that might contribute to the presence of $CX_3CR1^{+/GFP}$ cells in the circulation of recipients indicated that the purity of the CX_3CR1+ fraction injected may have been insufficient and included CX_3CR1- HSCs that reengrafted in the BM of recipients, resulting in the continued production of $CX_3CR1^{+/GFP}$ cells. In future experiments, the $CX_3CR1^{+/GFP}$ fraction will be sorted twice through FACS, increasing the purity of the cell fraction injected. Although we are in the process of refining this experimental protocol, my results to date suggest that both $CX_3CR1^{+/GFP}$ BM cells and RFP+ cells derived from definitive hematopoiesis accumulate in the spinal cord.

In the studies outlined in chapters 4 and 5 of my thesis, statistically significant differences in the accumulation of BMDCs in control and mSOD spinal cords were not obtained. This likely represents a statistical Type II error (false negative) due to the limited sample sizes evaluated in both of these studies and a high degree of variability within experimental groups. I anticipate that increasing

the sample size included in each study will result in obtaining statistically significant results.

6.1 Future Directions:

The impetus for this research was to improve the clinical potential of BMDCs to function as treatment modalities for neurodegenerative disease. There are currently no effective treatments for a variety of neurodegenerative diseases including amyotrophic lateral sclerosis (ALS), a fatal disorder characterized by the selective degeneration of motoneurons. One reason for the difficulty in treating neurological disorders with pharmaceutical agents is the inability of all large molecule and the majority of small molecule drugs to cross the blood-brain barrier (BBB) to reach affected regions within the CNS; the current repertoire of drugs capable of traversing the BBB have been ineffective at treating neurological disease. Therefore, better understanding of the factors that govern BMDC accumulation in the CNS and which cells within BM are capable of integrating into the cellular milieu of the CNS presents a novel a therapeutic modality for the treatment of neurological diseases.

The work presented in this thesis demonstrates that increased numbers of BMDCs accumulate in the spinal cord of mSOD mice compared to controls and the majority of these cells differentiate into populations of CNS-associated macrophages. Further examination of the morphology, anatomical location, and immunophenotype of BMDCs within the spinal cord indicate that a minority of BM-derived macrophages acquire the stellate morphology, parenchymal location,

and antigenicity characteristic of microglia. Several studies demonstrate that the

conditioning effects of irradiation are requisite for BMDC migration into the CNS;

however, in Chapter 4, I demonstrated that the conditioning effects of the

chemotherapeutic BU similarly result in BMDC accumulation in spinal cord,

providing evidence that alternative conditioning regimens to irradiation can be

used to potentiate BMDC accumulation in the CNS. In Chapter 5 I demonstrated

that the $CX_3CR1^{+/GFP}$ fraction of BM cells, which provides only transient

reconstituion of myeloid cells, accumulates in the spinal cords of mSOD and

control mice, indicating that replacement of host BM is not required for BMDCs to

accumulate in the CNS. Together, the results of these studies increase the

clinical potentital of BMDCs to function as treatment modalities, as

preconditioning with BU leave the immune system of recipients intact and the

ability of CX_3CR1+ BMDCs to accumulate in the CNS indicates that replacement

of host BM is not required.

The next steps in this research should examine the efficacy of BMDCs that

have been engineered to overexpress neurotrophic factors at delaying disease

progression in models of neurodegenerative disease. Neurotrophic growth

factors are secreted proteins that support neuronal function and survival.

Previous clinical studies employing intrathecal delivery of brain-derived

neuorotrophic factor (BDNF) into the cerebral spinal fluid were inefficacious at

slowing disease progression in ALS patients (Henriques et al., 2010). However,

if and to what degree BDNF can pass from the CSF across the BBB into the

parenchyma of the CNS is not known (Pan et al., 1998). In unpublished work by

Jennifer Solomon, mSOD mice irradiated and transplanted with BM from mice that overexpress BDNF did not improve motor function, motoneuron survival, or extend time to disease end-stage. A suggested reason for the observed lack of benefit was that limited numbers of BDNF-overexpressing BMDCs migrated to sites of neurodegeneration in the mSOD spinal cord. As such, one way to address this issue would be to examine factors that increase the accumulation of BMDCs into the CNS.

Treatment with granulocyte-colony stimulating factor (G-CSF) has been demonstrated to increase the number of BMDCs within the circulation. Previous studies employing a murine model of Alzheimer's disease (AD) have demonstrated that treatment with G-CSF increases the number of microglia and the number of BM-derived macrophages in the CNS of BM chimeric mice (Sanchez-Ramos et al., 2009). Therefore, treating BDNF-overexpressing BM chimeric mSOD mice with G-CSF might similarly result in increased BMDC accumulation in the diseased spinal cord and a therapeutic benefit of BDNF might be observed.

6.2 References

Ajami B, Bennett JL, Krieger C, Tetzlaff W, Rossi FM (2007) Local self-renewal can sustain CNS microglia maintenance and function throughout adult life. *Nature Neuroscience, 10*(12), 1538-1543.

Barba P, Pinana JL, Valcarcel D, Querol L, Martino R, Sureda A, et al. (2009) Early and late neurological complications after reduced-intensity conditioning allogeneic stem cell transplantation. *Biology of Blood and Marrow Transplantation : Journal of the American Society for Blood and Marrow Transplantation, 15*(11), 1439-1446.

Cardona AE, Pioro EP, Sasse ME, Kostenko V, Cardona SM, Dijkstra IM, et al. (2006) Control of microglial neurotoxicity by the fractalkine receptor. *Nature Neuroscience, 9*(7), 917-924.

Fogg DK, Sibon C, Miled C, Jung S, Aucouturier P, Littman DR, et al. (2006) A clonogenic bone marrow progenitor specific for macrophages and dendritic cells. *Science (New York, N.Y.), 311*(5757), 83-87.

Gavins F, Yilmaz G, Granger DN (2007) The evolving paradigm for blood cell-endothelial cell interactions in the cerebral microcirculation. *Microcirculation (New York, N.Y.: 1994), 14*(7), 667-681.

Ginhoux F, Greter M, Leboeuf M, Nandi S, See P, Gokhan S, et al. (2010) Fate mapping analysis reveals that adult microglia derive from primitive macrophages. *Science (New York, N.Y.), 330*(6005), 841-845.

Hassan M, Ehrsson H, Ljungman P (1996) Aspects concerning busulfan pharmacokinetics and bioavailability. *Leukemia & Lymphoma, 22*(5-6), 395-407.

Henriques A, Pitzer C, Schneider A (2010) Neurotrophic growth factors for the treatment of amyotrophic lateral sclerosis: Where do we stand? *Frontiers in Neuroscience, 4*, 32.

Massengale M, Wagers AJ, Vogel H, Weissman IL (2005) Hematopoietic cells maintain hematopoietic fates upon entering the brain. *The Journal of Experimental Medicine, 201*(10), 1579-1589.

Neumann H, Medana IM, Bauer J, Lassmann H (2002) Cytotoxic T lymphocytes in autoimmune and degenerative CNS diseases. *Trends in Neurosciences, 25*(6), 313-319.

Pan W, Banks WA, Fasold MB, Bluth J, Kastin AJ (1998) Transport of brain-derived neurotrophic factor across the blood-brain barrier. *Neuropharmacology, 37*(12), 1553-1561.

Sanchez-Ramos J, Song S, Sava V, Catlow B, Lin X, Mori T, et al. (2009) Granulocyte colony stimulating factor decreases brain amyloid burden and reverses cognitive impairment in alzheimer's mice. *Neuroscience, 163*(1), 55-72. doi:10.1016/j.neuroscience.2009.05.071

Solomon JN, Lewis CA, Ajami B, Corbel SY, Rossi FM, Krieger C (2006) Origin and distribution of bone marrow-derived cells in the central nervous system in a mouse model of amyotrophic lateral sclerosis. *Glia, 53*(7), 744-753. doi:10.1002/glia.20331

APPENDIX 1: PROTOCOLS

G93A Mutant SOD Mouse Genotyping

Reagents:

Proteinas K

Ribonuclease A

Chelex 100

Deoxyribonucleotide triphosphates (dNTPs)

Primers (custom sequences obtained through Invitrogen):

      Sense (mSOD1): CAT CAG CCC TAA TCC ATC TGA

      Antisense (mSOD2): CGC GAC TAA CAA TCA AAG TGA

Solutions:

TE, pH 8.0:
      10mM TrisCl: 60.55 mg
      1mM EDTA: 16.81 mg
      Top up to 50mL with ddH2O

Low TE, pH 7.6 : 10x dilution of TE with ddH2O

Proteinase K: 20mg/mL in ddH20

RNase A: 10mg/mL in ddH20

Chelex : 5% w/v in low TE

dNTPS (2mM): 10 μL of dCTP, dTTP, dGTP, dATP in 460 μL ddH2O

Protocol:

1. Collect ear tissue (store at -20°C)
2. DNA Extraction Buffer → volume per 2 samples:
    a. Chelex – 250 μL
    b. Proteinase K – 25 μL
    c. RNase A – 25 μL
3. Add 150 μL of buffer to each tissue sample and place in 55°C water bath for 30 min (vortex at 15 min)
4. Place in 100°C water bath for 10 min
5. Centrifuge at 12x10^3 rpm for 5 min
6. Use 1 μL of supernatant from each sample as DNA template immediately or store at -20°C
7. For PCR reaction, for each sample add:

    a. Primer 1 – 0.5 µL
    b. Primer 2 – 0.5 µL
    c. 10x Buffer – 2.5 µL
    d. dNTPs – 2.5 µL
    e. MgCl2 – 0.5 µL
    f. ddH2O – 17.2 µL
    g. Taq – 0.3 µL
8. PCR Cycle conditions:

# of cycles	Temp (°C)	Time
1	95	5 min
30	94	30 sec
	56	30 sec
	72	30 sec
1	94	30 sec
	56	30 sec
	72	10 sec
∞	4	∞

9. Run on a 1% agarose gel in 1x TBE running buffer
10. Add 1-2 µL bromophenol blue to PCR product and load 10 µL of PCR product + dye to each column of gel
11. Run add 100V for ~30min
12. Presence of 132 bp band indicates mSOD transgene

Bone Marrow Transplantation

Solutions:

ACK RBC Lysis Buffer (Invitrogen)

FACS Buffer:
      1xPBS - 500 mL
      2% FBS – 10 mL
      2mM EDTA -

Procedure:
1. Euthanize BM donor mouse with CO_2
2. Cut skin on abdomen at xyphoid process; pull skin down to expose legs
3. Cut legs from body and remove surrounding muscle/fat from femur and tibia
4. Place bones in dish with PBS
5. Cut bones at each end to expose marrow cavity
6. Using a syringe filled with FACS buffer fitted with 25 ¾ gauge needle, flush marrow from cavity into petri dish; flush from both ends of bone
7. Remove clumps in BM + FACS buffer by sucking up and ejecting with syringe without needle
8. Transfer BM + FACS buffer into Falcon tube (15 mL or 50 mL depending on volume) and centrifuge at 1500 rpm for 5 minutes
9. Remove supernatant and resuspend BM in 1 mL RBC lysis buffer; let stand for 10 min on ice.
10. Top up Falcon tube with FACS buffer and centrifuge at 1500 rpm for 5 min
11. Remove supernatant and resuspend in 1 mL PBS
12. Pass through 40 μm filter
13. Count cells using hemocytometer:
    a. Add 10 μL of cell solution to 1 mL PBS
    b. Add 10 μL of diluted cells into chamber of hemocytometer
    c. Count number of cells in 4 grids surrounding centre grid
    d. Cells per mL: Total cells counted/4 x 100 x 10000
14. Dilute cells with PBS to 5x10^6 cells per 400 μL
15. Lethally irradiate recipient mice with 9.5-11 Gy gamma radiation
16. Inject ~5x10^6 BM cells (~400 μL) per recipient mouse via tail vein injection
17. Collect blood samples 3 weeks post-transplant to assess BM reconstitution by FACS analysis